UiT
THE ARCTIC UNIVERSITY OF NORWAY

FACULTY OF SCIENCE AND TECHNOLOGY

Department of Geosciences

The role of diapiric mound structures in the overburden fluid plumbing systems of the Vøring Basin

Lene Loug Hansen

Master's thesis in Geology, GEO-3900

May 2018

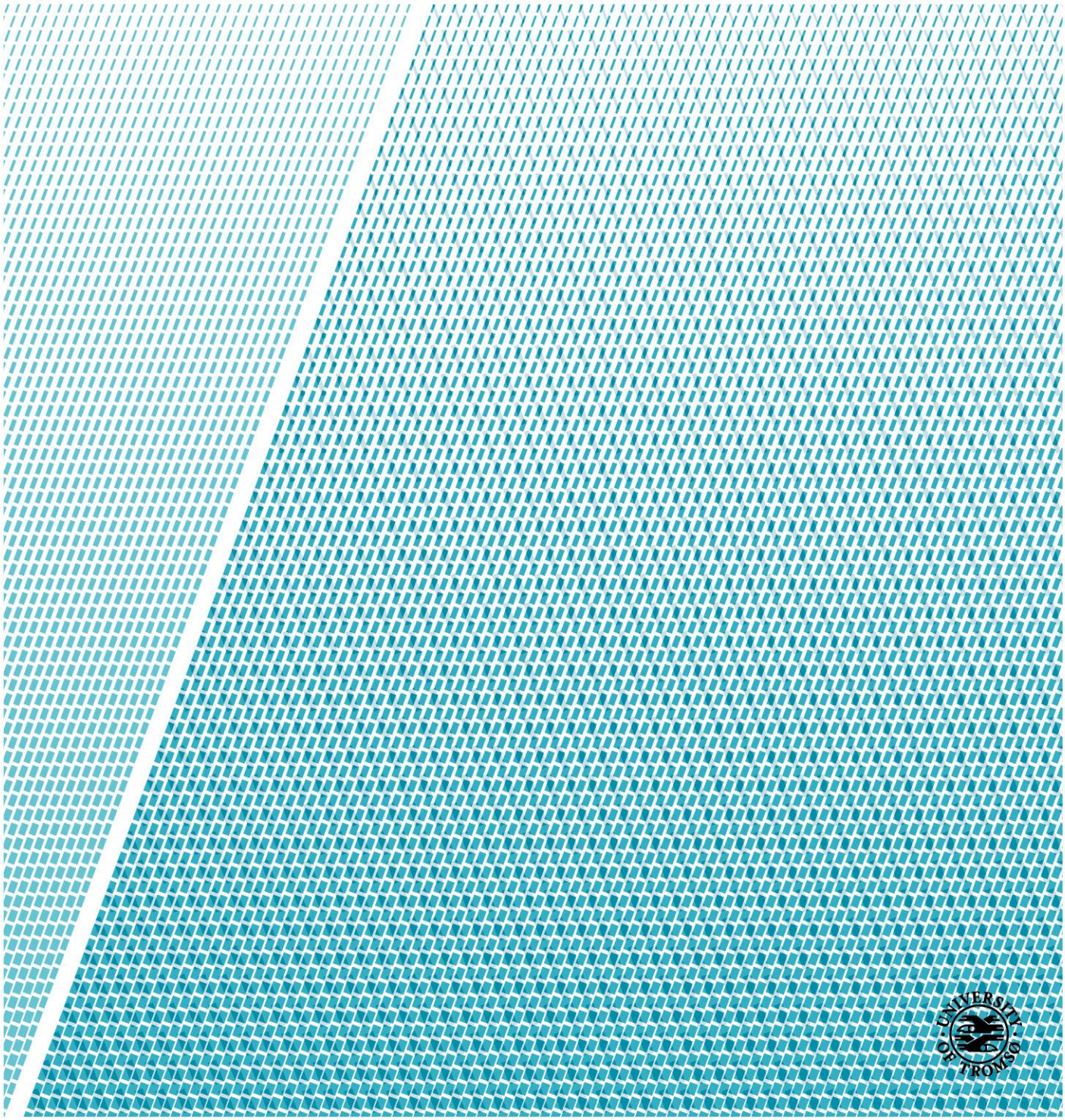

Abstract

The overall aim of this thesis is to better understand the development and emplacement of diapiric mound features in the Vema Dome area, located in the Vøring basin on the mid-Norwegian continental margin. Two 3D seismic surveys, ST9603R99 and BPN9601, were interpreted in this study, in order to investigate the diapiric mounds and their relationship with an underlying fluid plumbing system including magmatic sill complexes and fluid flow features observed in the seismic. The 3D seismic data was kindly provided to the Arctic University of Norway through access to the DISKOA national data repository for exploration and production related data that is shared by both Authorities (mainly NPD) and oil companies.

Eleven diapiric mounds have been identified in the study area. Ten of these mounds are located at the top Naust formation and have a thin layer of recent sediments deposited on top. The remaining mound is located cutting through the base Naust reflection, indicating that diapirism have been active in the area during the deposition of the Naust formation, but with a possible hiatus. The mounds have a clear upper boundary with a strong continuous reflector, and a lower boundary with low seismic amplitude and are semi-continuous. The internal seismic structure of the mounds are hummocky and chaotic, with very low to almost no internal seismic reflections. There are four separate magmatic sill intrusions interpreted in the seismic data, particularly recognized in RMS amplitudes attribute volumes. These anomalies are very well defined in the seismic data, as the amplitude signature does not fade around the edges, but rather is an abrupt change to an increased amplitude. The sills are crosscutting the regular sedimentary strata, are mostly sub-parallel to the strata configuration and are saucer shaped. The plumbing system beneath the diapirs are seen as vertical columnar features of lowered seismic amplitudes interpreted as chimneys, pipes and small faults. These have been divided into two groups, where some of them are hydrothermal vents that can be correlated to the sill complexes, and the others has been related to overpressure in the subsurface. All these features have acted as pathways for fluids and sediments migrating and expulsing on the seafloor.

This study suggest that diapirism over the Vema Dome is a result of the combination of at least three factors; 1) the emplacement of sills leading to hydrothermal vents and other chimney features representing good pathways for fluid migration, 2) buoyancy due to density difference of oozes overlain by glacigenic debris flows, and 3) the uplift of the Vema Dome leading to faults and fractures.

Acknowledgement

I would first like to thank my supervisor, Professor Stefan Bünz for giving me the opportunity to write this thesis and for giving me the opportunity to join two seismic cruses over the last year, introducing me to on-board seismic processing.

I would like to thank all my friends at UiT for all the lunches and coffee-breaks and for making my two years here in Tromsø great. I would also like to thank Kate Alyse Waghorn for all your support, good discussions and correcting my grammar. Also thanks for all the dinners at Rå Sushi and Casa inferno and many, many glases of wine.

Finally, I would like to thank my family and Renate for all their support.

Table of Contents

1 Introduction

On the Vøring marginal high on the mid-Norwegian continental margin, three fields of diapir features have been identified, and named the Vema, Vigrid and Vivian diapir fields. This thisis focuses on the Vema diapir field located over the Vema Dome located in the Vøring Basin by studying two 3D seismic cubes located over the Vema Dome and on the eastern side of the dome. The diapiric features has previously been studied by Hjelstuen et al., (1997) and Hovland et al., (1997).

1.1 Objectives

The main focus of this thesis is to map diapiric mound structures in the Vema Dome area in the Vøring Basin on the mid-Norwegian continental margin, in order to get a better understanding of the development and the controlling factors of these structures, and how they relate to underlying fluid flow features.

The outer Vøring Basin has been studied in detail, but there has not been much focus on the large diapiric mound structures in the area. Sill complexes and hydrothermal vent complexes have been mapped in the Vøring Basin by for example Planke et al., (2005), and the diapiric mound structures have previously been documented by Hovland et al., (1998) and Hjelstuen et al., (1997). Newly released 3D seismic data from the area of the Vema Dome provides new insight into their subsurface structure and their plumbing system. Two 3D seismic surveys have been used, ST9603R99 and BPN9601. Figure 1.1 shows a structural map modified from npd.no with the location of the 3D seismic surveys.

1.1.1 Thesis outline

This thesis is divided into three main components. The first three chapters will give some background information, covering some fundamental theory about fluid migration in sedimentary basins and typical fluid flow features and how they are imaged in seismic, introduction to the study area and introduction to the seismic datasets used in this study. Next there will be a chapter where the results and findings will be presented and interpreted. Last there will be a discussion of the results.

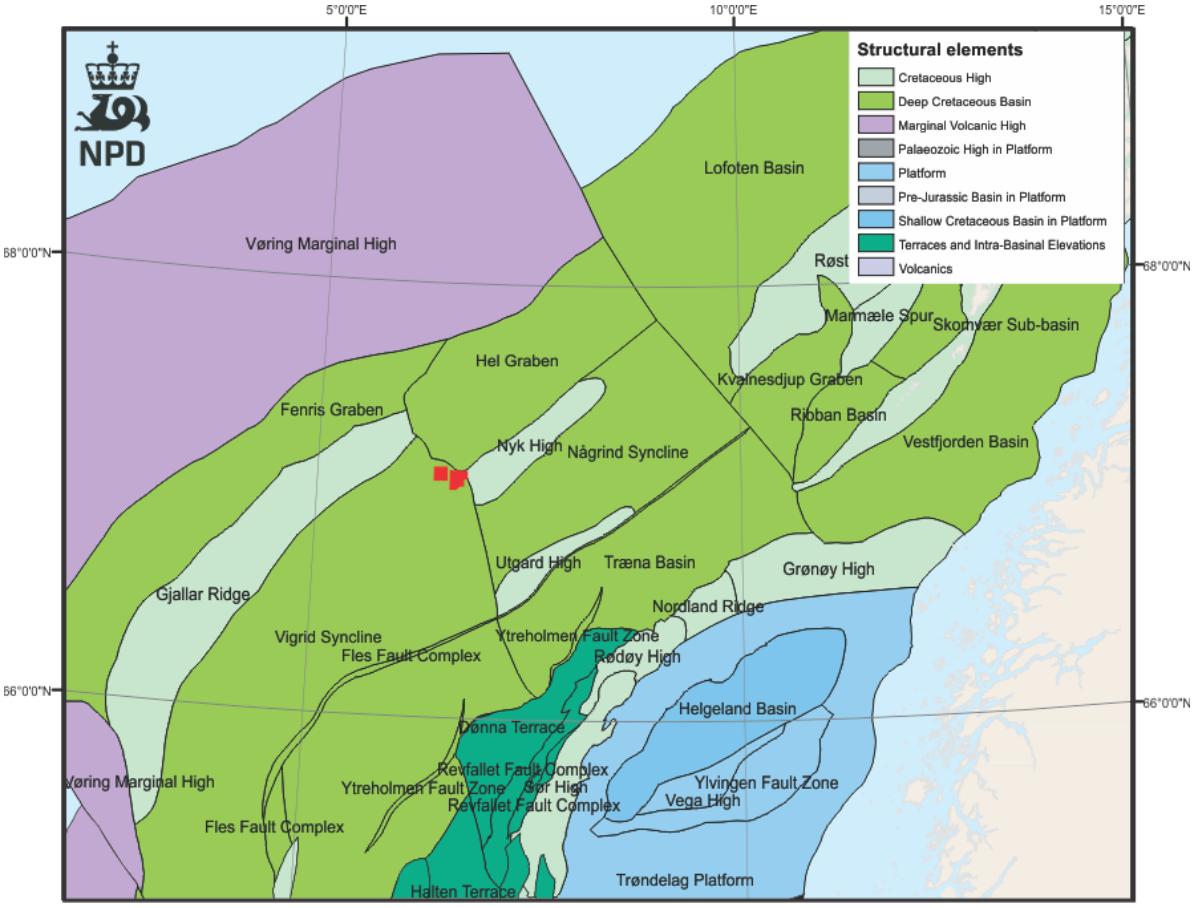

Figure 1.1 Overview map modified from npd factpages. Red polygons indicate the location of the seismic surveys.

2 Fundamental theory

The following sub-chapters will give an introduction to fluid flow and associated fluid flow features in sedimentary basins. The characteristics of these features are described according to their look in seismic.

2.1 Fluid migration in sedimentary basins

Fractures and pore spaces in sediments are usually filled with fluids, either in a gaseous form, liquid form or both (Guzzetta and Cinquegrana, 1987). The movement of gas and liquid through the subsurface is referred to as fluid flow. Migration of fluids in the subsurface can be triggered by a variety of mechanisms including, but not limited to; a heat source warming deep fluid, compaction reducing pore space and bouyancy and compressibility characteristics of fluid contained in the pore space (Huuse et al., 2010, Andresen, 2012). Mechanisms include earthquakes, tectonic stress and widespread faulting, sea level fluctuations, depositional loading, differential and disequilibrium compaction, lateral pressure transfer, overpressure caused by influx of fluids from deeper levels, diagentic transformations, hydraulic failure and man-made drilling operations (Andresen, 2012).

Fluid flow in the subsurface can be recognized with several distinct features, such as diapiric structures, pockmarks, chimneys and pipes (Andresen, 2012). Pipes, chimneys and faults are part of fluid flow systems as pathways for pore fluids to migrate from depth towards the subsurface (Berndt, 2005). When the fluid flow structures reach the seafloor, there are numerous features that form in response to fluid expulsion, dependent on the fluid contents and the way the fluids are expelled. For example, when the fluid has a high mud content, a mud mound may form, while pockmarks can be formed when fluid expulsion at the seafloor creates turbidity making a low relief structure as opposed to a high relief mound (Berndt, 2005). Figure 2.1 shows an illustration of fluid flow features commonly found on continental margins (Huuse et al., 2010).

An understanding of the fluid flow systems on the continental margins is important as it affects hydrocarbon migration, ecosystems on the seabed, poses potential geohazard, which could be a threat for seafloor installations and can trigger submarine landslides (Berndt, 2005). The study of focused fluid flow is also important regarding basin analysis (Andresen, 2012). Studying the trigger mechanisms, sources, migration pathways and when fluid flow has been active in an

area, can give important information about the basin evolution regarding sedimentation and tectonic history as well as presence and extent of hydrocarbons (Andresen, 2012).

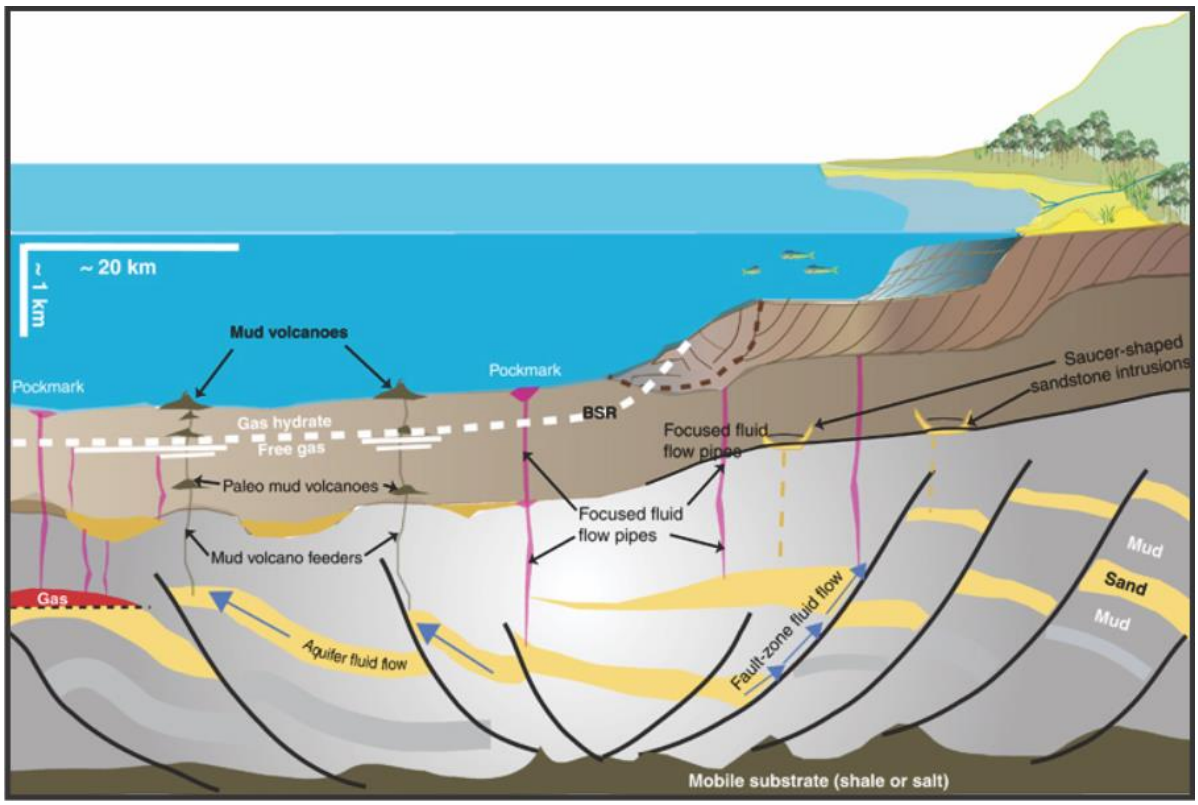

Figure 2.1 Illustration of the large-scale sediment remobilization and fluid flow features typically found on continental margins. Features include mud volcanoes, sand intrusions, pockmarks, focused fluid flow pipes, and fluid flow along faults and sedimentary planes. (Huuse et al., 2010)

Timing of fluid flow events can be determined if it is possible to indicate the age of the subsequent features. Pockmarks and mud and sand diapirs/volcanoes are usually extrusive features, meaning they penetrate the surface when they form. If a basal reflection is present, indicating the oldest possible age of formation, timing and longevity of the fluid flow event can be determined. It is hard to determine the age of fluid flow features that do not reach the surface or do not have distinct onset paleo-surface marker, such as vertical features as chimneys and pipes (Andresen, 2012).

The amount of fluid released to the surface during periods of fluid flow can be hard to determine due to variable factors such as flow mechanisms, fluid composition, and mechanisms of overpressure and erosion (Andresen, 2012).

2.1.1 The physics of fluid migration

Migration of fluids in a sedimentary basin follow the laws of fluid dynamics, and the main driving force is buoyancy (Schowalter, 1979). During burial of sedimentary strata, increasing load of sediment reduces pore space within the material. Fluid is less compressible so any fluid contained within the pore space is forced to migrate (Brown, 1990). If the pressure is more than the hydrostatic gradient at a specific depth, the pore fluid becomes overpressured, and can start to migrate (Osborne and Swarbrick, 1997). Fluids are driven to flow from high pressure gradients to lower pressure gradients. The fluid potential is defined as (equation 1) (Bjørlykke, 2010):

$$F_p = P - \rho g h \qquad Equation\ 1$$

Where P = Fluid Pressure, ρ = Density of the fluid, g = Acceleration of gravity and h = distance to reference level (e.g. the sea level).

The density of a liquid in the subsurface is dependent on pressure and temperature. This also applies to gases which in addition is also dependent on the ratio of mass to volume (Schowalter, 1979).

Fluid flow through a permeable media can be described by Darcy's law (equation 2). Permeability (k) is the resistance of flow of a fluid in porous media. Migration of fluids are dependent upon differences in pressure and density, and will normally migrate from areas with high pressure towards areas with lower pressure (Bjørlykke, 2010).

$$Q = \frac{kA(P_b - P_a)}{\mu L} \qquad Equation\ 2$$

Where:

Q = Total discharge/Rate of flow (m^3/s), k= Permeability (m^2), A= Cross sectional area (m^2), P_b-P_a = pressure difference, μ = Viscosity of the medium (Pa*s).

Capillary pressure is the main resisting force acting against the buyancy forces and migration of fluids (Schowalter, 1979, Bjørlykke, 2010). In order for fluids to migrate in the subsurface, the buoyancy force has to exceed the capillary pressure. The capillary pressure is determined by the radius of the pore throats where the throat restrict the free passage for fluids, and contact

tension between the fluids in the system, e.g. water and gas, and can be excpressed by equation 3 (Schowalter, 1979, Berg, 1975).

$$P_c = \frac{2\gamma}{r} \qquad Equation\ 3$$

Where P_c=Capillary pressure; γ = interfactial tension between hydrocarbon and water; r = the radius of the drop (Berg, 1975).

2.1.2 Fluid flow features

Fluid flow in the subsurface can have a variety of expressions which, when observed in geophysical data or analogue sites, are indicative of specific modes of fluid flow. The resulting identifiable characteristics are often a result of the type of fluid migrating. Gas, oil, groundwater/deep fluid circulation (Andresen, 2012) and magmas (quasi/non-Newtonian) are all fluids capable of migrating and often have unique features associated. When sediment is entrained in fluid flow, an additional range of features form in response. Fluid accumulations in the subsurface can be resolvable in seismic data if the fluid changes the physical properties of the host rock enough to induce a seismic response. Generally the change in physical properties is large enough to increase reflectivity and create an amplitude anomaly when hydrocarbons are present in the pore space, however in marine sediments non-hydrocarbon fluids will normally not induce a seismic response. Therefore, specific features forming in response to fluid flow are necessary to determine the state of sub-surface fluid migration. Fluids migrate through faults and cracks, or they can migrate along sedimentary planes. Fluid flow structures on the seafloor are representative of fluid migration breaching the seafloor and features which form in response are depression structures such as pockmarks and craters or build-up features such as mounds or black-smokers. The difference in morphology is largely determined by the content of the fluid, for example, mud is less cohesive so builds up into large circular mounds with relatively low relief while hydrothermal fluids contain minerals that, when they precipitate out, create tall thin ‘chimneys’. Fluid flow features in the subsurface, represented in seismic sections, are usually related to the long-term rock-property alteration by continued fluid flow and express as vertical column features such as chimneys and pipes, sediment injections, carbonate mounds, seeps and related diagenetic phenomena (Andresen, 2012).

Andresen 2012 divided fluid flow features into three groups based on the cause of their formation. These groups are shown in figure 2.2. The features are divided into "subsurface sediment remobilization, vertically focused fluid flow and laterally extensive fluid flow" (Andresen, 2012).

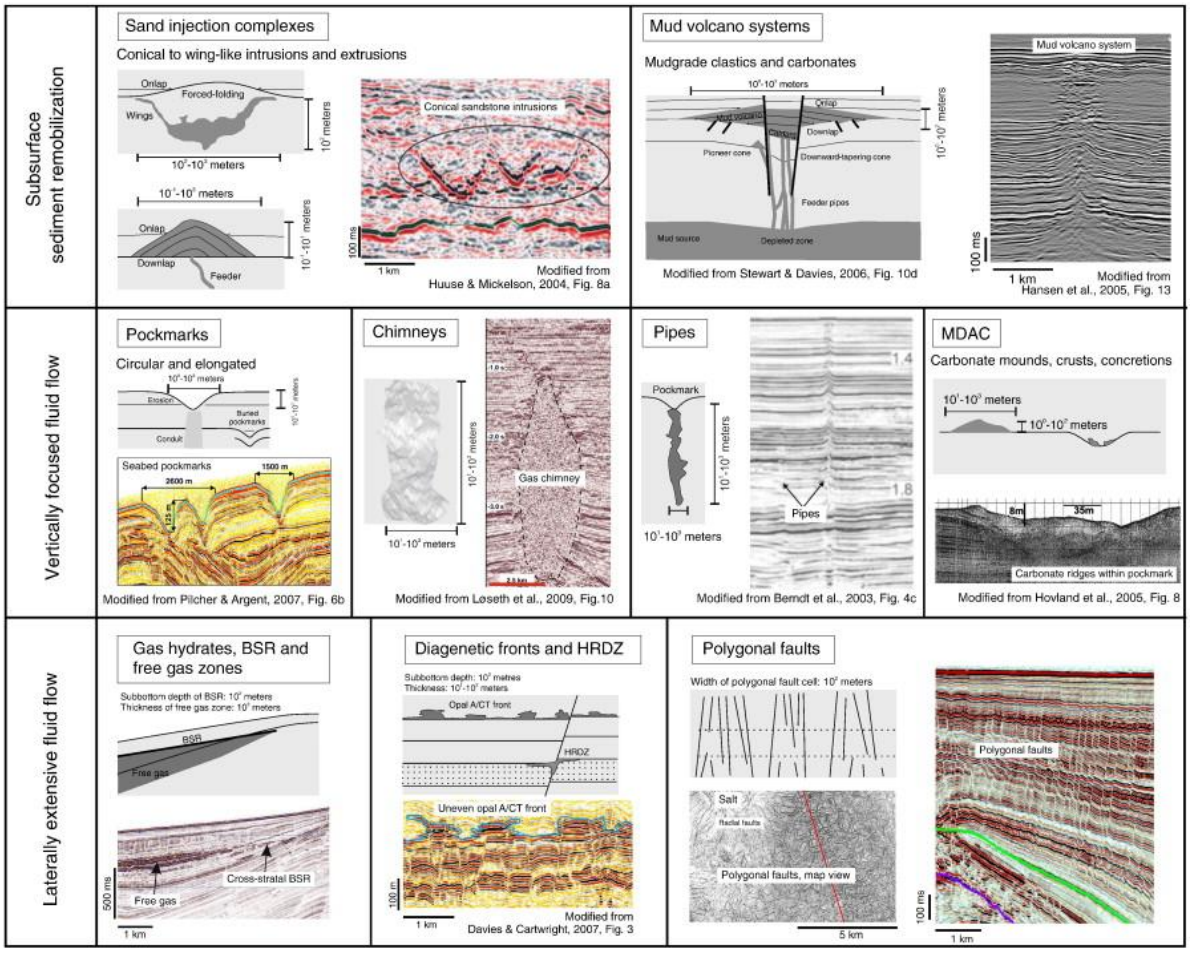

Figure 2.2 Illustrations and seismic examples of fluid flow features divided into three groups: 1. Subsurface sediment remobilization, 2. Vertically focused fluid flow and 3. Laterally extensive fluid flow. MDAC = methane derived authigenic carbonates, HRDZ = hydrocarbon related diagenetic zones, BSR = bottom simulating reflector. From (Andresen, 2012).

Focused fluid flow and subsurface sediment remobilization include features made by build up and remobilization of material due to fluid flow overpressure (Andresen, 2012). Sand intrusions, mud volcano systems, mobilized salt and igneous intrusions are such features (Andresen, 2012). For this study, mud volcano systems and igneous intrusions are of special interest. Vertically focused fluid flow include pockmarks, chimneys, pipes and methane derived authigenic carbonates, where chimneys and pipes are of interest here (Andresen, 2012). The last group, laterally extensive fluid flow include gas hydrates, BSR (bottom simulating reflector), free gas zones, diagenetic fronts and polygonal faults (Andresen, 2012). Laterally

extensive fluid flow features can occur when fluid flow is focused in specific stratigraphic levels, such as high porosity beds or at specific depths in the subsurface (Andresen, 2012). From this group we will take a closer look at the opal A/CT diagentic front and polygonal faults (chapter 2.3.2).

The following subchapters will give an introduction to the fluid flow features of interest for this study, where mud diapirism and faults have been given separate chapters (2.3 and 2.4).

2.1.2.1 Chimneys and pipes

Long vertical columnar features seen in seismic crossing the stratigraphy are usually referred to as chimneys and pipes (Andresen, 2012). They are often characterized as zones of low or high amplitude anomalies and low coherency (Andresen, 2012).

Chimneys and pipes can represent high fluid-flux paths, and are often seen in relation to other fluid flow features, e.g. terminating in pockmarks, diapirs or high amplitude anomalies associated with gas accumulation (Cartwright, 2007). Generally we distinguish between chimneys and pipes after their size. Pipes are usually regarded as small vertical features (diameter <200m) (fig. 2.3), while chimneys are much wider zones (fig. 2.4) (Lüdmann and Wong, 2003, Andresen, 2012).

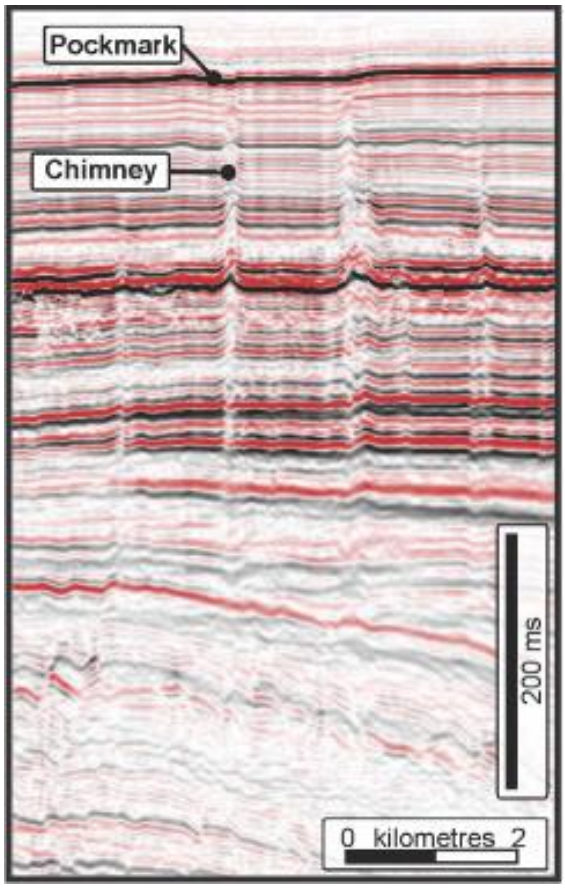

Figure 2.3 Seismic example of several vertical pipes (Cartwright and Santamarina, 2015)

When interpreting seismic, it is important to not confuse small pipes with disturbances and artefacts in the seismic. Seismic artefacts can be related to artefacts caused by migration, scattering artefacts or lateral velocity anomalies (Andresen, 2012).

The internal structure of chimneys and pipes are thought to vary with how they were formed. Some are interpreted to be vertical stacks of pockmarks. Some show more chaotic reflection patterns, interpreted to be highly deformed sediments with small folds and faults (Cartwright, 2007).

Hydrothermal vents is a type of vertical columnar fluid flow feature that are associated with igneous intrusions. They form due to high fluid flux migration often associated with sill complexes and are usually seen at the tip of sills (fig. 2.5) (Cartwright, 2007). In seismic, hydrothermal vents often characterized by a vertical columnar zone with disturbed seismic data, where the reflections often have lowered acoustic reflections. These vents often start at the tip of sill intrusions and terminates in a characteristic upper part seen as a dome or crater feature often described as an eye-shape (fig. 2.5 and fig. 2.6).

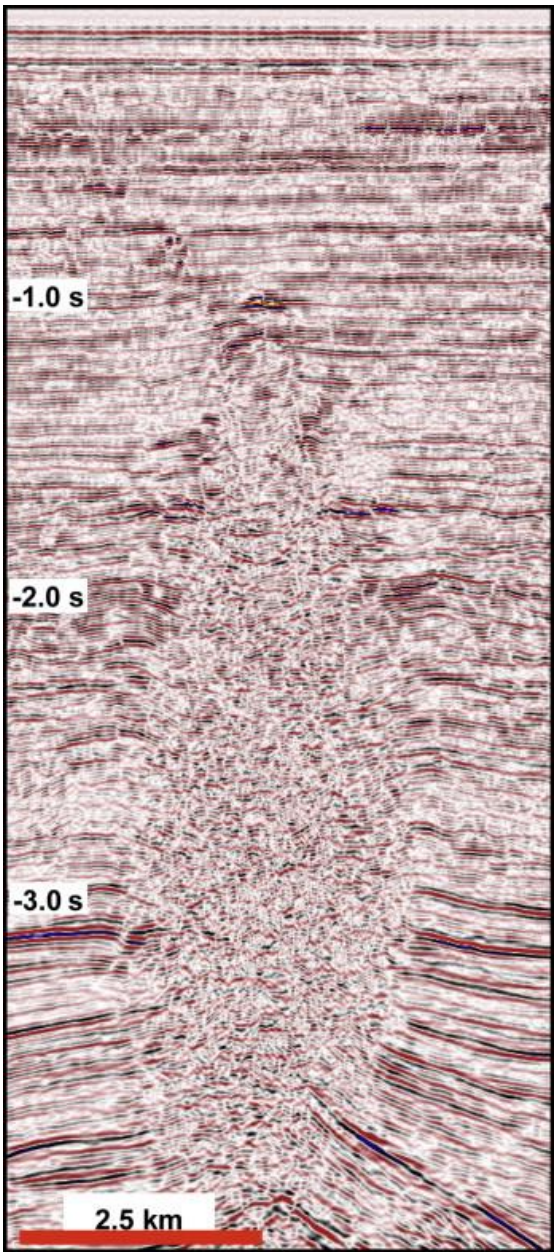

Figure 2.4 Seismic example showing a wipe-out zone which has been interpreted as a chimney feature. (Løseth et al., 2009)

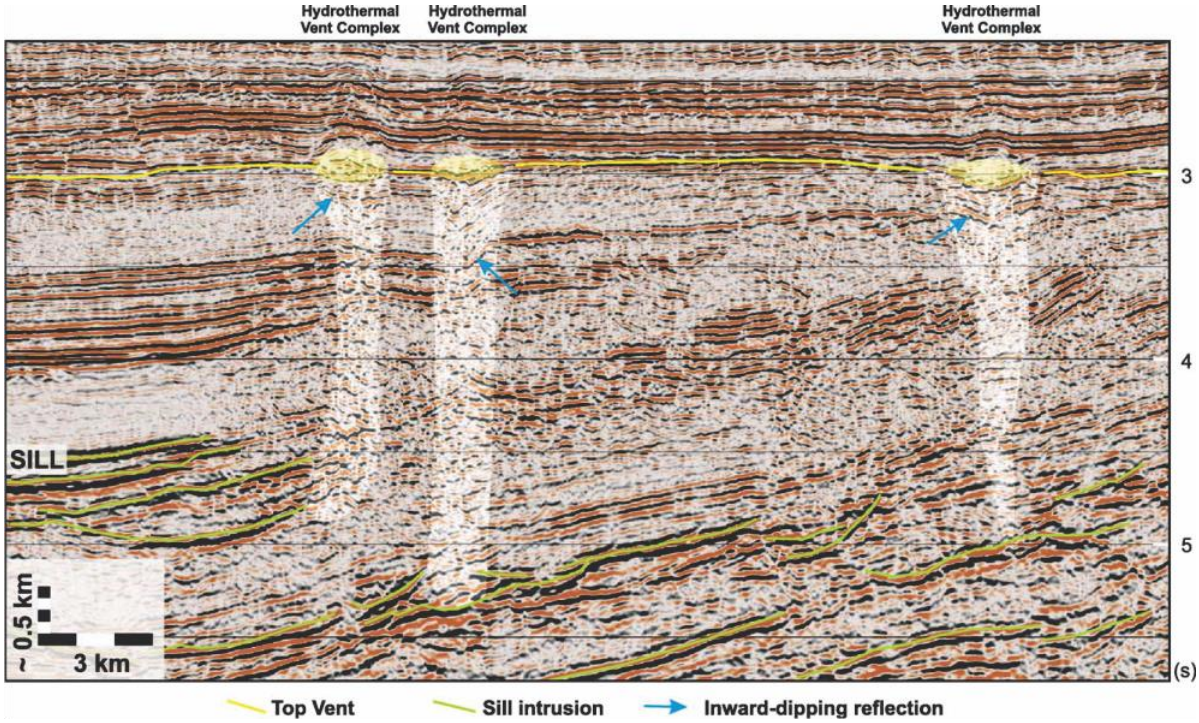

Figure 2.5 Hydrothermal vent complexes as seen in a seismic section. This example is from the Vøring Basin and shows the characteristic features of hydrothermal vents with doming in the upper part. (Planke et al., 2005)

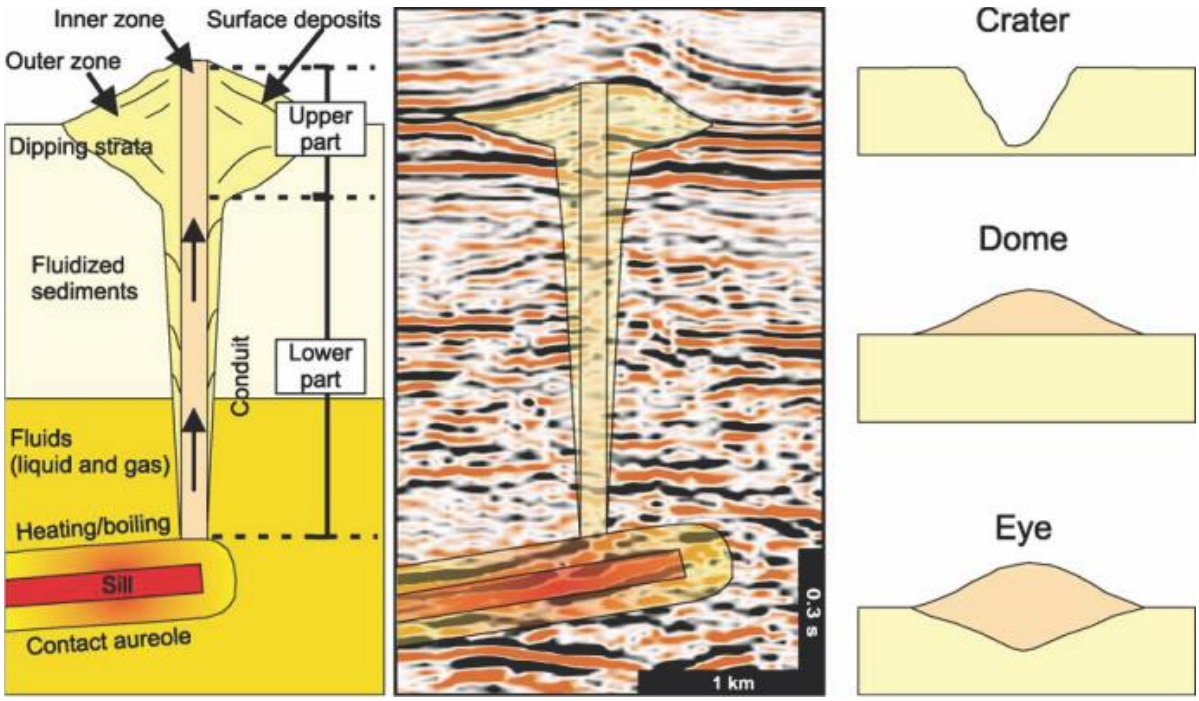

Figure 2.6 Sketch and seismic example of hydrothermal vents with the characteristic upper eye shape and vertical vent from the tip of a sill (Planke et al., 2005).

2.1.2.2 Opal A/CT transition

The Opal A/CT transition is a diagenetic front occurring in the subsurface where there is a transformation from opal A to opal CT during diagenesis (fig. 2.7). The formation of this transition is linked to oxidation of migrating hydrocarbons leading to carbonate cementation where the host rock is usually poorly consolidated sandstone (Løseth et al., 2009). This transition can be seen as a high amplitude reflection often semi-parallel to the seafloor, and can be followed over large distances (Andresen, 2012).

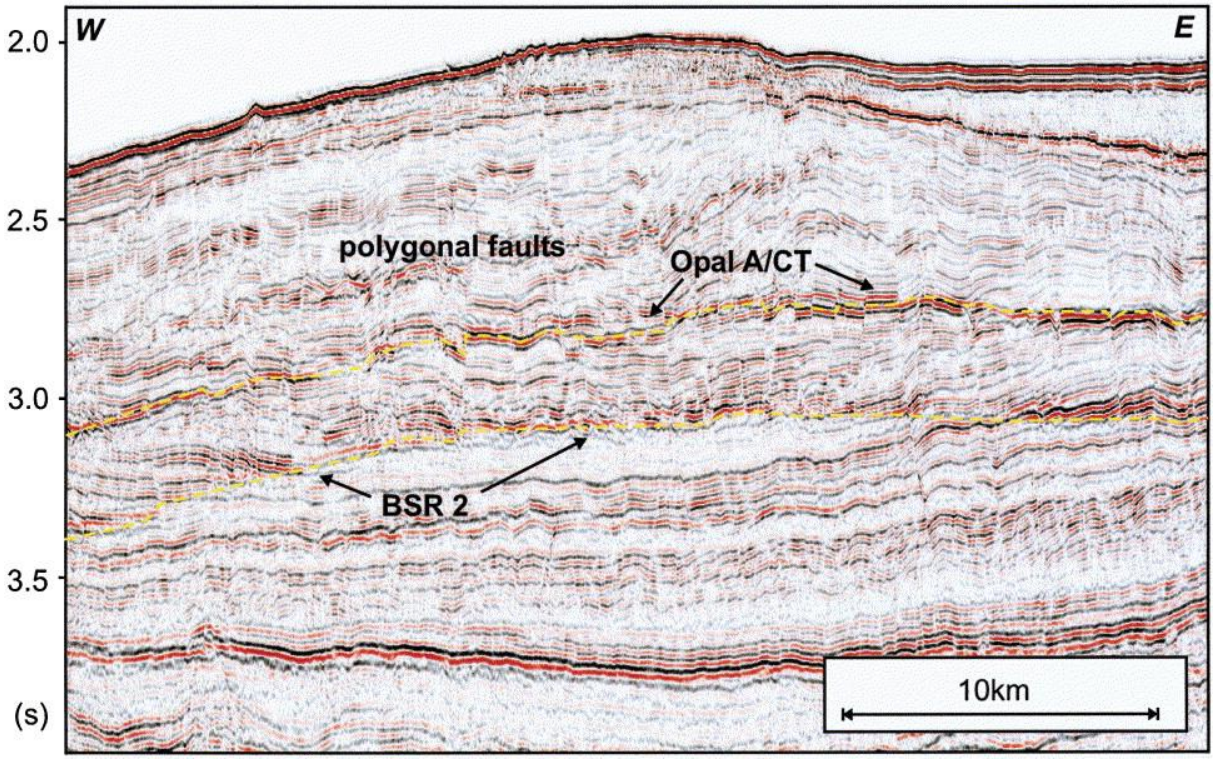

Figure 2.7 Seismic example showing opal A/CT diagenesis from the mid-Norwegian margin (Berndt et al., 2004)

2.1.2.3 Sill intrusions

Volcanic processes and deposits can have a big influence on continental margins and sedimentary basins (Planke et al., 2005). Sills are igneous intrusions that are normally parallel to sedimentary layers, and often close to horizontal when they first intrude the surrounding stratigraphy, and can locally cross-cut the stratigraphy (Planke et al., 2005). Sill complexes can affect sedimentary basins by deformation, uplift, heating of host rock, metamorphism, maturation of petroleum and boiling of host rock fluids (Planke et al., 2005). Boiling of pore fluids in the vicinity of the sill intrusions can cause overpressure and formation of hydrothermal vent complexes (fig. 2.5 and fig.2.6) (Jamtveit et al., 2004).

Sills are recognized in seismic as reflections with high amplitude, local transgression and abrupt terminations, and are often seen with a concave shape (fig. 2.8) (Planke et al., 2005). The Møre and Vøring Basins are volcanic basins linked to the Late Paleocene rifting and continental breakup (Planke et al., 2005). Sill intrusions are therefore very common to find in this area.

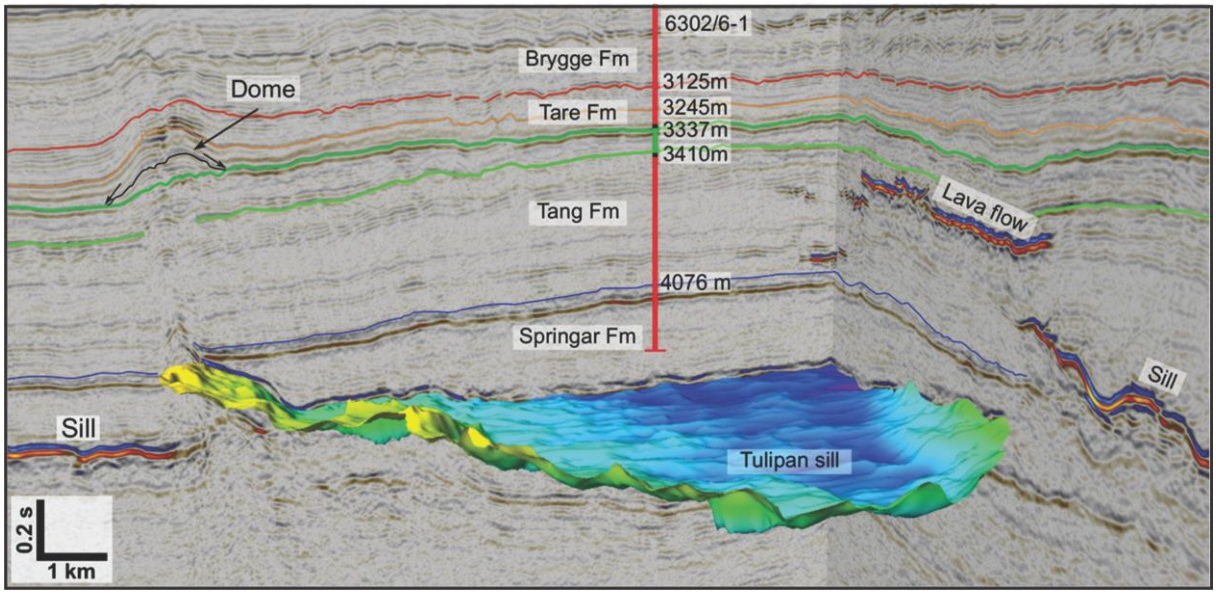

Figure 2.8 Seismic example showing an interpreted sill feature, and two overlying sills (right) in the seismic as well as an hydrothermal vent ending in a dome structure (left) (Kjoberg et al., 2017).

2.1.2.4 Seismic indication of hydrocarbons

Common indicators for gas include bright spots, dim spots, flat spots and polarity reversal (Ligtenberg, 2005) When gas is present in sediments causes a drastic change in the p-wave velocity, affecting the acoustic impedance (Andreassen et al., 2007). This can be seen in the seismic as high amplitude anomalies. As there are several geological phenomena (e.g. sill intrusions, salt, carbonates) that changes the acoustic impedance and are seen as high amplitude anomalies, or bright spots, several hydrocarbon indicators should be seen together in order to interpret the anomalies as hydrocarbon accumulations.

Figure 2.9b shows a geological model with free gas in the sediments. The figure shows that a low velocity within the layer containing gas gives a negative reflection coefficient at the top boundary, and a positive reflection coefficient at the lower boundary (Andreassen et al., 2007).

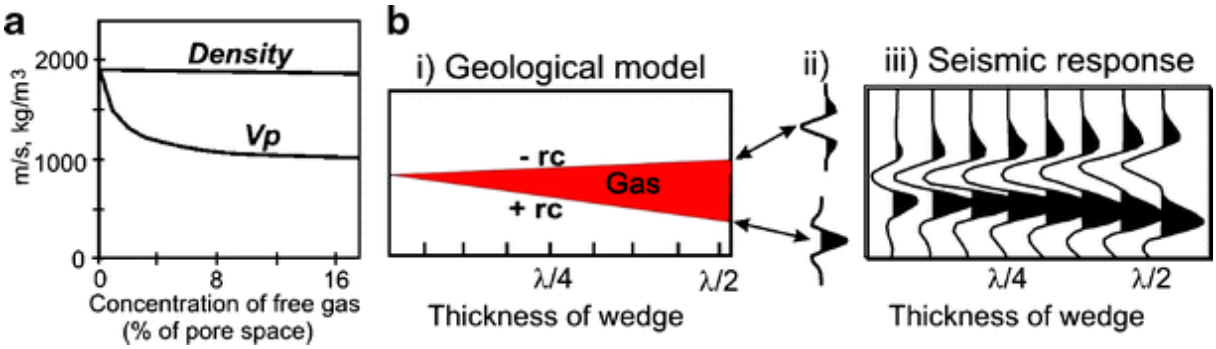

Figure 2.9 A. Graph showing the response of density and p-velocity with presence of free gas in the sediment pore space. B. Geological model of a wedge with gas thinning to the left (Andreassen et al., 2007)

2.2 Mud diapirism

The term mud diapirism is used to describe sediment remobilization structures consisting of material classified by grain size as mud (Brown and Westbrook, 1988, Pérez-Belzuz et al., 1997). Mud diapirism occurs in a number of different tectonic settings, both onshore and offshore. Areas with mud diapirism have been found and studied in accretionary wedges, extensional settings and also in tectonically inactive settings (Pérez-Belzuz et al., 1997). Most of the research on mud diapirism focusses on sedimentary remobilization in accretionary wedges as the compressional setting here is ideal for decreasing pore space and forcing non-compressible fluids to flow and entrain unconsolidated sediment as fluidization velocity is reached (Huuse et al., 2010).

The terms mud diapirs and mud volcanoes can be used in a broad sense, and are sometimes used as synonyms. However, Hjelstuen et al., 1997 described the difference between mud diapirs and mud volcanoes as follows: mud diapirs from when material moves upwards from a source area in a constant flow, while mud volcanoes are sourced from a shallower source and erupt as a series of discrete events. The resulting diapiric features also differs in that mud diapirs the expected morphology is a relatively homogenous plug of mud breccia, while mud volcanoes have distinctive debris flows with some pelagic material (Hjelstuen et al., 1997). The fluid content of the mud can also be a control mechanism when describing diapiric structures. Plastic muds with low fluid content are often associated with mud domes and ridges, while muds with a higher fluid content is associated with mud volcanoes (Brown, 1990).

The driving mechanisms of mud diapirism are still not fully understood, however there is agreement that buoyancy forces due to contrasts in bulk density play a major role. Other important factors are presence of gas in sediments and tectonism (Hovland et al., 1998).

If the migrating fluid is vigorous enough and reaches a critical velocity, which is in part reliant on the particle size to be entrained and called fluidization velocity, then unconsolidated material can be entrained in the flow (water phase). Tectonic compression can also reduce pore space, as can disequilibrium compaction and changes in fluid volume (i.e. through diagenesis, temperature changes). If hydrocarbons are present in the fluid, pressure differentials are elevated, driving flow in the hydrocarbon phase (often occurring after the water phase). Fluid velocity, relative density and particle size are important factors. Viscosity appears to be important in triggering flows with a very heterogeneous distribution of grain sizes (Hjelstuen et al., 1997, Brown, 1990, Hovland and Curzi, 1989).

Once the mud is mobile and starts to migrate upwards, it will often use faults and fractures as pathways (Hjelstuen et al., 1997). The mud diapirs can be completely detached from the original source region. Gas escape structures are often associated with diapiric structures, and can often be seen directly below the features (Lüdmann and Wong, 2003).

Diapirs are recognized in seismic as having an irregular surface and the seismic internal structure is often chaotic and hummocky with low seismic amplitudes (fig. 2.10) (Hjelstuen et al., 1997).

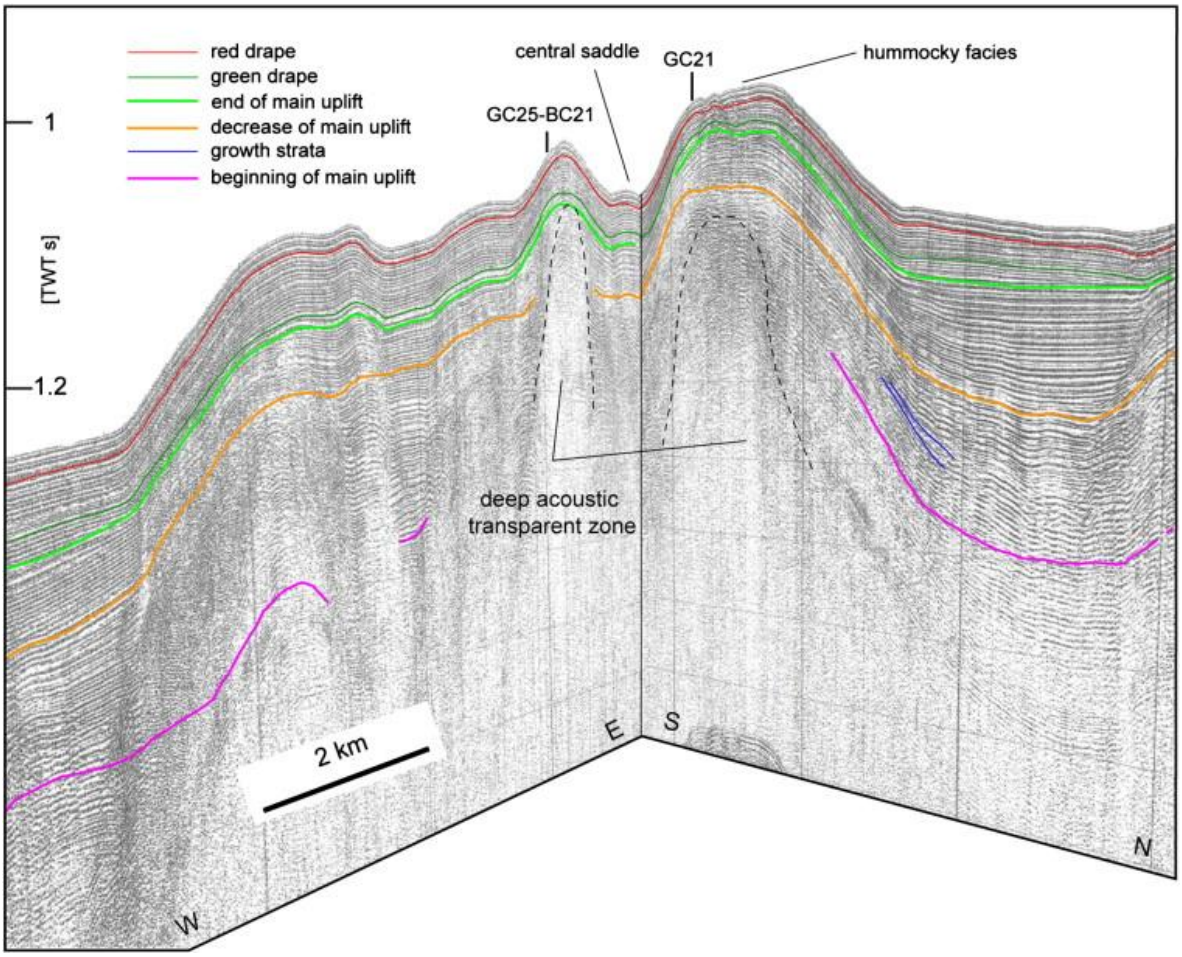

Figure 2.10 Example of a mud diapir from the southern Tyrrhenian Sea (Rovere et al., 2014).

2.3 Faults

A fault is defined as "*a surface or narrow zone in the Earth's crust along which one side has moved relative to the other in a direction parallel to the surface or zone" (Twiss and Moores, 1992).*

Faults are some of the most important pathways for fluid migration. The Norwegian Sea has undergone several stages with tectonic activity, resulting in a complex structural setting. An understanding of faults and their distribution in the study area is necessary in order to understand their importance regarding fluid flow activity and the formation of diapirs.

2.3.1 Faults in relation to fluid flow

Faults act as fluid flow pathways by creating a pressure differential in the subsurface. This differential is utilized by migrating fluids as the 'path of least resistance' (fig. 2.11)

(Gudmundsson, 2001). This implies that the structural fabric and background stress environment is important in determining how fluid will migrate in the subsurface, either by providing fluids with a convenient migration pathway or by trapping fluids (Sibson, 2003). Zones with lowered pressure through faults generally imply an amount of permeability within the fault zone, where the damage core often is characterized as the zone of highest permeability. Rheology plays a role in defining the permeability of the fault zone, however secondary processes as a consequence of fluid flow, such as mineral precipitation, may lower the permeability locally in faults (Sibson, 1996). Fluids may also force re-activation of faulting, or create new fracture networks by shear amount of fluid pressure on the surrounding rock. In the case of hydrothermal systems, it has been shown, especially in compressive environments, that fluids are more likely to utilize small offset fracture networks for flow rather than large offset major faults, especially when the tectonic environment dictates that a fault is 'sealed' (Sibson, 2003).

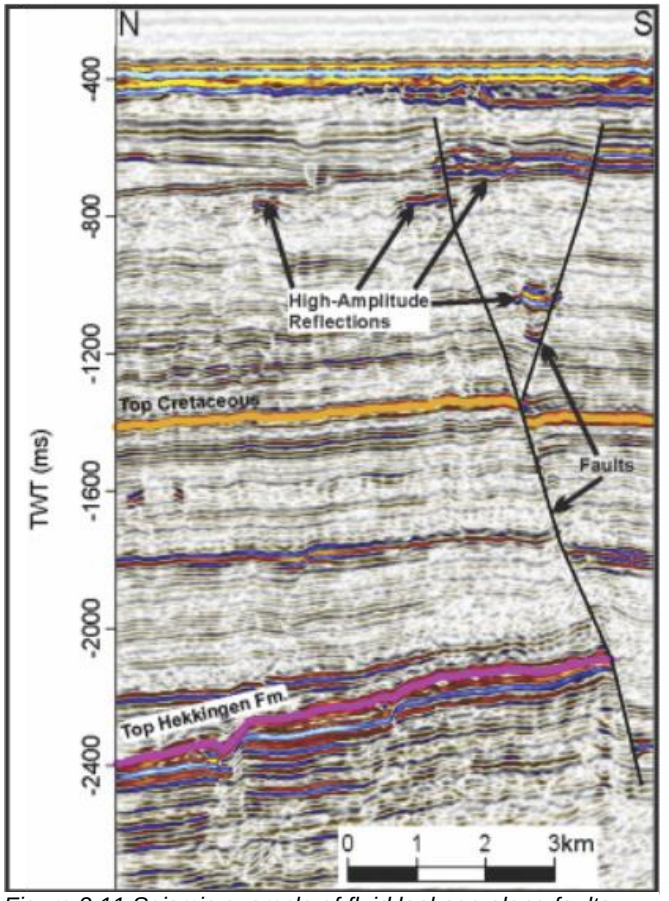

Figure 2.11 Seismic example of fluid leakage along faults. The high amplitude anomalies along the two faults, indicates migration and accumulation of gas (Vadakkepuliyambatta et al., 2013)

A fault zone can be divided into two separate parts with different permeabilities, the core and a surrounding damage zone (Gudmundsson, 2000). The core is where the main fault slip occurs. The core usually has a low permeability during periods of low seismic activity due to breccia and cataclasis. The damage zone however, has a lot of faults and fractures, giving a much higher permeability (Gudmundsson, 2000). As mentioned, faults can either act as a migration pathway, or can trap fluids (Gudmundsson, 2001). In order for a fault zone to work as a migration pathway, the permeability in the fault zone must be greater than the surrounding rock.

Since fault behaviour changes with time, whether they act as migration pathways or as traps can also change with time (Gudmundsson, 2001). The breccia associated with the core of the fault reduces permeability and limits fluid migration, but the amount of breccia present varies and are not found everywhere in the core. This means that the fault zones can also act as pathways and a barrier for fluid flow in different parts of the system, and not just vary with time (Gudmundsson, 2001).

2.3.2 Polygonal faults

Polygonal faults are a type of fault system not related to tectonics, and often occur within fine-grained deposits in sedimentary basins (Berndt et al., 2003). It is important to have an understanding of polygonal fault systems as they can be a controlling factor of fluid migration on a regional scale (Berndt et al., 2003)

Cartwright et al. (1998) show seismic data from 28 sites with layer bound faults. By using a system of polygonal faults in the lower Tertiary interval in the North Sea Basin, present seven criteria for polygonal faults that should be identifiable in seismic data, where the first six are restricted to 3D seismic data (fig. 2.12) (Cartwright and Dewhurst, 1998):

1. Polygonal faults are identifiable in map view, and can be seen as a hexagon fault pattern.
2. Polygonal faults have a limit of vertical extent. They are bound to specific layers, and are found in stratigraphic units that can be correlated on a regionally scale.
3. They also have a specific areal extent, and are often found over large parts of a basin.
4. Polygonal fault systems are normal faults, with small vertical throws, normally 10-100 m.
5. The faults are found with 100-1000 m spacing from each other.
6. The sections affected by the polygonal faults may be subdivided into two or more tiers.
7. The last criteria, which also is possible to see in 2D seismic data is that the faults can switch from synthetic to antithetic in fault polarity.

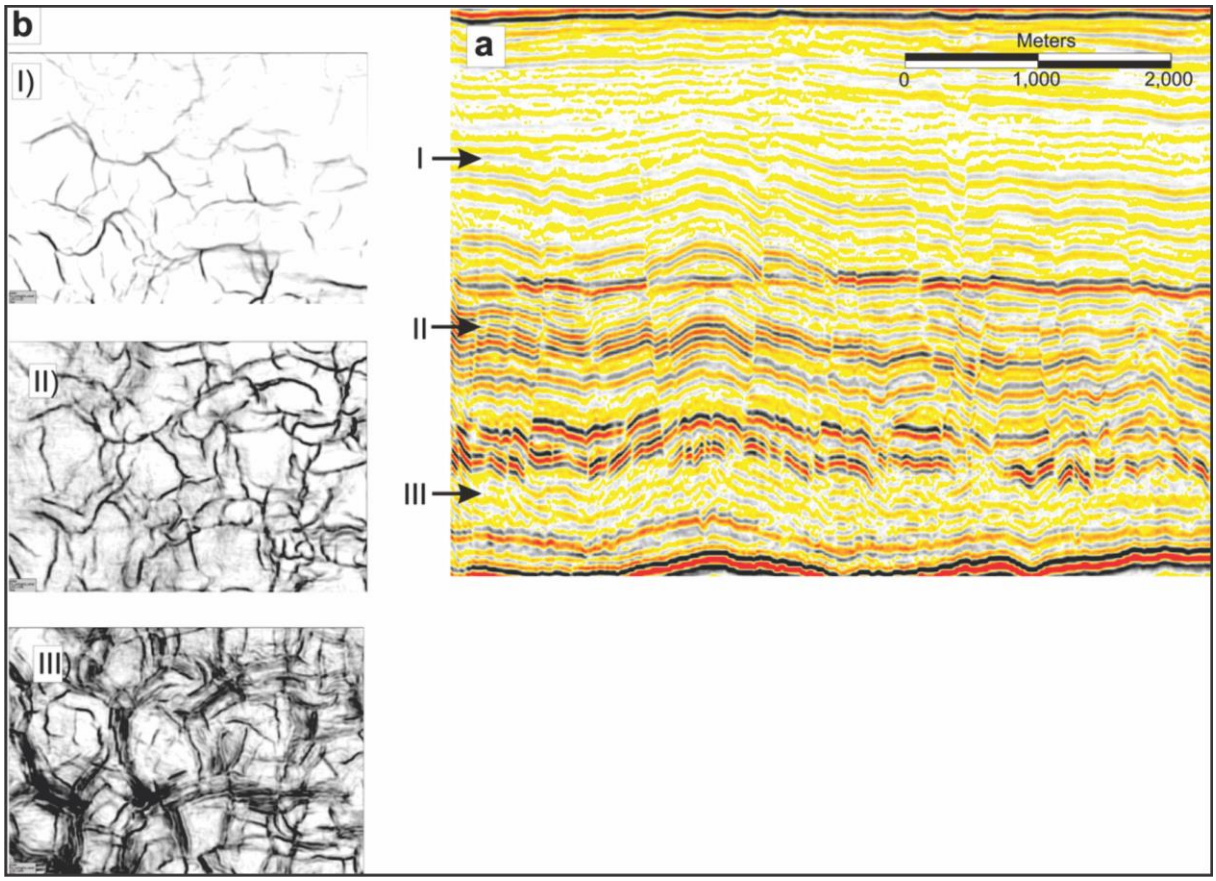

Figure 2.12 A. Polygonal faults shown in a seismic profile. The arrows indicate the position of coherent maps in figure b. B. Coherence timeslices though the polygonal faults. Their positions are marked in figure a (Cartwright, 2011)

Polygonal faults are found in material with an ultrafine grain size and very low permeability, such as biogenic oozes, mudstones, clays and claystones (Cartwright and Dewhurst, 1998). Since they are only found in these materials, the grain size should therefore play a role in the formation mechanism (Cartwright and Dewhurst, 1998). The formation mechanism of polygonal faulting, is still debated and several mechanisms have been proposed, some of them being syneresis, thermal and chemical contraction due to diagenesis, and density inversion (Cartwright, 2011, Dewhurst et al., 1999, Cartwright and Dewhurst, 1998). Syneresis is when a material acting in a gelatinous way contracts and pore fluid is expelled (Cartwright and Dewhurst, 1998). Syneresis is considered to give the best explanation of formation of polygonal faults because it take into account the volumetric strain observed in fault offsets. Syneresis can also explain why polygonal faults are only found in very fine grained sediments (Cartwright et al., 2003)

3 Study area

The Vøring Plateau is a large flat area on the Norwegian Continental Margin, which can be divided into the Vøring Marginal High to the west and Vøring Basin to the east. It is located between ~65-68 °N and ~2-10 °E, at water depths of 100-1500 m (Hovland et al., 1998). The main focus area in this study is the Vema dome (fig. 3.1), which is located in the north-western part of the Vøring basin. The Vema Dome itself is a structural high, which has undergone multiple phases of tectonic events, and is buried at Oligocene level. The Vøring Basin is part of a larger series of basins and platforms which make up the Mid-Norwegian Continental Shelf (Faleide et al., 2008), an area which has been well studied due to its hydrocarbon potential (Blystad, 1995).

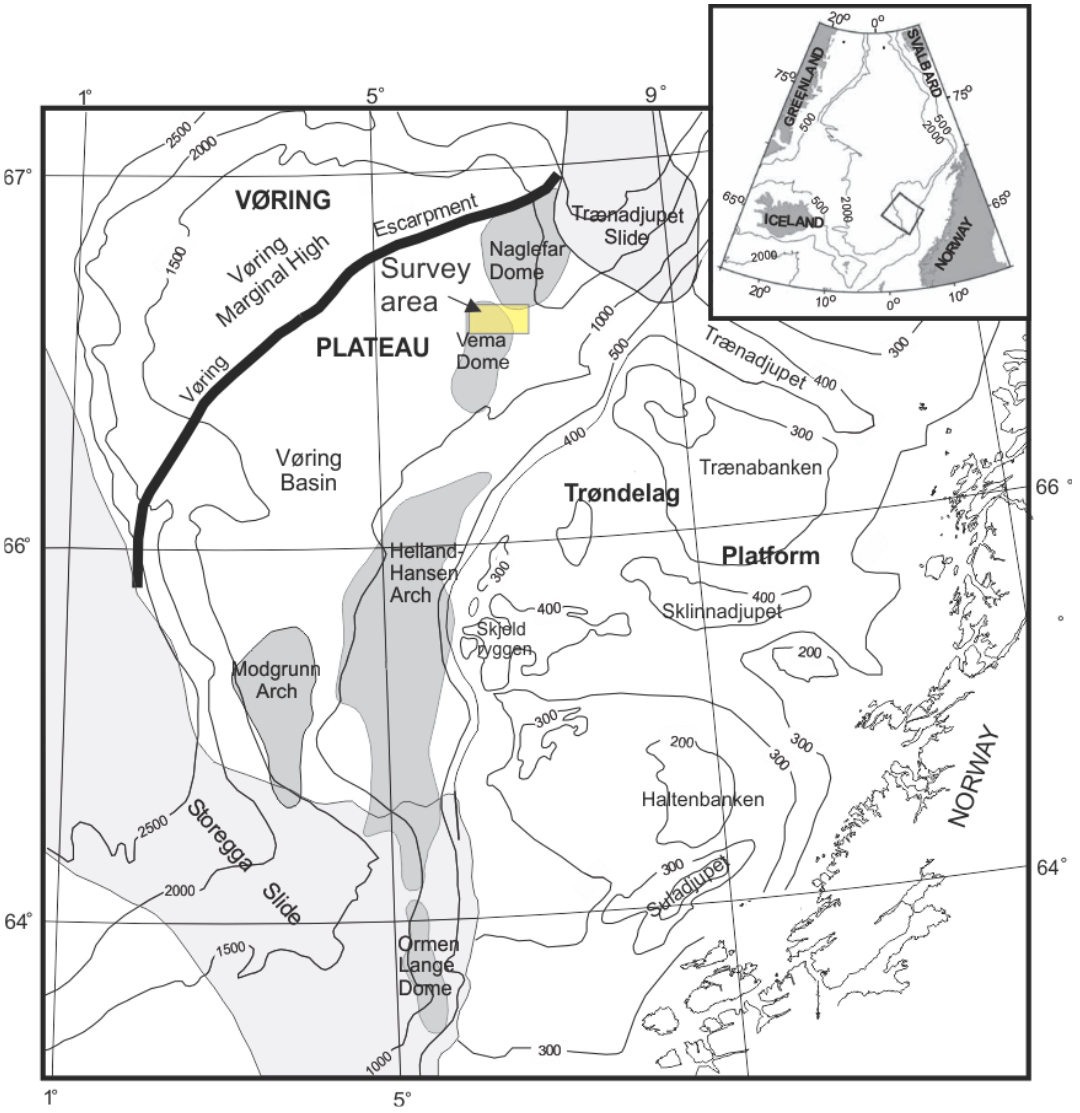

Figure 3.1 Map over the mid-Norwegian margin where the study area over the Vema Dome is marked with a yellow square (Hjelstuen et al., 2004b).

3.1 Tectonic development of the Vøring Basin

Since the late Ordovician (~485-443 Ma) times, the tectonic development of the Vøring Basin can be summarized into six major events.

The Caledonian Orogeny occurred as the Laurentian and Fennoscandian Margins collided and closed the Iapetus Ocean (Skogseid et al., 1992). During this mountain building phase the study area was in a compressional tectonic regime, and was characterized by regional lithospheric thickening and thrust fault development (Bukovics and Ziegler, 1985). During the Devonian (~419-358 Ma), the lithosphere was unbalanced due to the thickening in the late Ordovician which resulted in large-scale gravitational collapse and crustal thinning. Extension mainly occurred via reactivation of Caledonian Orogeny thrust faults, forming half graben structures along the Vøring Basin (Bukovics and Ziegler, 1985). After this phase of gravitational collapse and lithospheric readjustment, several episodes of extension, and/or regional rifting have been documented. Late Carboniferous-early Permian (~307-290 Ma) is characterized by both basement involved faulting and regional rifting, mid/late Triassic (~227-208 Ma) is characterized by basement-involved faulting and finally in the late Triassic-early Jurassic (~208-190 Ma) the faulting regime developed into growth faulting, where basement faulting nucleates the onset of faulting in sedimentary strata above (Hardy and McClay, 1999).

The forth major tectonic event occurred in the late Jurassic to Early Cretaceous (~157-139 Ma), where subsidence began along reactivated fault blocks of the Mid-Norwegian Margin (Bukovics and Ziegler, 1985). Although the timing of this subsidence, which created the Vøring Basin has been debated, the Vøring Basin either developed in the later stage of this episode or subsided faster. Rifting between Greenland and Eurasia along the North Atlantic Ridge in the Paleocene-Eocene (~66-33 Ma) caused listric fautling in the Vøring Basin, along with major uplift and wide spread magmatic intrusions (Bukovics and Ziegler, 1985). The last major tectonic event occurred in the Neogene (~23-2.5 Ma) where regional uplift and erosion produced large amounts of sediment that was transported and deposited in the Vøring Basin, extending the continental shelf to its current position (Bukovics and Ziegler, 1985).

The Vema Dome specifically was formed during the Paleocene-Eocene rifting event. This event created a series of rotated fault blocks and graben structures. However, on the Vema Dome, the orientation of existing rift-related terrain forced the local faulting trend to an E-W orientation instead of the regional NW-SE axis of stress (Hovland et al., 1998). Locally the Vema Dome

was uplifted during this event. In the Oligocene and Miocene (~33-5 Ma) the North Atlantic Rift System created a regime of intraplate compression in the area of the Vema Dome. In the late Miocene (~11-5 Ma), minor reactivation events resulted in continued doming, and since then the Vema Dome has been steadily subsiding (Hovland et al., 1998).

3.2 Stratigraphy of the Vøring Basin

The sedimentary history of the Vøring Basin is largely a consequence of the tectonic development of the region. During periods of uplift and erosion around the Vøring Basin, large volumes of sediment were deposited to create the modern day shelf. During periods of subsidence, the accommodation space for sediment deposition was increased. However, while deep wells further into the continental shelf have given knowledge of the stratigraphy present in some areas of the Mid-Continental Margin, on the Vema Dome itself and in the Vøring Margin in general, much of the stratigraphy has relied on correlation of seismic data. Following rifting and subsidence of the Paleocene-Eocene rifting events, large amounts of material have been deposited in the Vøring Basin, with the base Cenozoic as one of the earliest stratigraphic horizons in the basin (Hansen et al., 2005).

There are three major stratigraphic groups on the Vøring Bain, which can further be divided into formations and reflections of known age. The major groups are the Rogaland group (Deegan and Scull, 1977, Dalland et al., 1988) of Palaeocene age, the Hordaland group (Deegan and Scull, 1977, Dalland et al., 1988) which is of Eocene-Lower Miocene age, and the Nordland group (Deegan and Scull, 1977) of lower Miocene to recent age (table 3.1). Figure 3.2 shows a lithostratigraphic chart over the Norwegian Sea.

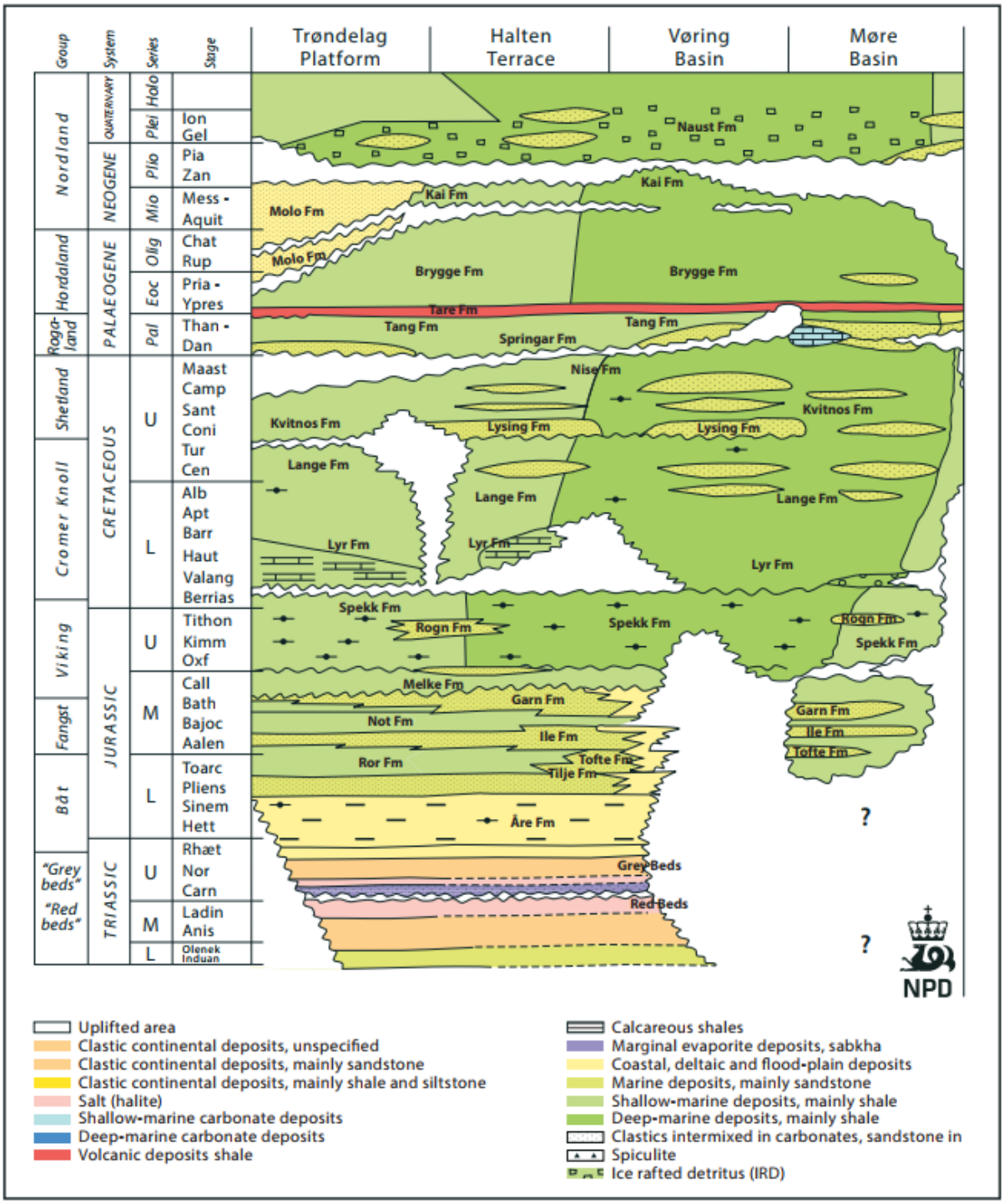

Figure 3.2 Lithostratigraphic chart of the Norwegian Sea. From the Norwegian petroleum directorate (NPD).

On the Vema Dome, published well data (Ren et al., 2003) suggests that sedimentation consists largely of silty shales and sandstone from the upper cretaceous to recent, however recovery appears to be sparse. The major hydrocarbon reservoir in the area appears to be the Cretaceous rotated fault blocks which are believed to be of deep marine sediments (Hovland et al., 1998). The Vema Dome Brygge Formation appears to correlate to the same material found in other

locations in the Vøring Basin. The Kai formation onlaps the flanks of the Vema Dome while the Naust Formation is above the structural delineament of the Vema Dome (Hovland et al., 1998). Table 3.1 shows the identified Cenozoic sequences on the Norwegian continental margin with a description of their characteristic seismic facies and lithologies (Hjelstuen et al., 2004a).

Table 3.1 Table of identified sequences, seismic facies characteristics and lithologies from (Hjelstuen et al., 2004a)

Sequence boundary *(reflector name)*	Formation (Dalland et al., 1988)	Seismic pattern	Lithology
	Naust	High amplitude reflectors separating sub-sequences of non-structurally, weakly layered and chaotic seismic facies. Well-stratified seismic units deposited outside the prograding wedge on the Vøring margin	Diamicton, hemipelagic/ glacimarine sediments, till
Base Late Pliocene (BP)			
	Kai	Parallel medium amplitude reflectors. Small-offset faults.	Siliceous ooze
Lower Miocene (LM)			
		Parallel low to medium amplitude reflectors. Small-offset faults.	Clay
Intra Oligocene (IO)	Brygge	Chaotic/non-structural to weakly layered	
Middle Oligocene (MO)			
		Band of parallel, non-faulted, high amplitude reflectors characterise the upper unit. An acoustic non-structural seismic pattern dominate the lower unit.	Clay
Top Paleocene (TP)			

3.2.1 Hordaland group

The Hordaland group consists of the Brygge Formation, deposited from Early Eocene to Early Miocene (~55-18 Ma) (Rise et al., 2010). The Brygge Formation is widely distributed on the mid-Norwegian continental margin, with the thickest accumulation found in the Møre and Vøring basins with sediment thickness approximately 500-700 m in the Vøring basin (Rise et al., 2010, Eidvin et al., 2007). In the Møre and Vøring basins the formation mainly consists of ooze, deeper marine sediments, while the present day shelf is dominated by clay (Eidvin et al., 2007). Small-scale polygonal faults have been identified within the ooze sediments (Eidvin et al., 2007). Remobilization of sediments are also identified within the Brygge formation, one of these processes being the diapirism seen around the Vema Dome (Eidvin et al., 2007).

3.2.2 Nordland group

The Nordland group is subdivided into the Kai formation (Lower Miocene-Upper Pliocene) and the Naust formation (Upper Pliocene). These subdivisions consists of claystone, however also contain sandstones in the Kai formation and sandstones interbedded with limestones in the

Naust formation (Hansen et al., 2005). The Naust formation is largely the product of large debris flows, with much glacigenic input (Henriksen and Vorren, 1996).

3.2.2.1 Kai Formation

The Kai Formation consists of mainly biogenic ooze, deeper marine sediments (Rise et al., 2010). Kai has been correlated to the Molo formation found on the Trøndelag Platform, consisting of more sand deposits indicating a shallower, coastal environment (Rise et al., 2010). The Kai formation can be found on top of the "mid Miocene unconformity" which has been related to a regional uplift during Mid-Miocene times (Eidvin et al., 2007). In the Vøring Basin the sediments of the Kai formation is classified as clay with ooze. The same polygonal faults found in the Brygge formation can also be seen in Kai (Eidvin et al., 2007).

3.2.2.2 Naust formation

Naust is the youngest formation and was deposited during late Pliocne-Pleistocene (last ~2.8 Ma) (Rise et al., 2010). The sedimentation rate largely increased during this time with a mean sedimentation rate of ~25 cm per 1000 years due to regional uplift, and 'onset of major glaciations in Scandiavia' (Rise et al., 2010). Due to the increase in sedimentation rates, more than 1000 m thick sequences of the Naust formation has been found on the outer shelf and upper slope. The formation is subdivided into five depositional sequences, N being the oldest, A, U, S and T being the youngest (Rise et al., 2010).

Naust is characterized with sediment wedges which thins westward and downlaps onto the underlying Kai Formation (Rise et al., 2010).

The sediments was either deposited in a glacimaine environment or are redistributed glacial deposits from gravitational processes as mass movement and glacial debris flows (Rise et al., 2010).

3.3 Prior research of fluid flow features in the Vøring Basin/Norwegian continental margin

The Mid-Norwegian continental margin is a well explored area due to hydrocarbon exploration. As the Mid-Norwegian margin is a volcanic rifted margin, it is characterized by large basalt complexes, including sills and dykes (Kjoberg et al., 2017). Large systems of hydrothermal vents are associated with the sill complexes, often terminating in features associated with fluid flow and sediment mobilization such as pockmarks and mound features (Kjoberg et al., 2017).

In the Vøring basin, three diapir fields has been identified, the Vema diapir field, the Vigrid diapir field and Vivian diapir field. Table 3.2 shows an overview of the studies of fluid flow features mostly concentrated in the Vøring basin focusing on mounded structures related to fluid flow and mud mobilization. Kjoberg et al., (2017) article on sill intrusions and hydrothermal vent complexes in the Møre basin has been included here as it is relatable to the study in the Vøring basin.

Table 3.2 Overview of important papers on fluid flow features in the Vøring basin.

Authors	**Area (basin)**	**Area specified**	**Features**
Hovland et al., (1998)	Vøring basin	Vema dome	Mud diapirs
Hjelstuen et al., (1997)	Vøring basin	Vigrid syncline	Mud diapirs
Hansen et al., (2005)	Vøring basin	Gjallar Ridge	Mounded structures related to fluid flow and mud mobilization
Planke et al., (2005)	Møre and Vøring basins		Volcanic intrusions and hydrothermal complexes
Kjoberg et al., (2017)	Møre basin		Sill intrusions and hydrothermal vent complexes

Hovland et al., (1998) studied the diapiric structures over the Vema dome to determine why diapirs have formed on the Vema dome, yet not over Nyk High (east of the dome) even though the deposited sediments in the two areas are very similar (Hovland et al., 1998). The study concluded that that there are at least three factors involved as trigger mechanisms; buoyancy forces due to sediments of low density and high porosity buried, the Vema dome itself and migration of light hydrocarbons through faults and fractures. They also mention that tectonic instability can also be a trigger mechanism (Hovland et al., 1998).

Hjelstuen et al., (1997) agree with Hovland et al., (1998), but do not come up with a complete explanation as to how the diapirs are formed. They suggest that the mobilization of mud started in late Pliocene by buoyancy forces, and that gas chimneys act as conduits for the migrating mud (Hjelstuen et al., 1997).

Planke et al., (2005) mapped volcanic intrusions and hydrothermal vent complexes in the Møre and Vøring basins. They concluded that the hydrothermal vents was formed by eruptions of gas, liquids and sediments due to the emplacement of sill complexes, and that these vents have then acted as fluid migration pathways (Planke et al., 2005).

4 Data and Methods

High quality 3D seismic has led to improvements in surface imaging regarding fluid flow processes over 2D seismic grids. By using line spacing of ~25 m instead of the few kilometres typical of 2D grids, increased spatial resolution and image quality make it possible to image smaller features that are not visible in 2D (Cartwright, 2007).

4.1 Datasets

This study is based on two 3D seismic data sets, BPN9601 and ST9603R99 located over the Vema dome and on the eastern flank of the dome (fig. 4.1). The two surveys are located approximately 3 km from each other. Two wells within the survey area was also provided for correlation of the stratigraphy. From here and through the rest of the thesis vertical distances in the seismic marked as ms, milliseconds two-way-travel time unless stated otherwise.

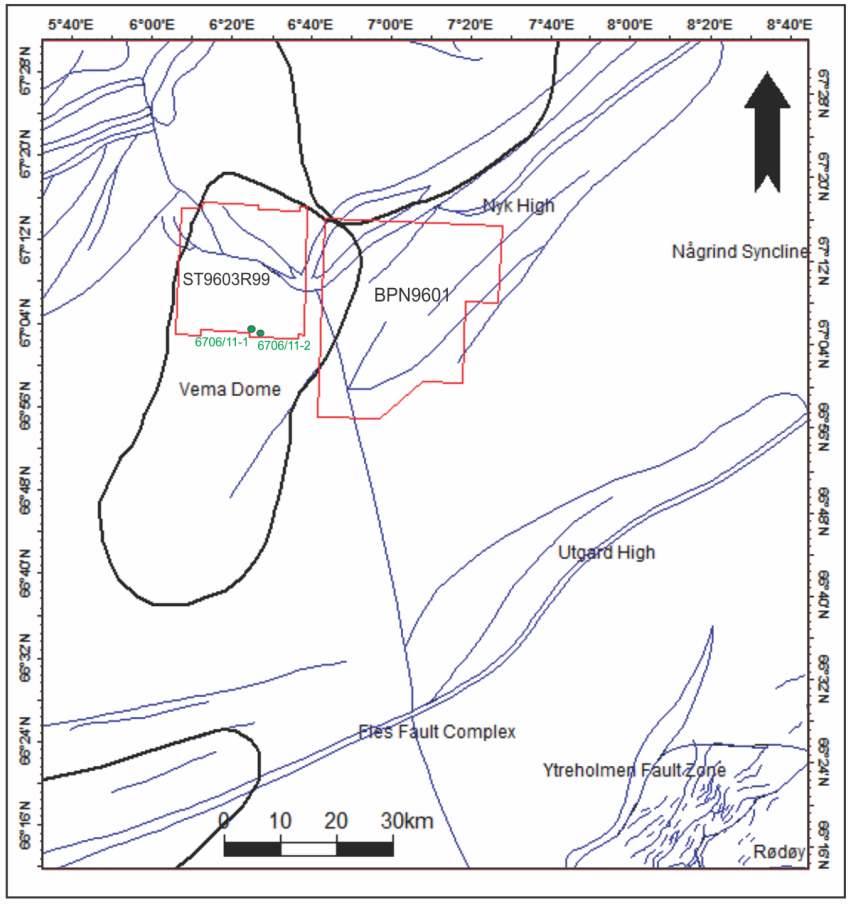

Figure 4.1 Overview of study area showing the location of the 3D seismic surveys (red polygons) and the wells (green circles). The blue lines shows the main structural elements in the Vøring basin, and the black outlines shows dome structures.

Survey BPN9601 was acquired in April and May 1996, and is owned by BP Norge. It was processed by CGG Norge (Oslo Processing Centre). When collecting the data, two airguns was used with a capacity of 2620 CU inch. The gun was towed at a water-depth of 6 m and the streamers at 8 m. Six streamers was used, each with a length of 3900 m. The recording length was 7 seconds, with a shot interval of 25m.

3D dataset ST9603R99 is owned by Statoil, and has been processed by CGG Norge, Oslo Processing Centre in 1999. The distance between the inlines were 18.75 m, and 12.5 m between the crosslines. The sample interval was 4ms. The ASCII header in petrel do not give any additional information about this 3D dataset.

Both datasets have been processed to a zero-phase polarity, which means that the reflectors have a normal European polarity (SEG). With a zero-phase polarity, a black peak represents a positive reflection coefficient. A zero-phase pulse is only theoretical as the reflection boundary is in the center of the peak. Showing reflections with this type of polarity is beneficial because the signal is shorter and has a greater amplitude compared to a signal with minimum-phase, giving a better signal-to-noise ratio (Yilmaz, 2001). Figure 4.2 shows a seismic section from the dataset BPN9301 showing zero-phase wavelets.

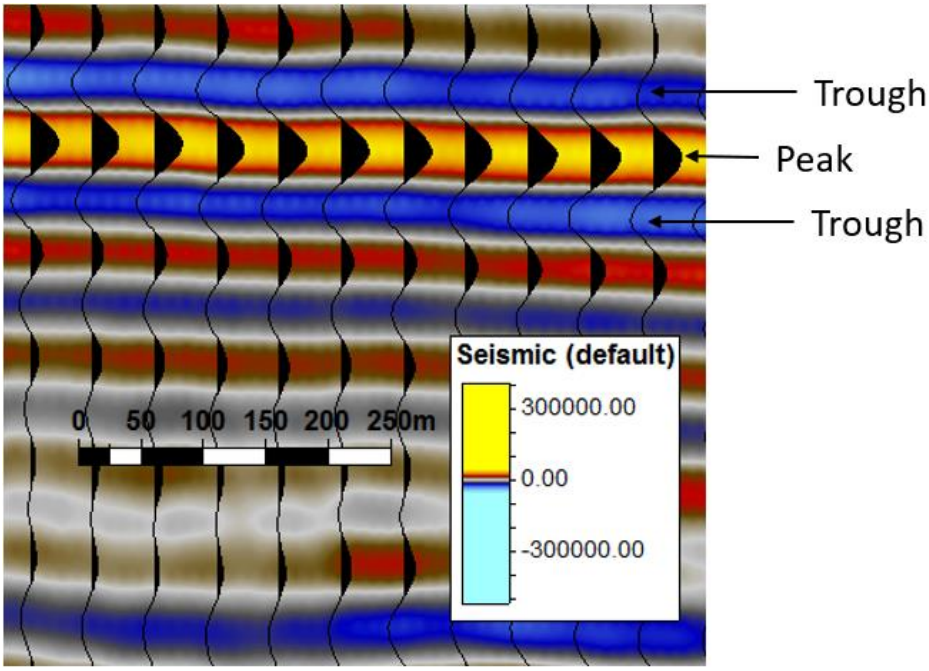

Figure 4.2 Seismic section from the survey BPN9601 showing a zero-phase polarity (SEG standard polarity).

4.1.1 Artefacts in the datasets

It is normal that there are some artefacts in seismic datasets. These can be due to coherent noise from the ship (e.g. ship motor and other instruments acting simultaneously), static artefacts such as two-way travel time changes between the source and receiver over the course of the survey or entering the dataset during the data processing workflow (such as migration artefacts). Static artefacts, relating to small changes in the two way travel time from source to receiver occur due to either; 1) a change in source depth over the survey 2) a change in receiver depth over the survey or 3) a combination of both. This is often due to tidal effects where a very small change in water depth can create an observable artefact and can therefore be seen in the same direction as the survey direction (inlines). It is important to be aware of these "footprints" as they otherwise can be misinterpreted as actual features (fig. 4.3) (Bulat, 2005).

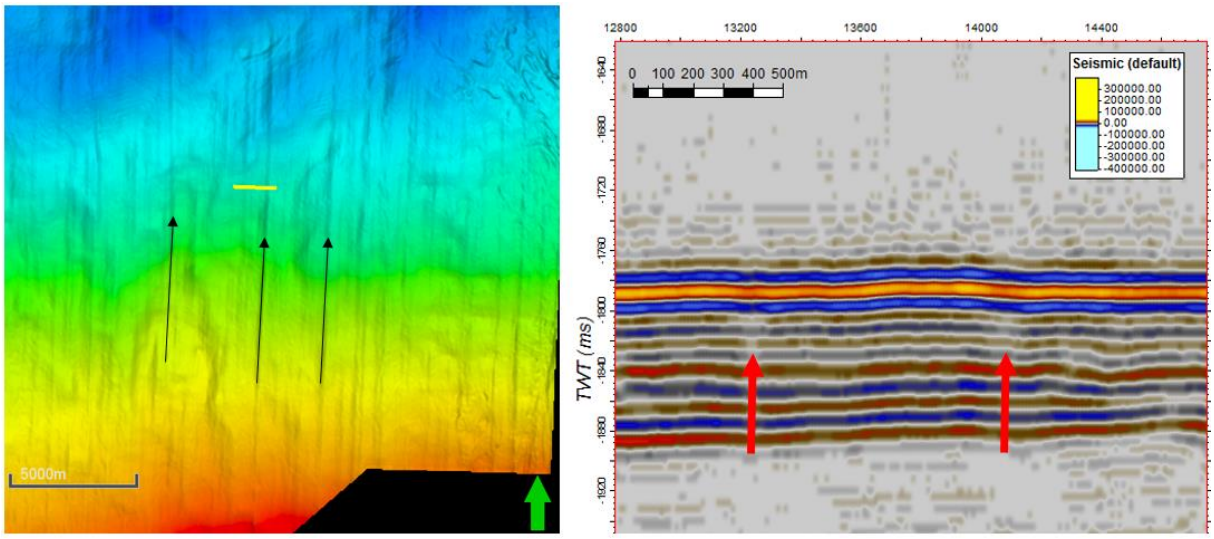

Figure 4.3 Survey footprints on the seafloor of the 3D survey BPN9601 (left). The artefacts are marked with black arrows. On the right, you can see the artefacts in a vertical cross section (marked with yellow on the figure to the right). Here the artefacts are marked with red arrows.

4.1.2 Well data

Data from wells 6706/11-1 and 6706/11-2 (fig. 4.1) was used to establish the seismic stratigraphy in the study area.

Tests from well 6706/11-1 showed that the Brygge Formation mainly consists of sediment ooze with a bulk density of 1.4 g/cm^3, e.g. very low density. There was not found significant amounts of gas in this well, and it was therefore abandoned (Npd Fact pages 2018). Well 6706/11-2 was drilled by Statoil in 2015 with the main goal of proving the presence of petroleum in the Late Cretaceous Nise Formation. A gas column of ~69m was found in the Nise Formation with the

top of the reservoir at 2375 m. The well was abandoned on 6th June 2015 as a gas discovery (npd fact pages 2018).

4.2 Seismic resolution

Resolution in seismic is defined as how close together features can be for them to be recognized as individual features. Resolution is usually separated into vertical and horizontal resolution (Yilmaz, 2001).

Wavelengths decrease with depth due to spherical divergence, absorption of energy, amplitude decrease caused by reflection-, refraction and scattering of energy, causing the resolution to decrease with depth. Due to an increase of density with depth, the velocity of rocks also usually increases with depth (Yilmaz, 2001).

During a seismic survey, the depth of the features of interest need to be taken into account, as this affects the choice of source, survey geometry and sampling rates. In a seismic survey, when the goal is to look into for example a sedimentary basin, which can have depths of 3-6 km, it is normal to use a source that generates frequencies between 30-50Hz. Higher frequencies than this will be absorbed by the earth (Bulat, 2005). So as a general rule, higher frequencies usually gives better resolution, but little penetration, and lower frequencies give lower resolution, but better penetration.

4.2.1 Vertical resolution

Vertical resolution is a measure of how thin a layer can be in order to be seen as a separate layer in a seismic profile. This limit is a function of the Nyquist frequency given by one-quarter of a wavelength of the dominant wavelength (Bulat, 2005) (Equation 4 and 5).

$$Wavelength = \lambda = \frac{v}{f} \qquad Equation\ 4$$

$$Vertical\ resolution = \frac{\lambda}{4} \qquad Equation\ 5$$

If the thickness of a layer is less than one quarter of the wavelength, the top and base will start to merge into one waveform, and the layer will not be visible in a seismic profile (Bulat, 2005)

The velocity of a seismic wave usually lies between 2000 and 5000 m/s in the subsurface (~1500m/s in the water column) and generally increases with depth (Yilmaz, 2001). The dominant frequency of a seismic signal decreases with depth and is usually 20-50 Hz. From the equation for dominant wavelength it shows that the wavelength also increases with depth. Because of this, layers or features that are deeper down in the subsurface, must be thicker than shallower ones in order to be resolvable (Yilmaz, 2001)

4.2.2 Horizontal resolution

As with vertical resolution, horizontal resolution defines how close two points can be horizontally to be seen as separate points (Yilmaz, 2001). Horizontal resolution on unmigrated sections is usually defined as the size first Fresnel zone. Seismic waves emitted from a source will hit an area, and not a single point. The area where most of the energy reflected back that has arrival times with less than half a period from the first break is known as the first Fresnel zone (Sheriff, 1985). The size of the first Fresnel zone, and therefore also the horizontal resolution is given by equation 6.

$$rf = \frac{v}{2}\sqrt{\frac{t}{f}} \qquad Equation\ 6$$

Where rf= Radius of the Fresnel zone (m), v = velocity (m/s), t = TWT (s) and f = dominant frequency (Hz).

It resolution is better the smaller the radius of the Fresnel zone (Yilmaz, 2001). By migrating 2D and 3D seismic, the Fresnel zone can be collapsed, focusing the energy, and thus better the resolution (Bulat, 2005).

4.3 Seismic interpretation

Frequency spectrum analysis extracted from the seismic, shows that the bandwidth filtering lies between 6-10 Hz as a lower boundary and approximately 80 Hz for the upper boundary in survey ST9603R99. The dominant frequency peaks at approximately 30Hz (fig. 4.4). Frequency spectrum analysis from survey BPN9601 shows a bandwidth filtering with a lower boundary of 6-10 Hz and an upper boundary of approximately 70 Hz (fig. 4.5).

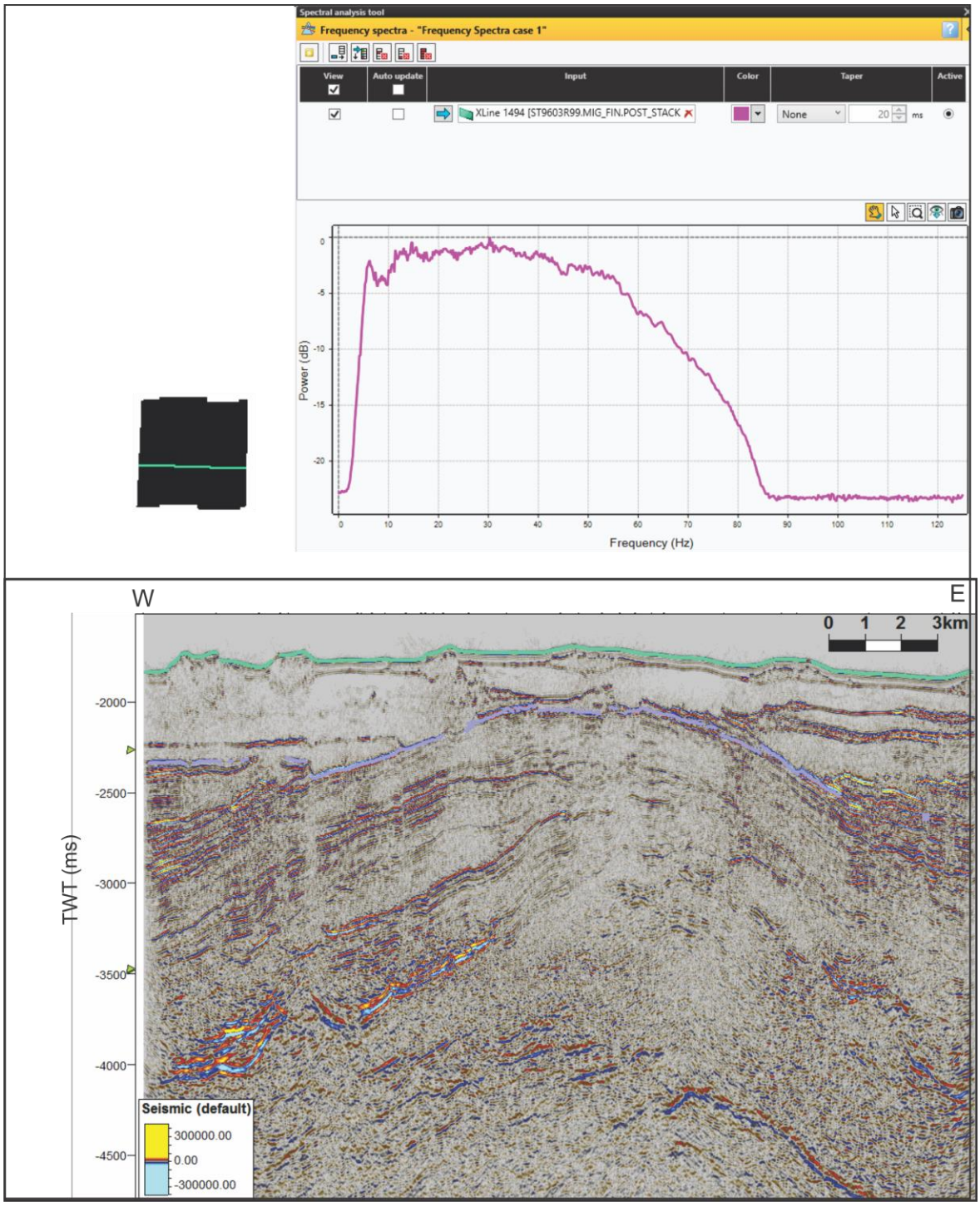

Figure 4.4 Above: Frequency spectrum analysis showing the bandwith of the seismic data with a lower boundary of 6-10 Hz and an upper boundary of approx. 80 Hz. Below: The seismic line from where the frequency spectrum analysis were extracted.

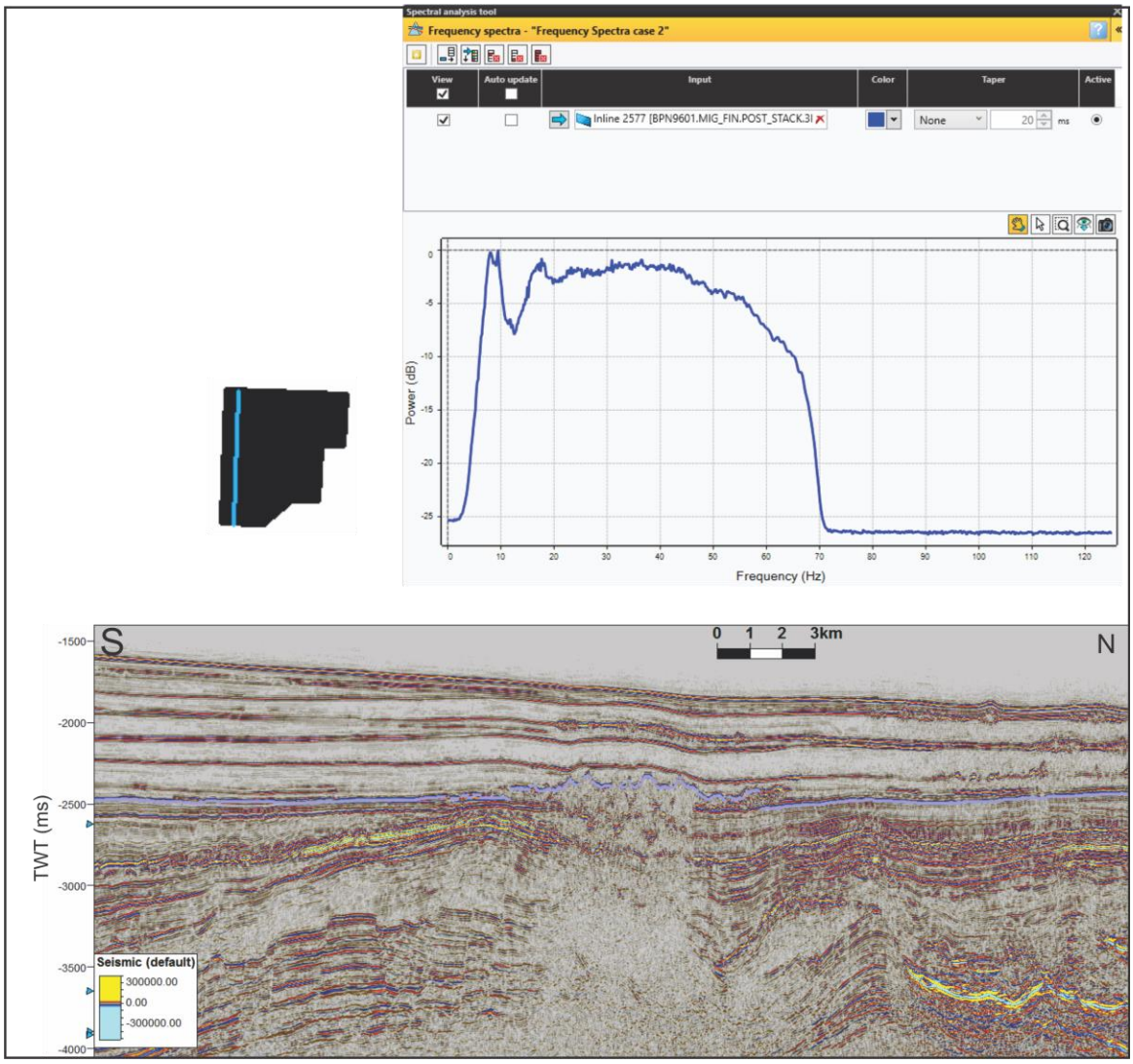

Figure 4.5 Above: Frequency spectrum analysis showing the bandwith of the seismic data with a lower boundary of 6-10 Hz and an upper boundary of approx. 70 Hz. Below: The seismic line from where the frequency spectrum analysis were extracted

For the interpretation of the seismic, the interpretation program Petrel2016 was used. The software is owned by Schlumberger and is a tool developed for the exploration and petroleum industry for seismic interpretation. Petrel allows for interpreting 2D and 3D seismic data, and to correlate this with well data. Seismic attributes and calculation can be used to generate useful maps in the software. The software uses negative TWT on its y-axis, meaning that many figures will show a negative value, while the text will show a positive value for TWT. In the results and discussion ms will mean ms TWT unless stated otherwise.

The horizons have been mapped by mostly using the 2D auto tracker. There are several methods to generate maps, but the one used here is by making polygons to mark the area of interest. After realizing the surfaces, attribute maps can be made. Different algorithms are then used to

generate useful maps. The attribute maps used in this study is mainly variance and RMS amplitude maps, and will be further discussed below:

4.3.1 Variance (Edge method)

The variance attribute shows signal coherency, by estimating trace to trace variability. As it shows the same response for the same seismic signature, discontinuities related to stratigraphic termination or structural lineaments are enhanced. The variance attribute is a useful tool for looking at faults (polygonal fault patterns), and can be used to map gas chimneys, also useful for analysis of seismic facies when interpreting the depositional environment (Schlumberger, 2015). Variance attributes can be generated as a 3D cube, allowing you to move up and down in time or depth.

Variance attribute map was generated for this study with parameters: Inline range 3, crossline range 3 and vertical smoothing 15.

4.3.2 RMS Amplitude

Calculates the root mean square (RMS) of single trace samples, over a specified vertical window with a length of n samples, for each sample in a input trace (Schlumberger, 2015). RMS amplitude map can be used for finding hydrocarbon indicators due to the AI contrast between water and hydrocarbons (Schlumberger, 2015).

5 Results

In this chapter, interpretations and observations from the two datasets BPN9601 and ST9603R99 will be presented (fig. 5.1). The main focus has been to map diapiric mound structures in the Vema Dome area in order to get a better understanding of the fluid plumbing systems in the Vøring Basin and the mechanisms developing the diapiric structures in the area. Deeper features like sill intrusions, fault systems and fluid flow features have been mapped and linked to the shallow diapiric structures. Seismic profiles, time-slices and attribute maps have been used to present the results.

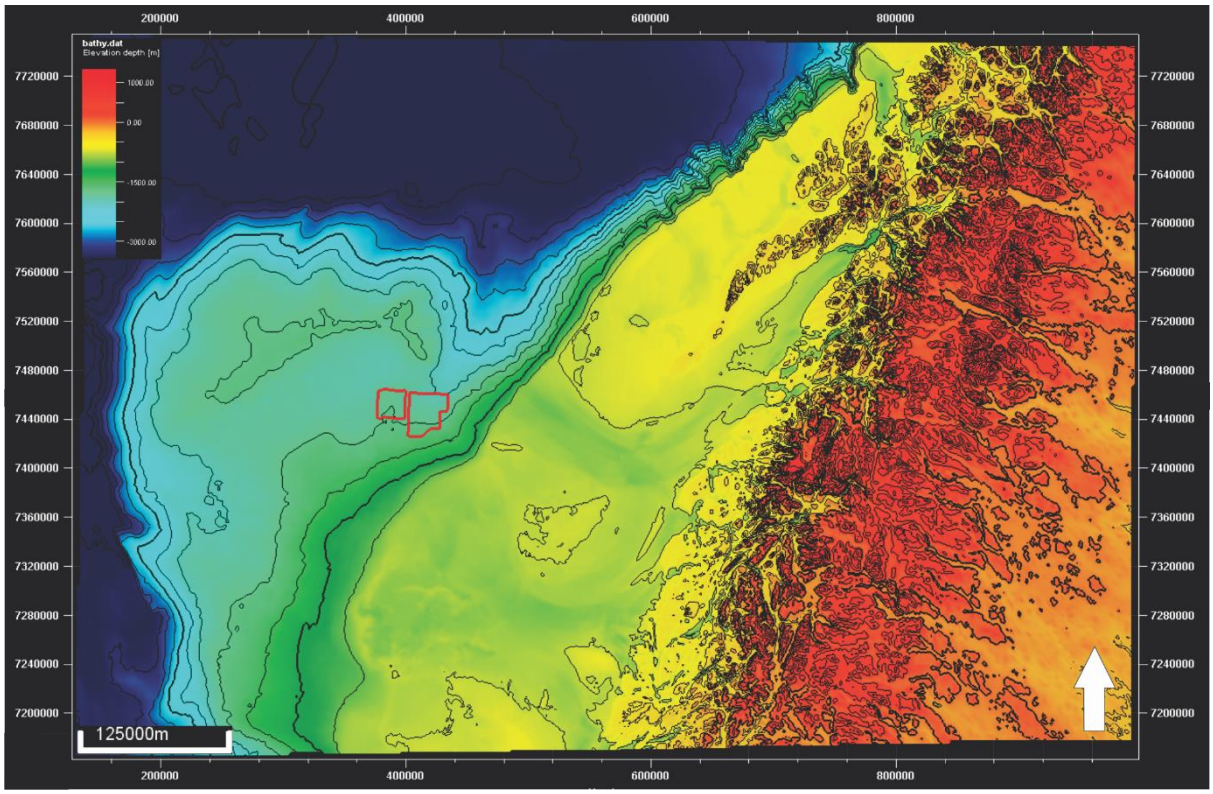

Figure 5.1 Bathymetry map showing the location of surveys ST9603R99 and BPN9601.

5.1 Seismic stratigraphy

The seismic stratigraphy of the Vema dome area is based on well data from the two wells located in the southern end of dataset ST9603R99, well 6706/11-1 and 6706/11-2 (fig. 5.2) as well as published papers from the area (Hovland et al., 1998, Chand et al., 2011). The wells available within the study area are located within survey ST9603R99 (fig. 5.2). As the two surveys do not overlap, the stratigraphic interpretation of survey BPN9601 was done based on Hovland et al., (1998), and by comparison of characteristic seismic facies with survey ST9603R99 (fig. 5.3).

This study focuses on the geologic history from Paleogene until present, and little attention has therefore been given to the deeper stratigraphy. The stratigraphic units interpreted for this study is the oldest Brygge Formation, and the youngest Naust Formation. Other studies have determined that Kai is not present over the Vema dome, but can be found on the flanks of the dome in between the Brygge and Naust formations (Hovland et al., 1998). However, as the well locations are on the Vema dome, where the Kai formation is not present, occurrence of the Kai formation could not be determined due to lack of stratigraphic control.

The two wells are located over the Vema Dome in the southern part of survey ST9603R99 with a distance of 3824 m from each other (fig 5.2). The stratigraphic units identified in the wells are Naust Fm., Brygge Fm., Springar Fm, and the Nise Fm. Springar and Nise Formation have not been interpreted as they are hard to distinguish in the dataset with discontinuous reflectors, and not relevant for this study. It is however interesting to mention that gas has been found in the Nise Formation in well 6706/11-2.

Figure 5.2 shows the interpreted stratigraphy in survey ST9603R99. The yellow shaded unit is the Naust Formation and the blue shaded unit is the Brygge formation. The top of the Vema dome follows the same interpreted reflector as the Base Naust/Top Brygge reflector.

Figure 5.3 shows the interpreted stratigraphy east of the Vema dome in survey BPN9601. The Naust formation is shown in the yellow shaded area. The Naust formation in this survey was interpreted by comparing the characteristic seismic facies with survey ST9603R99.

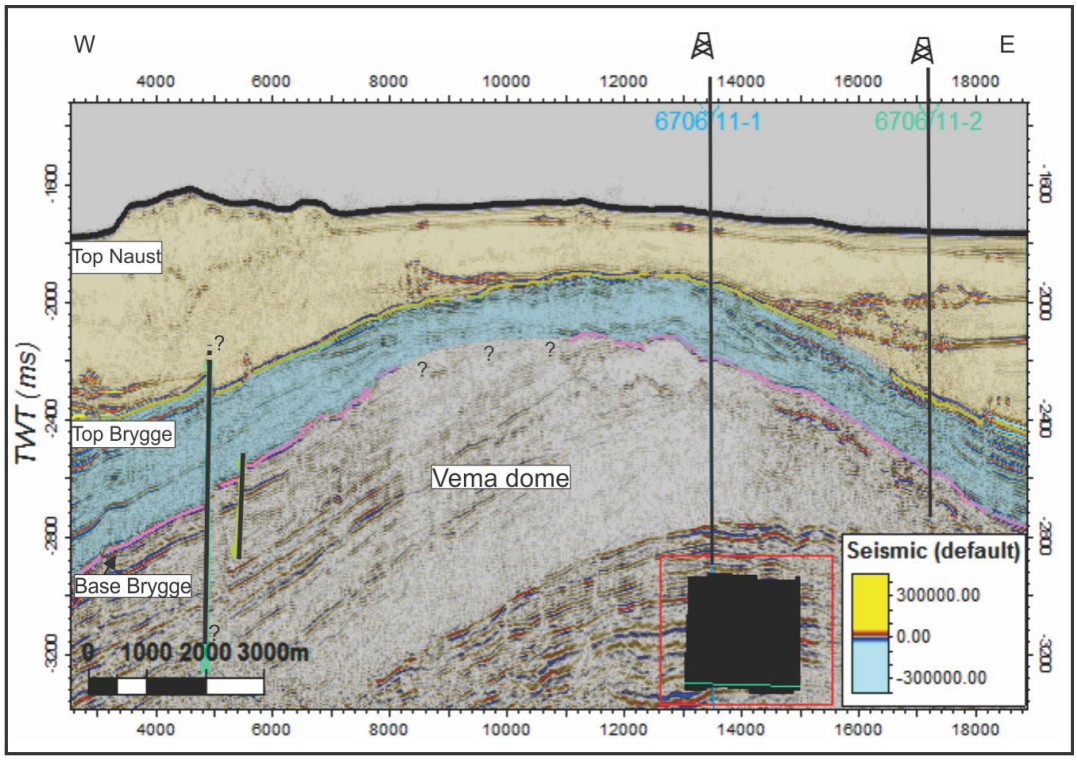

Figure 5.2 Seismic line from survey ST9603R99 showing the stratigraphy over the Vema dome. The Naust formation is coloured yellow and the Brygge formation is coloured blue. The black horizon indicates the seafloor, the yellow horizon is top Brygge and the pink horizon is base brygge. The base Brygge horizon could not be interpreted with high confidence over the top of Vema Dome. Location of the seismic line is shown with a green line in the polygon to the right in the figure. This line was chosen because it correlates with the two wells that lies within the survey area. Vertical exaggeration has been set to 10.

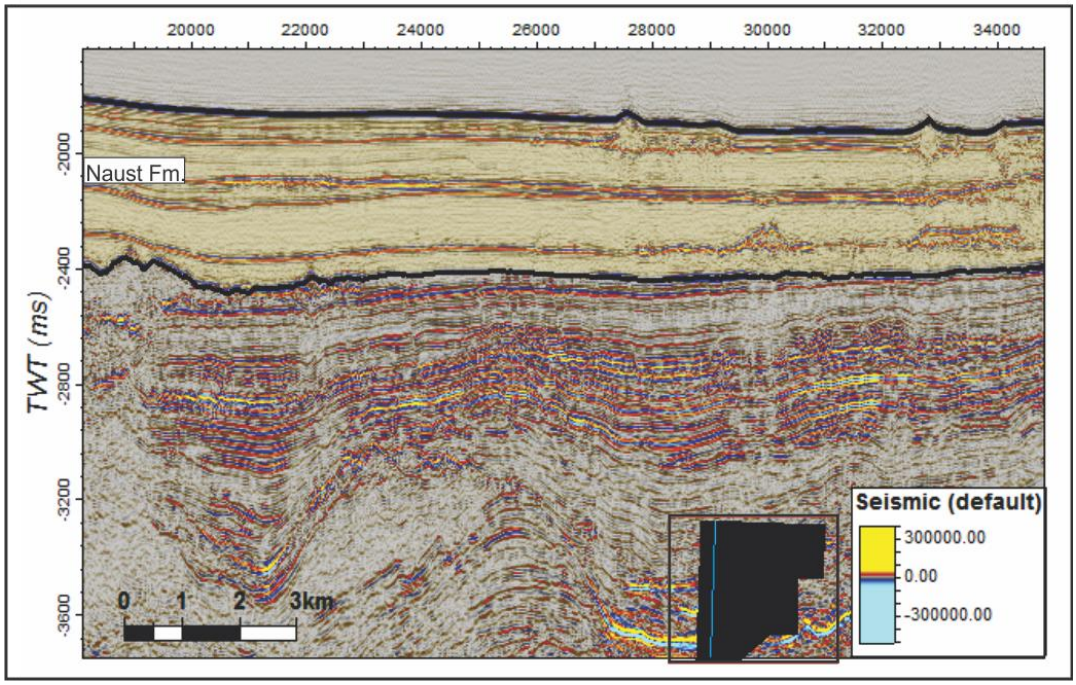

Figure 5.3 Seismic line from survey BPN9601 showing the interpreted stratigraphy in the survey area. The yellow highlighted section is the Naust formation, with top Naust and base Naust highlighted as black horizons. Location of the seismic line is shown with a blue line in the polygon to the right in the figure. Vertical exaggeration has been set to 10.

The reflector interpreted to represent base Brygge is identified at 2184ms (TWT) in well 6706/11-1 and at 2466 ms (TWT) in well 6706/11-2. The base Brygge reflection is a weak and discontinuous reflector making it difficult to follow. The reflection is only possible to follow in the southern part of survey ST9603R99. Here the reflector is cut by some faults small faults over the dome structure. Throughout the rest of the dataset, the reflections are disturbed and large areas show weak seismic amplitudes. It was not possible to follow the reflection laterally and continuously.

Sediments of the Kai formation are not recognized in the wells, and have therefore not been interpreted. It is however likely that the Kai formation is present in the study area, on the flanks of the Vema dome.

The reflector interpreted to represent base Naust is a fairly continuous reflector in both datasets, and easy to follow over the whole Vema dome (fig. 5.2 and fig. 5.3). The reflector has a strong positive reflection coefficient. In an S – N view, the reflector seems to steepen towards south direction, and in the E – W direction it has a concave shape over the Vema Dome. The Naust Formation are mostly made up of glacigenic debris flow deposits (Hovland et al., 1998), which are characterized by very little internal seismic reflections separated by each other by reflections with relatively high amplitude. The depth of the Naust formation varies from approximately 1825 ms over the Vema dome, to approximately 2500ms east of the dome, and reaches the seafloor, which varies from ~1530 ms TWT to 2070 ms TWT.

The Base Naust reflection lies unconformable on top of the Brygge/Kai formation. On the western side of the Vema dome, it onlaps the dome structure. Figure 5.4 shows the interpreted base Naust surface. The base Naust is shallowest in the west, where it lies on top of the dome structure.

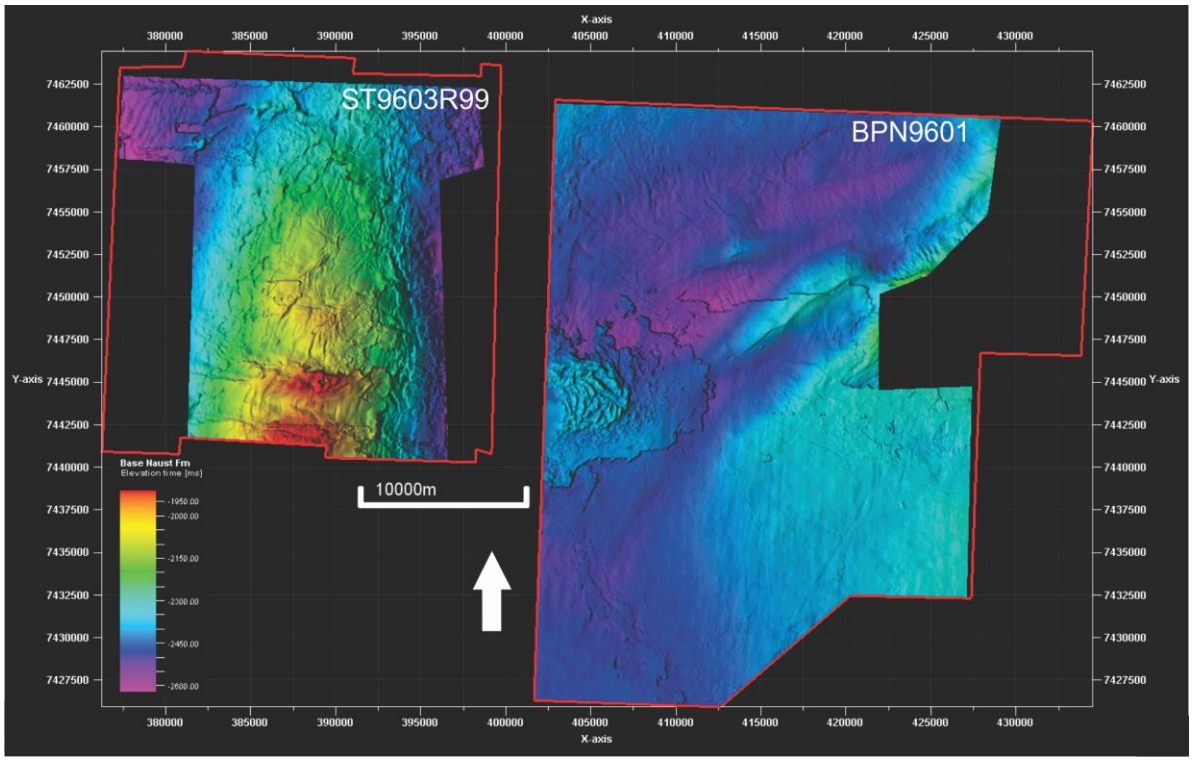

Figure 5.4 The interpreted base Naust surface which goes over the Vema Dome in survey ST9603R99 where it is at its shallowest.

The seafloor has a rugged topography in the western part of the survey area, and flatens out towards the east. This rugged topography is concentrated over the Vema dome in survey ST9603R99 (fig. 5.5).

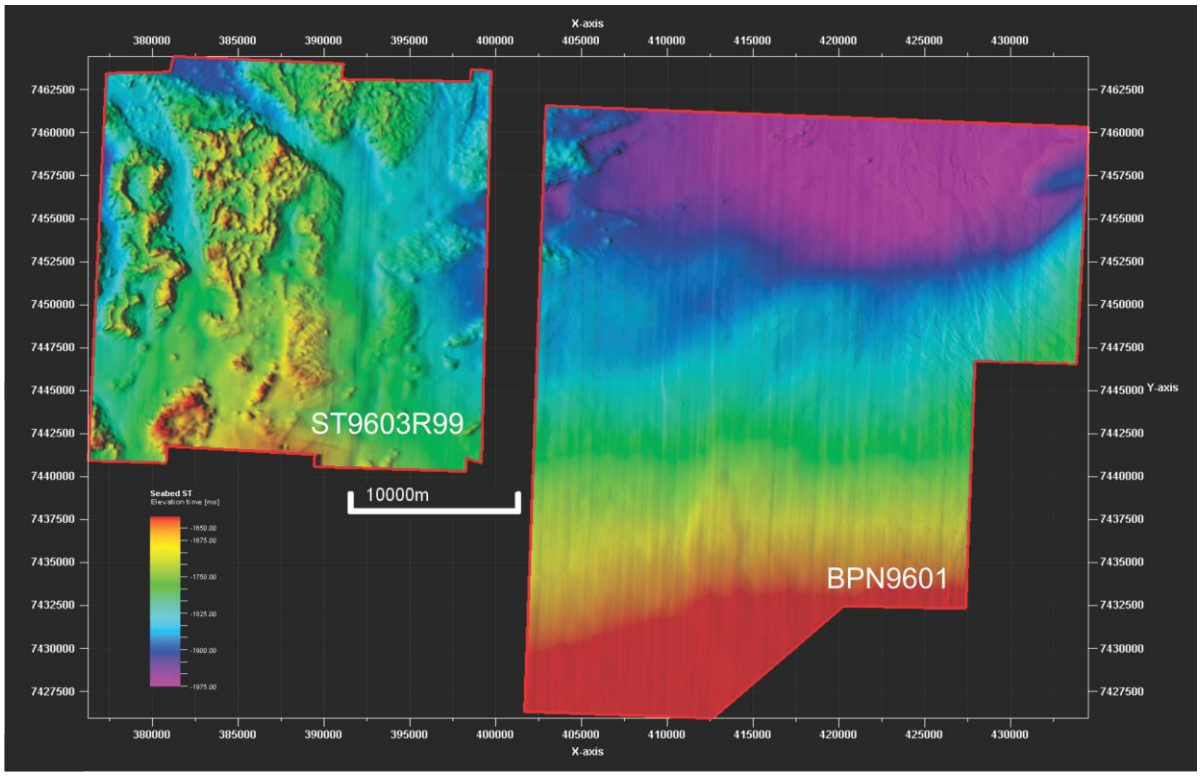

Figure 5.5 Map view of the seabed. The seafloor has a rugged topography over the Vema Dome and flattens out to the east.

5.2 Faults

Faults are generally recognised in seismic sections as vertical or near vertical discontinuities that offset reflections on either side. The fault plane itself often has a lower amplitude than the surrounding. Seismic attributes such as variance are also useful for identifying faults in 3D. Variance attributes measures dissimilarities in the waveform between two traces, and therefore highlights faulting.

Timeslices from the variance attribute shows a hexagonal pattern in the southern part of survey BPN9601 (fig. 5.6). The area stretches up to 13.6 km in the E-W direction, and up to 10.8 km in the N-S direction. This is a set of closely spaced blind faults, confined to approximately 2500 ms and 2990 ms on the seismic profiles, some of them terminating in the base Naust, but mostly (upwardly) terminating beneath the base Naust horizon, and seem to be confined to a specific stratigraphic interval with parallel, sub-horizontal reflections with low seismic reflection coefficients. This fault set cover an area of approximately 117 km^2. The faults strike randomly, with no specific preferred azimuthal orientation. Fault planes appear to be slightly curved or linear in planform (fig. 5.6a)

Cartwright et al., (2003) defined polygonal faults as layer bound faults confined to a stratigraphic interval of fine grained sediments which shows a wide range of fault strikes and shows a polygonal pattern in map view (Cartwright et al., 2003). The faults described here conform to this definition of faulting style so faults in this dataset have therefore been interpreted to be a tier of polygonal faults. No areas with polygonal faults was recognized in survey ST9603R99.

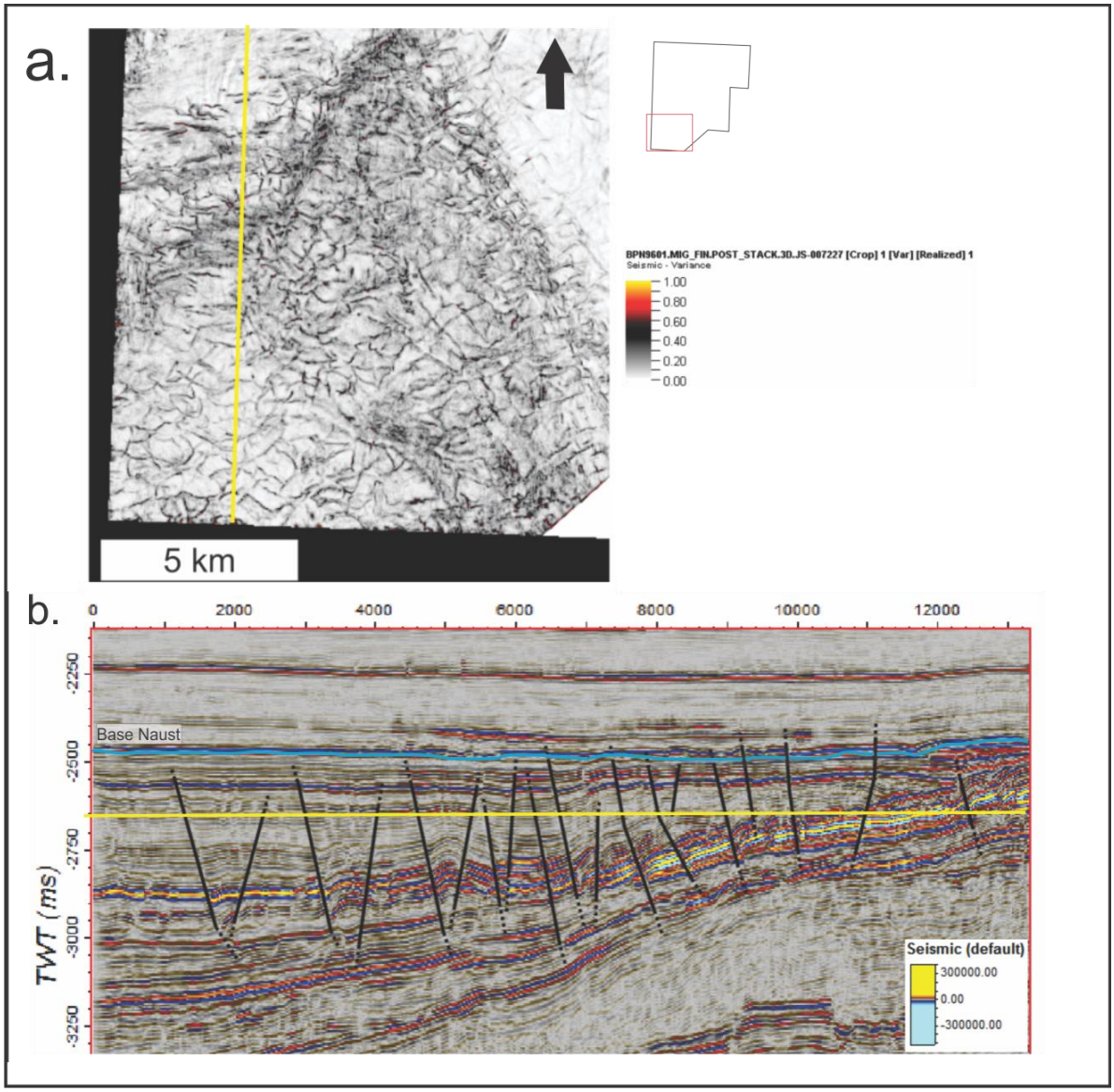

Figure 5.6 A) Timeslice from a variance cube showing a polygonal fault system in the southern part of survey BPN9601. The timeslice is marked with a yellow line in figure b, and the area is marked with a red square on the polygon to the right. B) a seismic section with the polygonal fault system. The seismic inline is marked by a yellow line in figure a. Base Naust is marked by a blue line.

As seen in figure 5.7, regional scale faults in the Vøring basin generally strike to SW-NE and NNW-SSE azimuths. Above the Vema dome, this regime changes, and there are two regional scale faults with a NW-SE direction.

5.3 Amplitude anomalies

In the north-western part of the survey area (fig. 5.7) the seismic data shows four areas (SI1-4) with high amplitude anomalies. These anomalies are very well defined in the seismic data, whereby the amplitude signature does not fade around the edges, but rather is an abrupt change to an increased amplitude (fig. 5.8). The amplitude anomalies have been recognized in the seismic between 4060 ms and 2795 ms. The amplitude anomalies have been mapped and interpreted by looking at timeslices of an RMS amplitude map and vertical seismic sections. There survey area is also largely affected by long vertical, columnar features with dimmed amplitudes reminiscent of acoustic masking due to gas in sediments (Løseth et al., 2009). These columnar features are associated with the high-amplitude anomalies and will hence be described and interpreted in this chapter. These features are marked as acoustic masking in the figures.

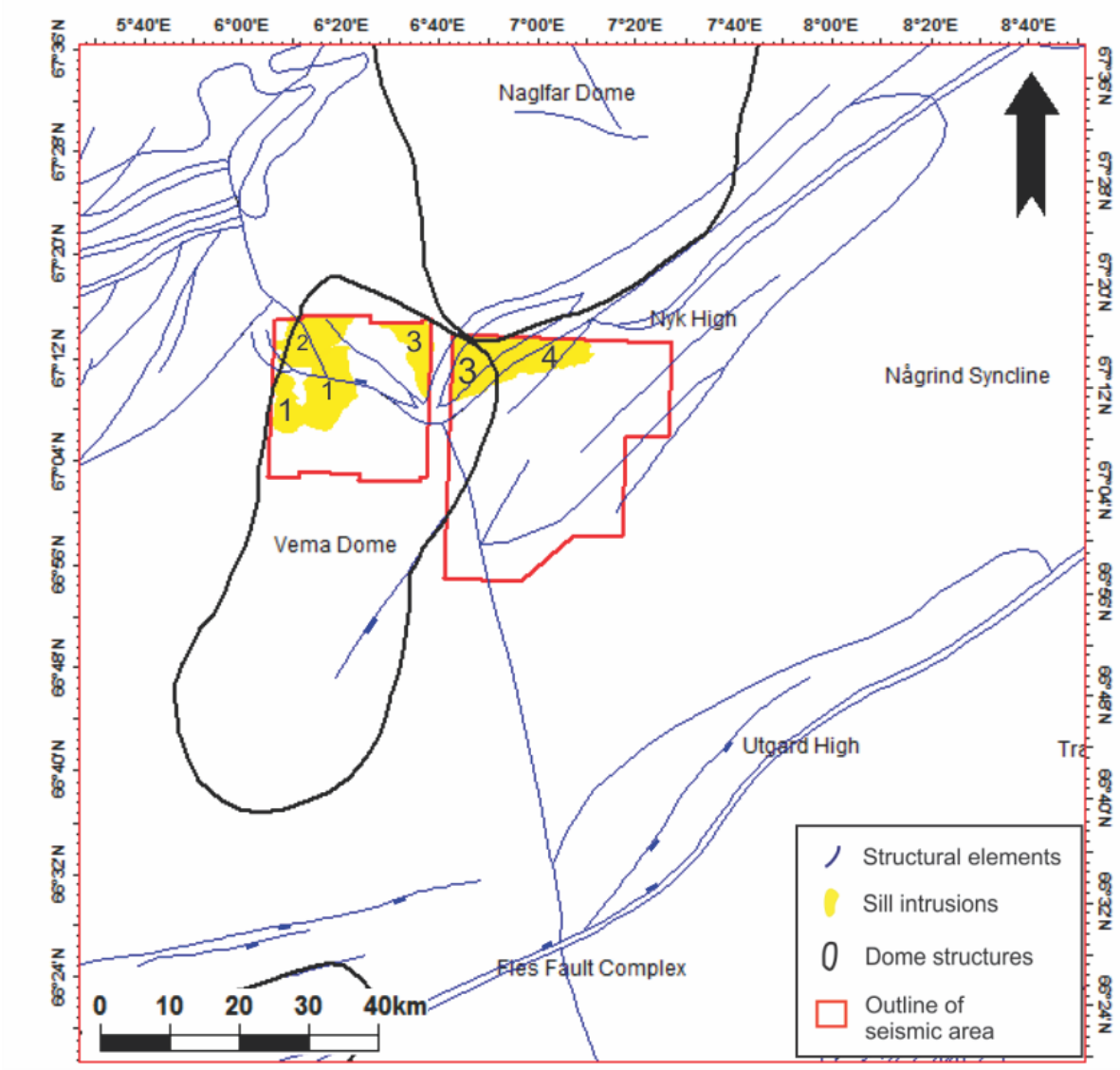

Figure 5.7 Overview map of amplitude anomalies interpreted as sill intrusions (yellow polygons). The dark blue lines show the main structural elements in the Vøring Basin, and the black outlines show dome structures. The red polygons show the outline of the seismic area. Notable is the regional scale faulting orientation change from SW-NE to NW-SW across the Vema Dome.

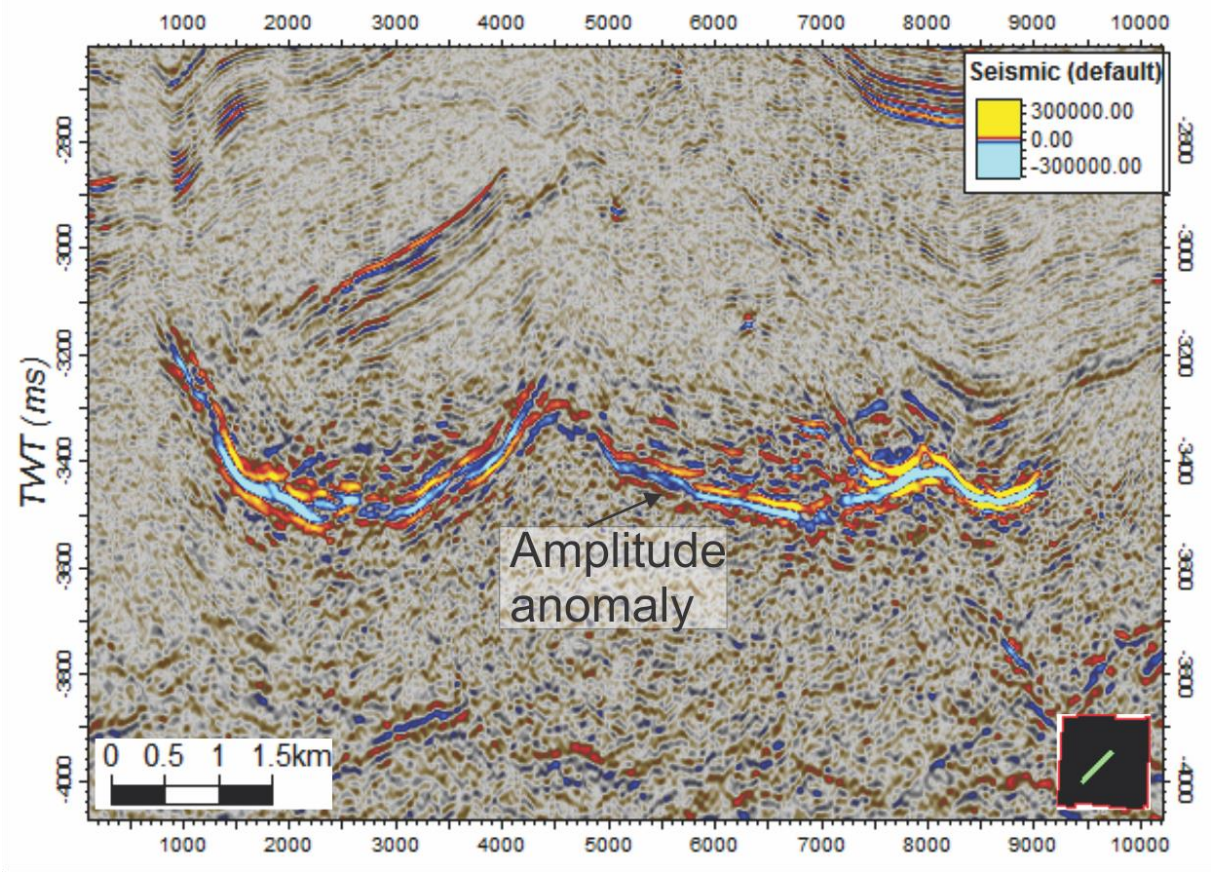

Figure 5.8 Seismic line showing an example of the high amplitude anomalies interpreted. The amplitude signature does not fade around the edges, but rather is an abrupt change to an increased amplitude.

The high amplitude anomalies have been named SI 1 – SI 4. SI 1 and SI 2 dip in the W-E direction towards the centre of the Vema dome (fig. 5.9). SI 3 dips in the opposite direction also towards the centre of the dome structure in its western end and flattens out towards the east. This indicates that the features causing these amplitude anomalies have been affected by the uplift of the dome structure. SI 4 is located to the east of the dome and is horizontal. SI 1 – SI 3 are saucer shaped, and SI 4 is elliptical. The features are crosscutting the regular sedimentary strata and are mostly sub-parallel to the strata configuration (fig. 5.10).

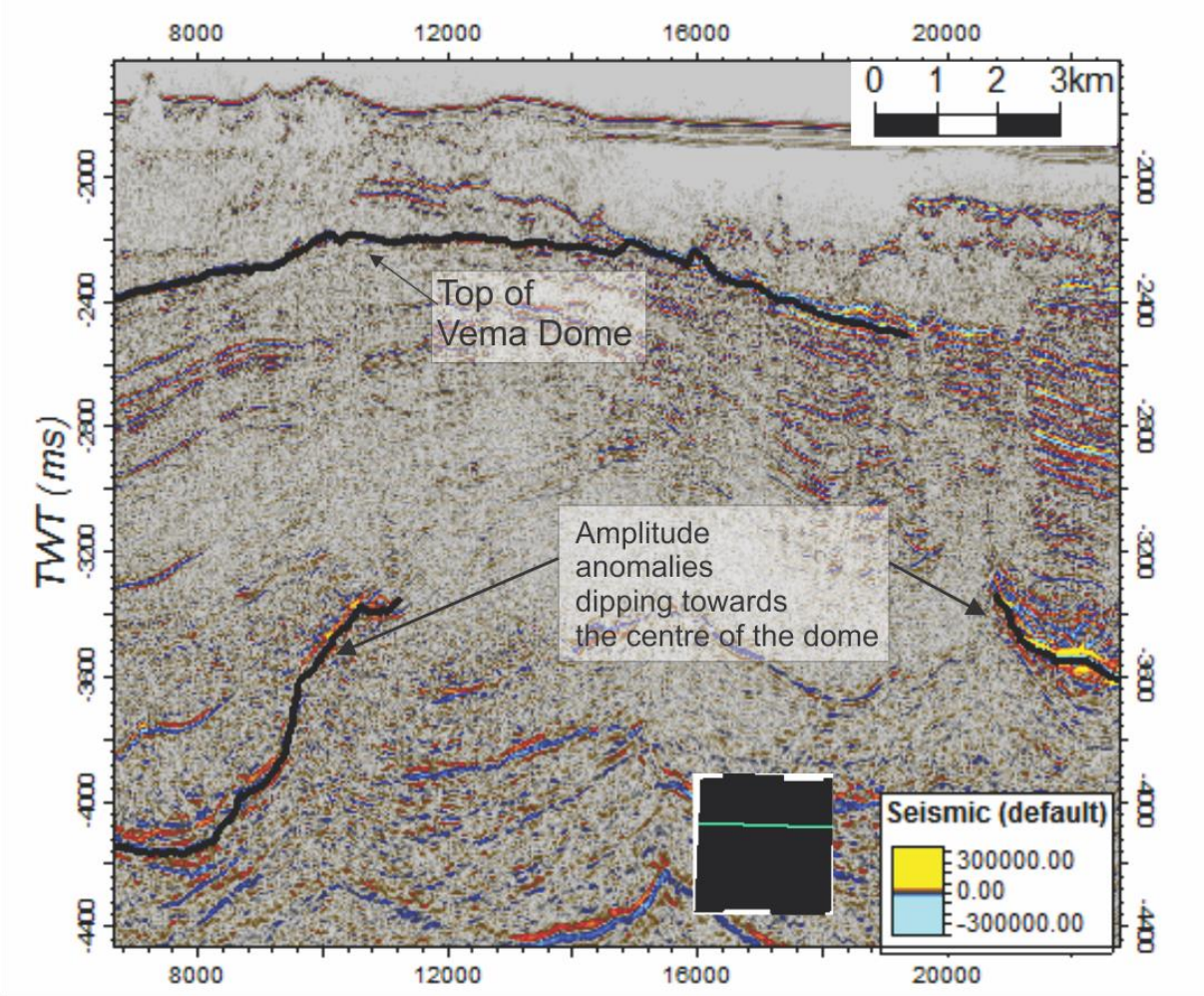

Figure 5.9 Seismic section showing interpreted high-amplitude anomaleis that are dipping towards the centre of the Vema Dome. The top of the dome and the amplitude anomalies are marked with black lines.

The mapped amplitude anomalies most likely extend outside the survey area, SI 1 to the west, and SI 1 – SI 4 further to the east.

These high amplitude anomalies described have the same seismic characteristics as features previously interpreted as sill intrusions in the Vøring basin by Planke et al., (2005), and in other regions for example by Kjoberg et al., (2017) and Magee et al., (2016).

Table 5.1 gives a summary of the vertical and lateral extent of the interpreted sill intrusions.

Table 5.1 Summary of sill intrusions (SI 1 – SI 4).

Sill	Long axis (m)	Short axis (m)	Area (km^2)	Top TWT (ms)	Base TWT (ms)
SI 1	11428	11208	82.7	3160	4490
SI 2	8200	6720	40	2635	3645
SI 3	2100	10600	103	3235	3980
SI 4	16100	4225	67.6	3320	3780

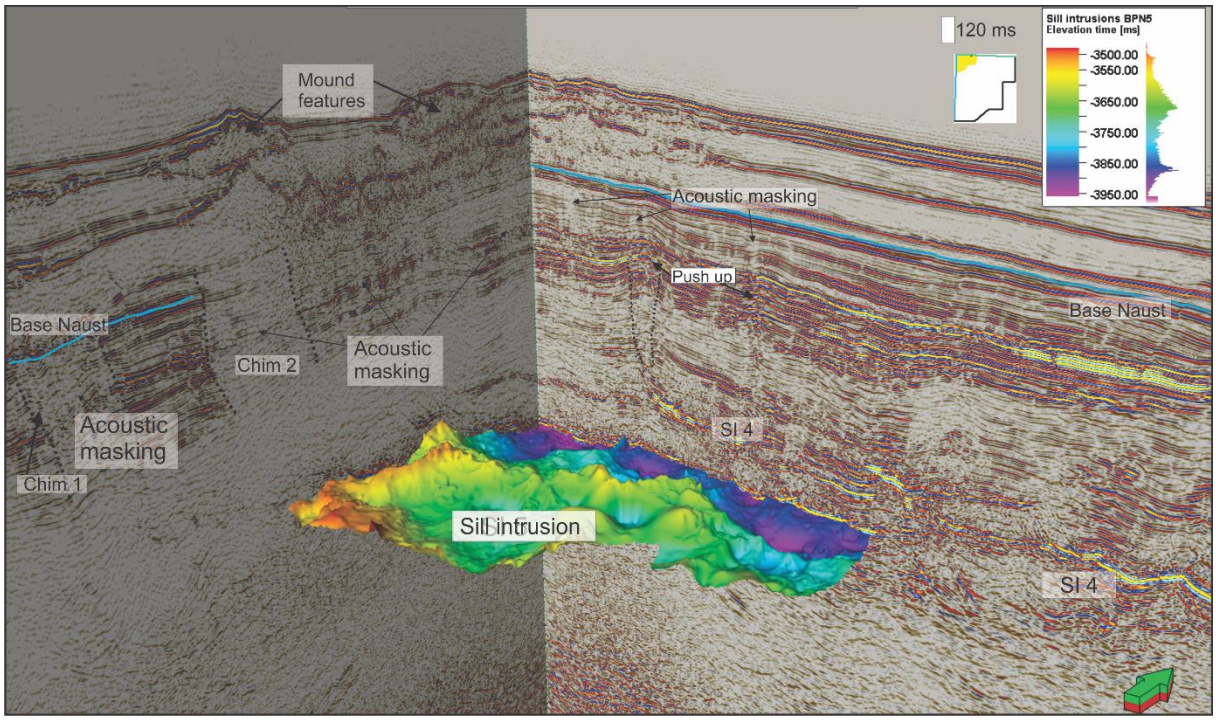

Figure 5.10 3D window showing the generated surface of SI 3 in survey BPN9601. The seismic sections show some mounded features reaching the seafloor and areas of acoustic masking above the sill intrusion and some push up effects. The blue line is interpreted as the base Naust reflection. Vertical exaggeration is set to 5. Note that the feature identified as a sill intrusion has a characteristic saucer shape and is emplacing parallel to the main sedimentary configuration.

Figure 5.10 is a 3D window showing SI 3 in survey BPN9601. The sill intrusion has a shallow dip in the N-S direction. The seismic sections also shows areas of acoustic masking above the sill intrusion. Close to the southern tip of the sill intrusion, there are two large areas of acoustic masking marked in figure 5.10 and figure 5.11. These sections of acoustic masking cuts the stratigraphy which otherwise shows parallel layers with strong amplitude coefficients. The areas are seen as vertical zones of weak and chaotic reflections. The vertical columnar feature in figure 5.11 marked chim1 has a diameter of approximately 1.3 km, and the feature marked

chim2 has an approximate diameter of 2 km. These features could be hydrothermal vents, as hydrothermal vent structures usually originate at the tip of sill intrusions. There are also some very thin vertical zones above the sills with acoustic masking. These are interpreted to be smaller pipe features. All these vertical features can act as possible fluid migration pathways as these represent fractured and reworked sediments.

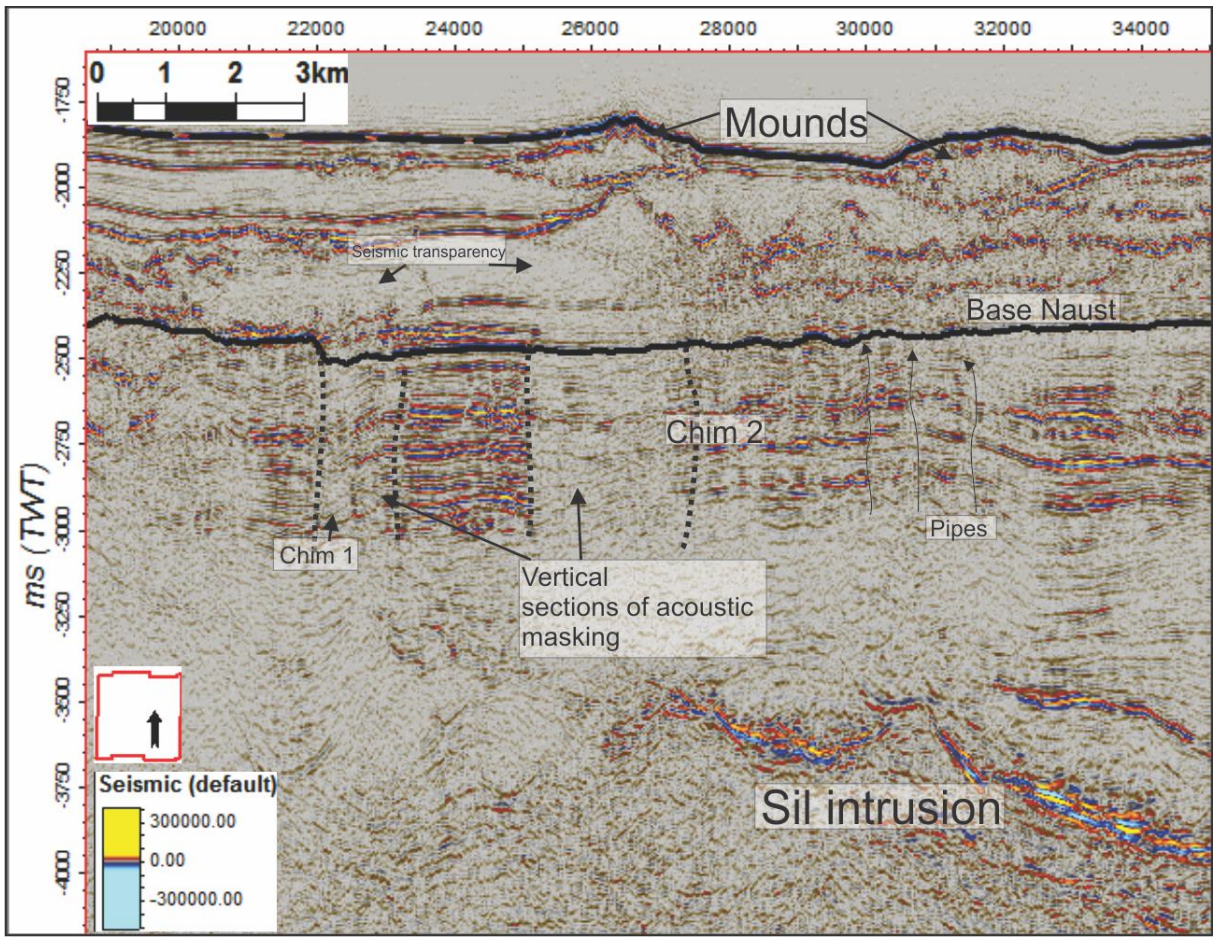

Figure 5.11 The same seismic section as shown in figure 5.8. Vertical columnar features with acoustic masking are marked with striped lines. High-amplitude anomalies interpreted as sill intrusions are found below the areas with lower seismic amplitudes (acoustic masking) and there are some mounded features above.

Figure 5.12 shows the seismic line shown in figure 5. 10 in the E-W direction zoomed in on the push-up effects found above the high amplitude anomalies interpreted as sill intrusions. These push up effects start at the tip of the sill intrusions and have a conical shape where the seismic reflections have been pushed up compared to the surrounding. These features share many similar characteristics as features Planke et al., (2005) interpreted as hydrothermal vents, including the push up/eye structure indicated by arrows in figure 5.12 and the seismically chaotic section joining to the sill beneath.

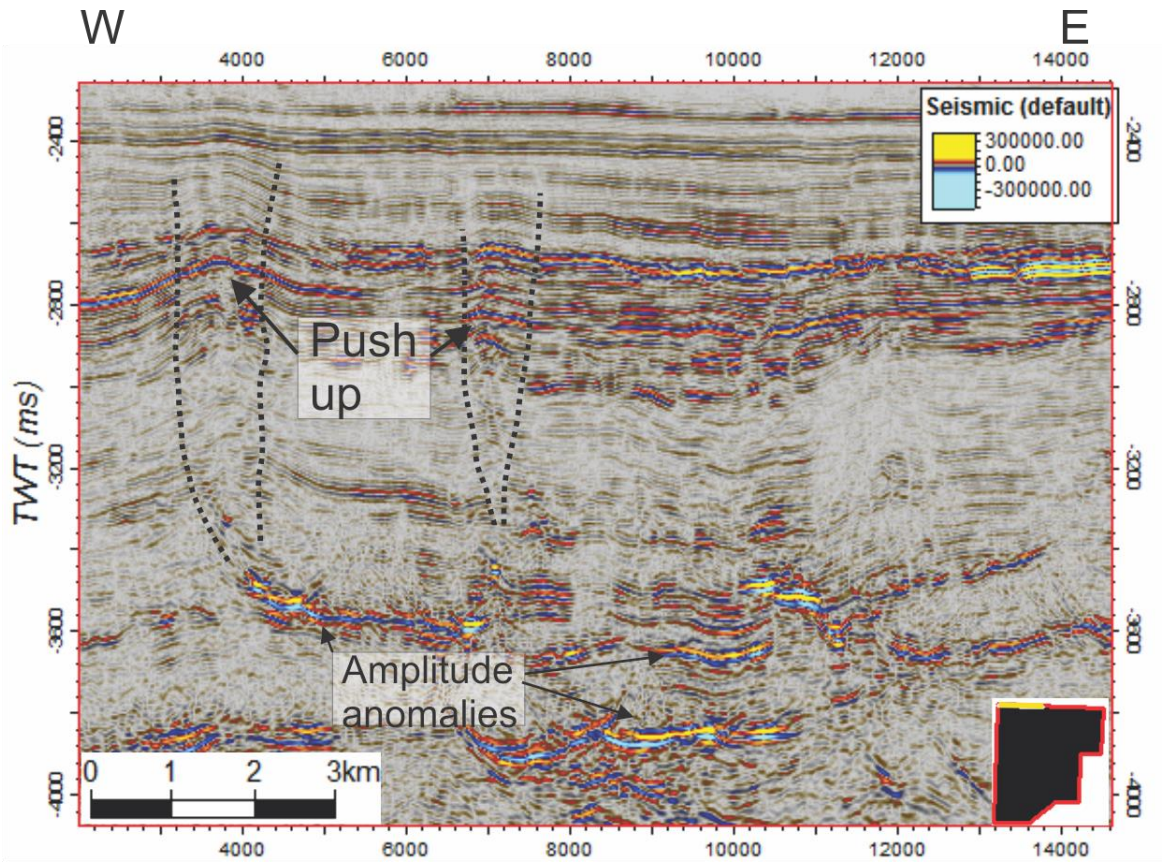

Figure 5.12 Seismic line showing some push up effect above high amplitude anomalies in the northern part of survey BPN9601. These features have been interpreted as hydrothermal vents after Planke et al., 2005. The edge of the disturbed sediment is marked by dotted lines and is representative of the area affected by fluid migration in repsonse to the sill emplacement. These features are often coincident with the tips of sill features.

Figure 5.13a shows a seismic line of the interpreted sill intrusion SI 3 and SI 4 in survey BPN 9601. There are some small, narrow zones of acoustic masking above the sill intrusions marked with black arrows in the figure. Figure 5. 13b shows a timeslice of a RMS attribute map showing the amplitude anomalies in figure a.

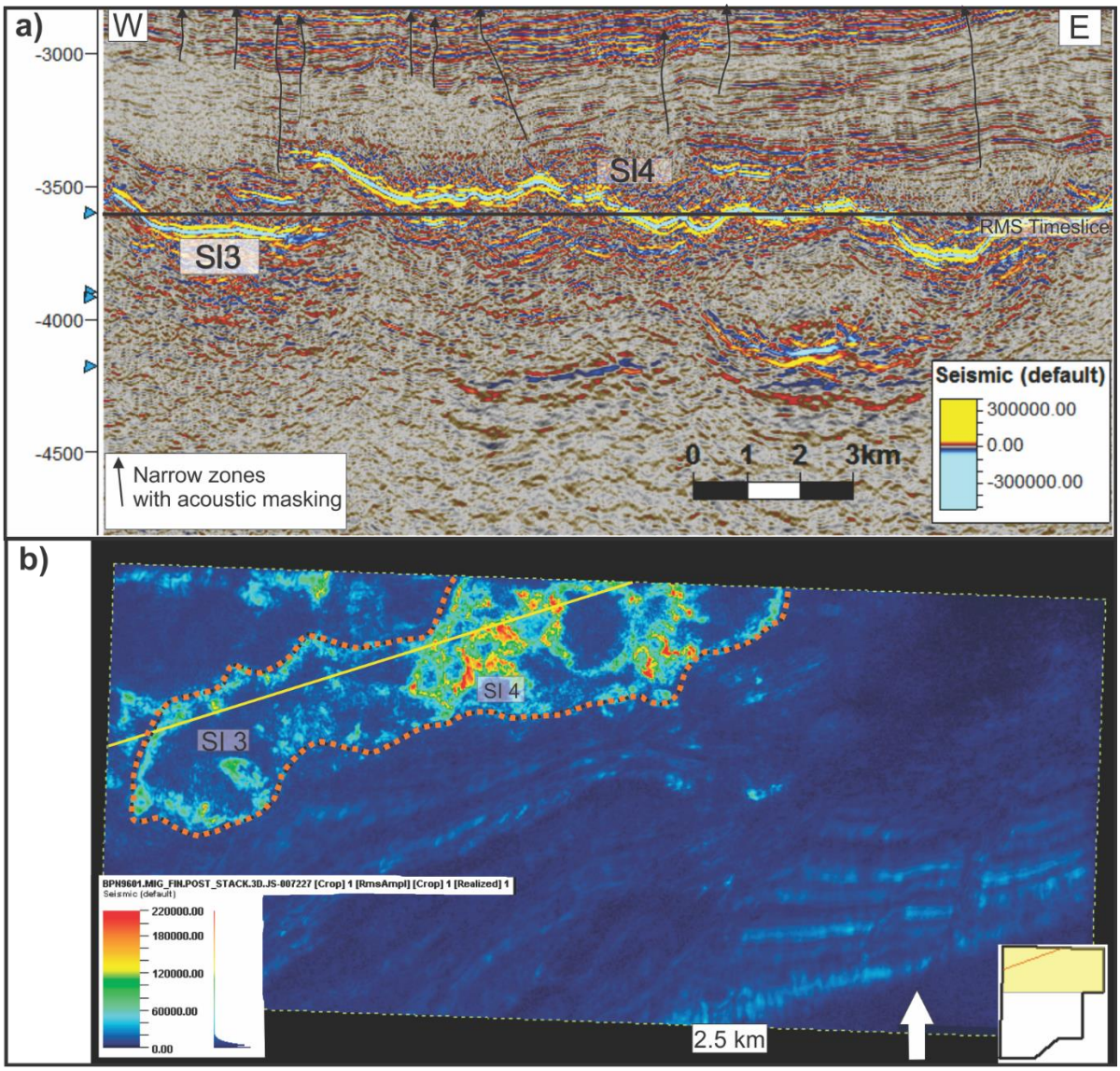

Figure 5.13 A. Seismic line showing high amplitude anomalies interpreted as sill intrusions in survey BPN9601. The black line indicates RMS timeslice in fig. b. Black arrows indicate narrow zones of acoustic masking. B. Timeslice of RMS amplitude map. The high amplitudes within the orange area are the interpreted sill intrusions.

Figure 5.14 shows a 3D window of SI 1. Areas of acoustic masking are found above the sill intrusion, crossing the stratigraphy, and there are mound features at the seafloor. There are some wider zones of acoustic masking, where two of these wide zones start at the tip of the sill intrusion and terminate beneath the mounds at the seafloor. These zones lie within the black dotted lines in the figure. There are also many smaller vertical features of acoustic masking that are marked in the figure with black arrows.

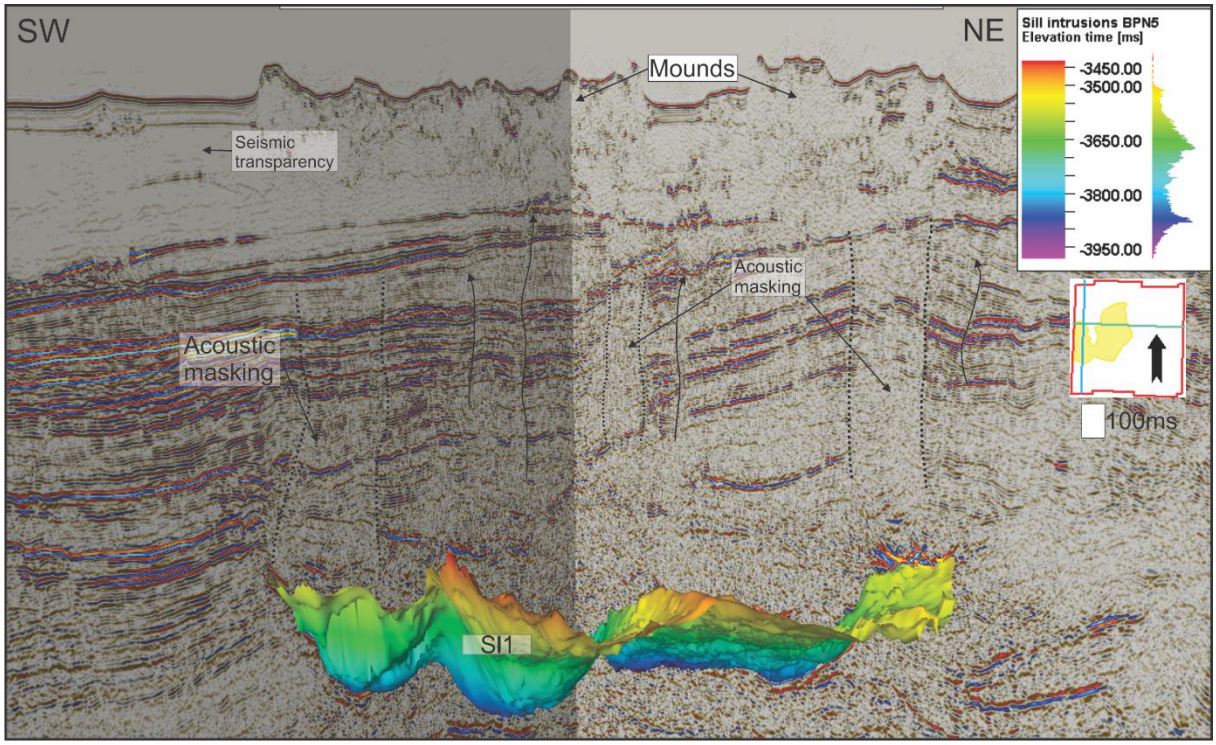

Figure 5.14 3D window of SI 1 and areas of acoustic masking and above laying mounds. The main structure of large vertical amplitude anomalies are indicated by black dotted lines while the smaller amplitude anomalies are marked with solid arrows. The sill exhibits the characteristic saucer shape- All the vertical amplitude anomalies are confined to the same area as the sills, and there is a correlation between mound features, vertical amplitude anomalies and sills.

Figure 5. 15 shows a seismic line in the southern part of ST9603R99 in the E-W direction over the Vema dome. There are some mound features almost at the seafloor and at approximately 4000-4400 ms there are amplitude anomalies interpreted to be sill intrusions. There are areas with vertical columnar features which have been highlighted in the inset of figure 5.15. These features shows low seismic amplitudes and chaotic reflections. These vertical features cut through otherwise strong continuous and parallel seismic reflections.

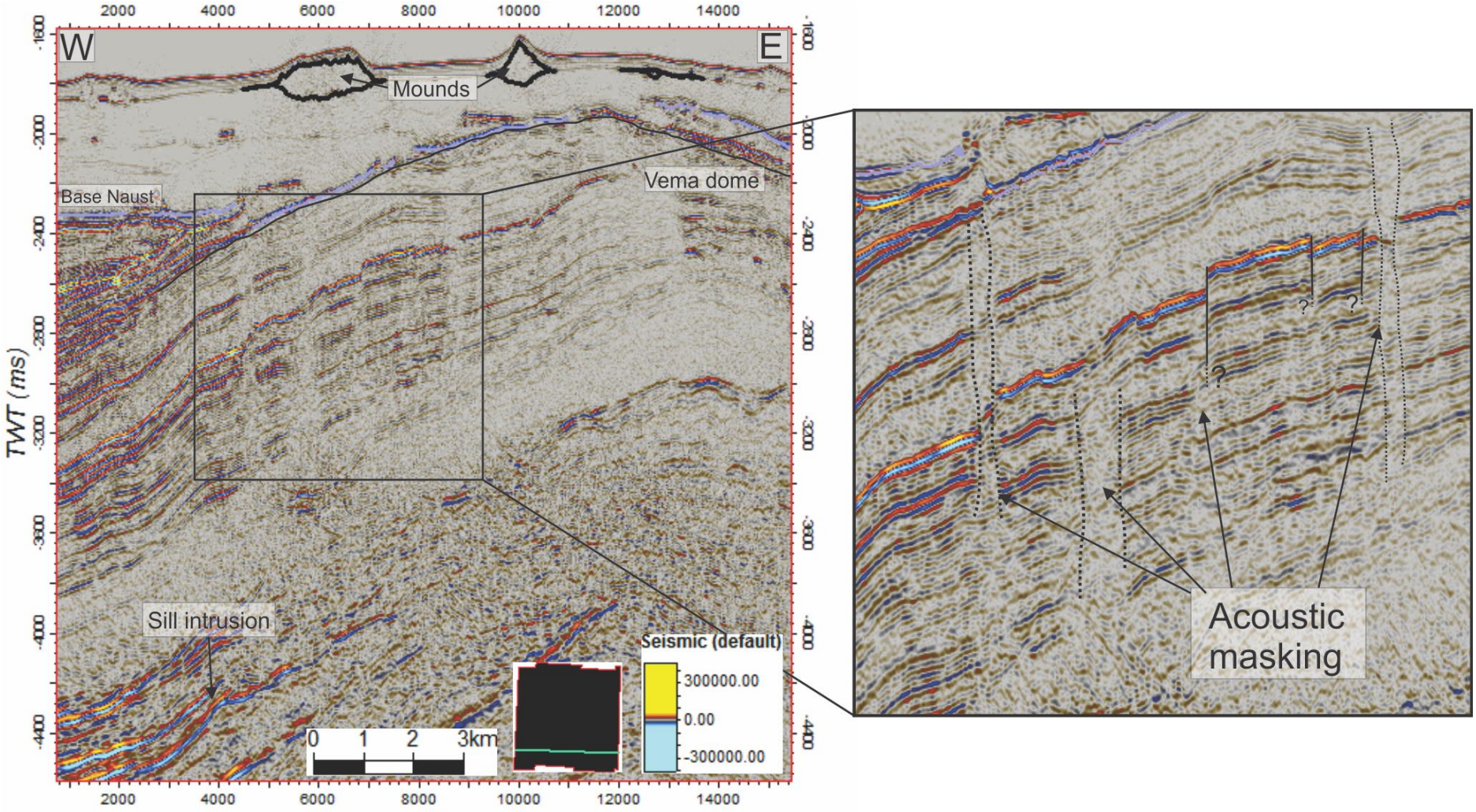

Figure 5.15 Left: Seismic section in the south of survey ST9603R99 over the Vema dome (Marked with green line). The purple line shows the reflector interpreted as base Naust. Some representative mounds are outlined in black. Right: Zoomed in square highlighting vertical columnar features (within the dotted lines). The purple horizon is the interpreted base Naust.

Figure 5.16 shows a seismic line in the W-E direction over the Vema dome. There is one big vertical columnar feature starting at the tip of the sill intrusion that can be followed up to the purple line indicating the base Naust reflector. There is also a big mound feature at the seafloor. The vertical feature is cutting through the surrounding seismic reflectors and is an area with low seismic reflection coefficients and the seismic has a chaotic appearance.

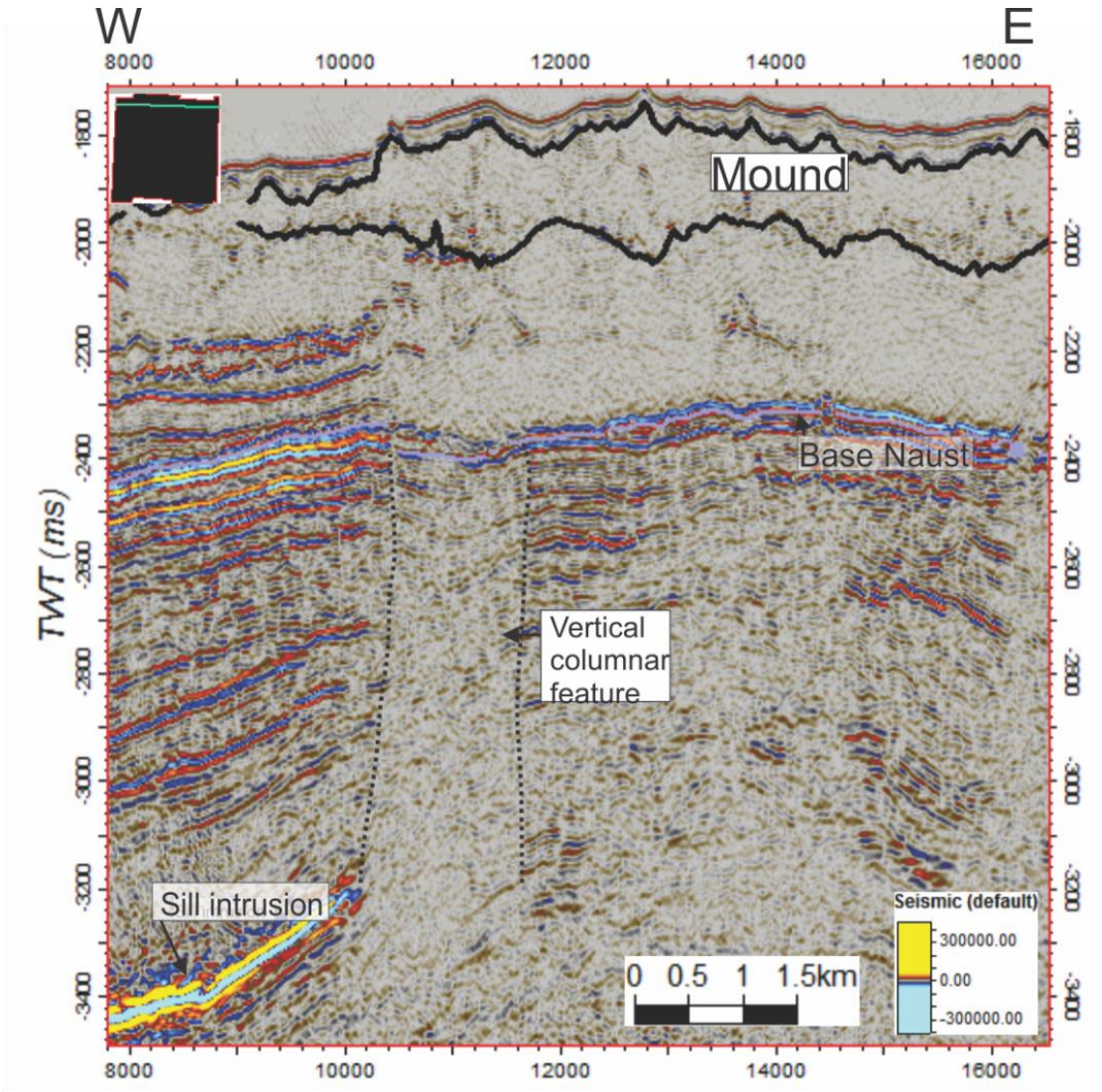

Figure 5.16 Seismic line in the norther part of survey ST9603R99 showing a sill intrusion, vertical columnar features as well as a mound feature.

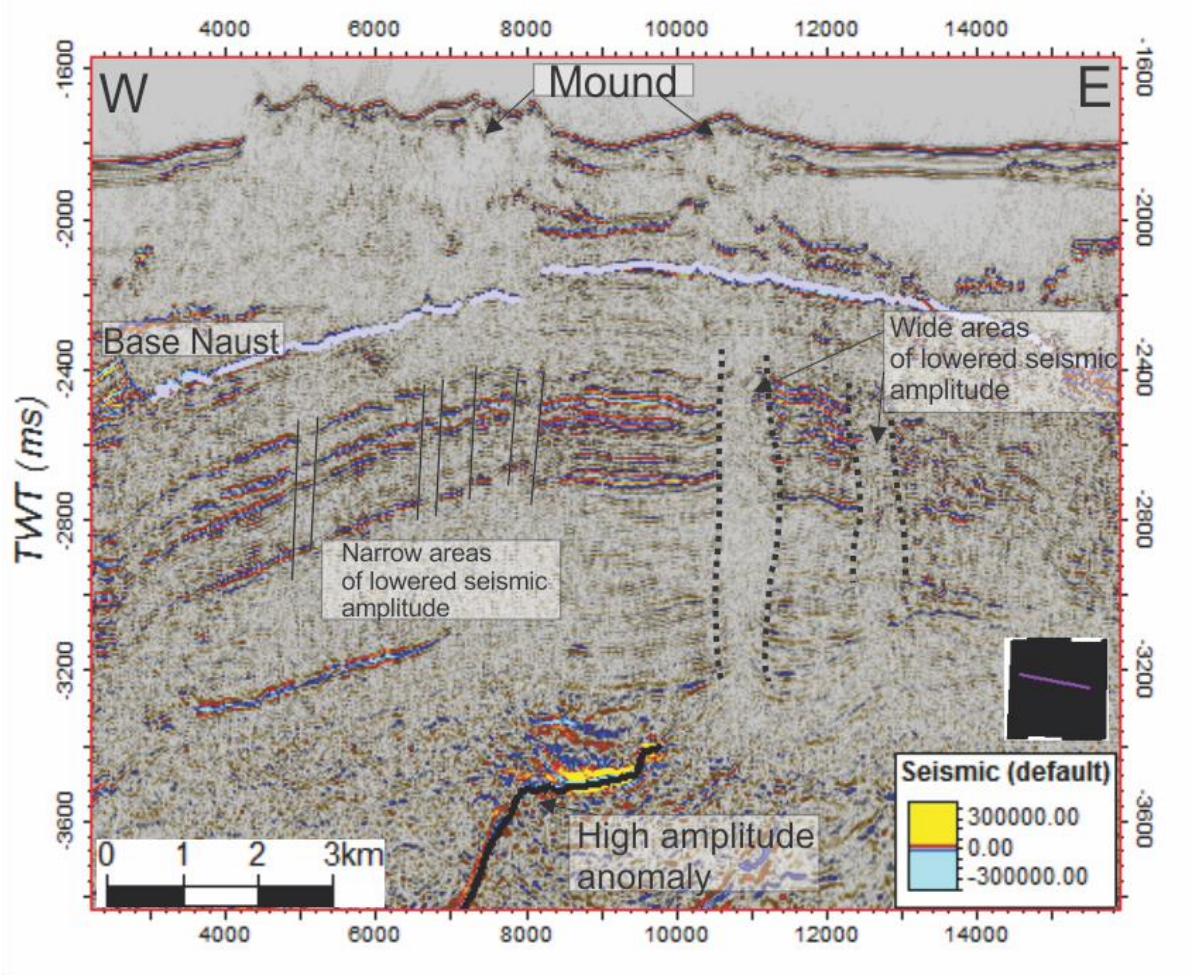

Figure 5.17 Seismic line showing big and small vertical columnar areas of lowered seismic amplitude. The big features can be correlated to the tip of the high amplitude anomaly. The reflection interpreted as the base Naust is indicated in light purple and there are also some mounds in the top of the Naust formation.

These vertical features with acoustic masking that have been described above can be divided into small features (marked with black lines) and big features (both marked with dotted lines) (fig. 5.17). These bigger features are interpreted to be hydrothermal vents originating from the sills, which can act as migration pathways for fluids. The smaller features are interpreted as faults and smaller chimney and pipe features which result from overpressure in the subsurface, also acting as fluid migration pathways. The bigger chimney features (fig. 5.11, fig. 5.14, fig. 5.16 and fig. 5.17) all seem to start at the tip of the high amplitude anomalies interpreted as sill intrusions. All vertical amplitude anomalies are coincident with sill emplacement features. The vertical amplitude anomalies are therefore interpreted to be fluid migration pathways which are acting as vent systems for release of heat from the sill emplacements.

5.4 Diapiric mound structures

Eleven mounded features have been mapped in the study area (fig. 5.18 and fig. 5.19), where ten of these are in the upper parts of the Naust formation, reaching the seafloor, while one penetrates the base Naust reflection.

The distribution of the mounded features are concentrated over the Vema dome. The mounded features decrease in size from west to east.

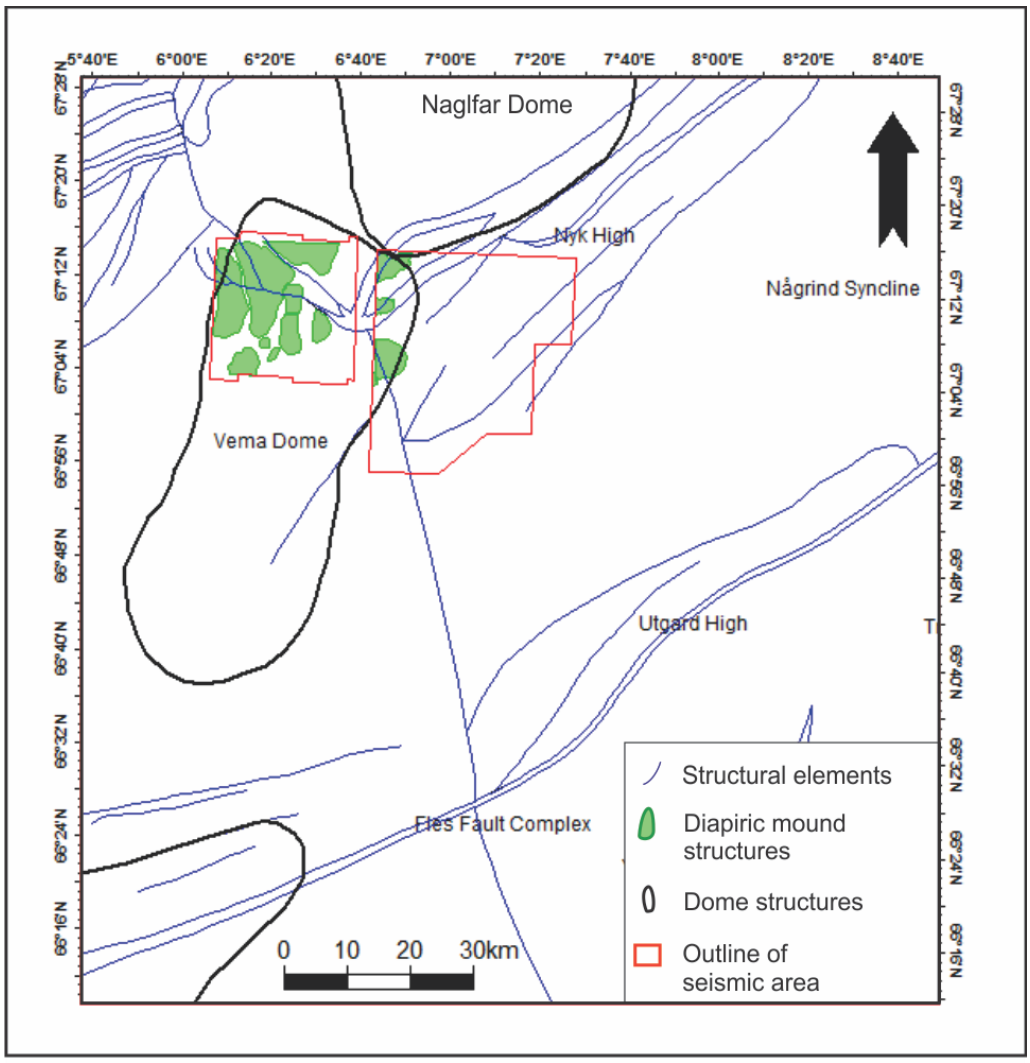

Figure 5.18 Map showing the interpreted mounded features (green) which are concentrated over the Vema Dome. The seismic survey area is marked with red polygons. The outline of dome features is marked with black lines and structural elements in the Vøring Basin is marked with blue lines.

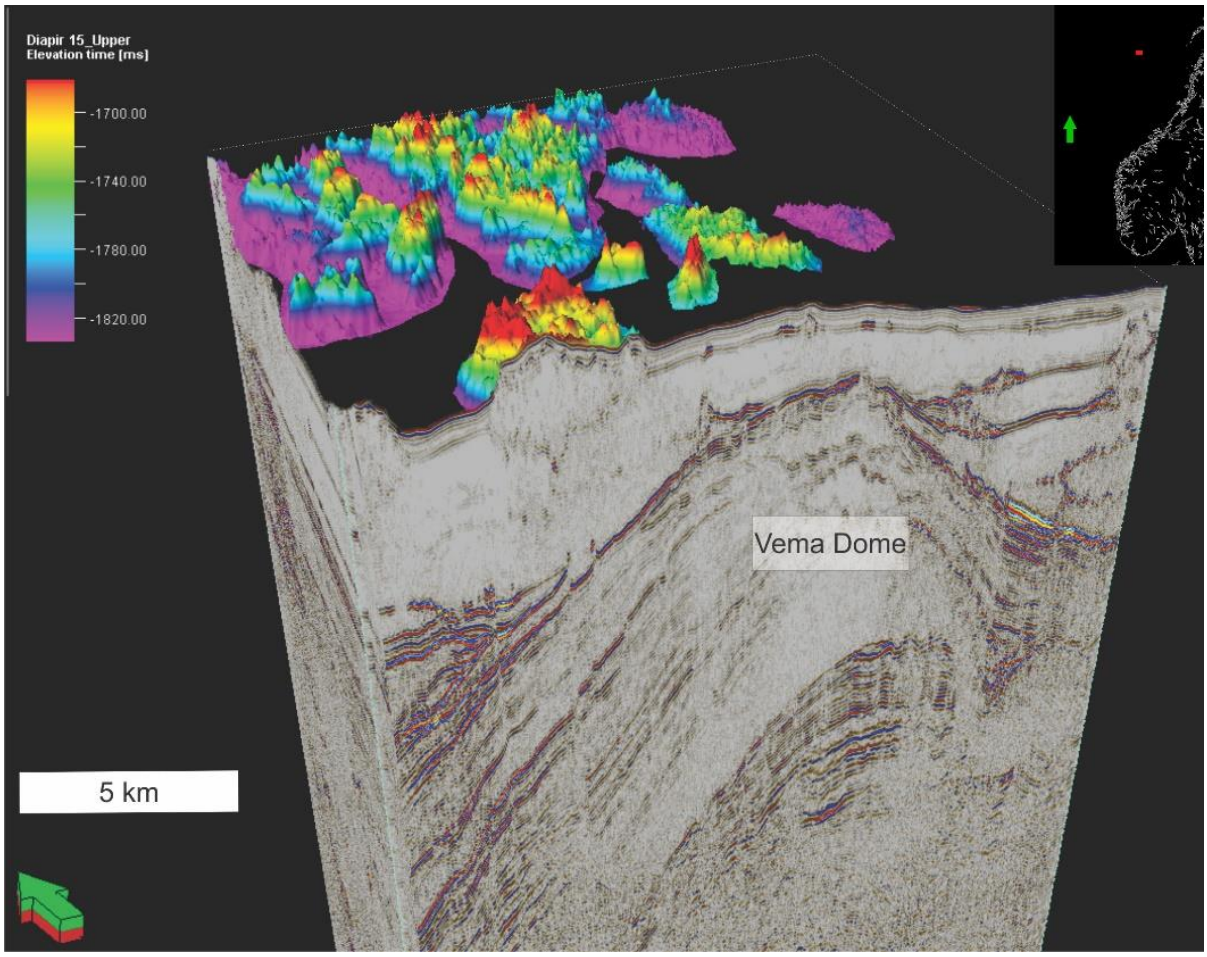

Figure 5.19 3D cube showing the mounded features in survey ST9603R99 with seismic lines showing the Vema Dome underneath.

When mapping these features, both an upper and lower boundary was defined. The upper boundary of the mounds follows a continuous reflector. The lower boundary was harder to define as the reflections are chaotic and have low amplitudes, and the underlying sediments are quite disturbed. A boundary was determined by following reflections that were semi-continuous. The diapirs almost reaching the seafloor shows a thin layer of stacked parallel reflections. This deposition on top of the mounds appears to be recent sedimentation infilling the rough topography of the uppermost diapiric structure, and there is no indication that this sedimentation was in place during emplacement of the features. Such indications include radial faulting around the emplaced feature, sediment sliding or slumping on the flanks and a non-uniform distribution of sediment over the features.

The internal seismic structure of the mounded features are hummocky and chaotic, with very low to almost no internal seismic reflections (fig. 5.20). Figure 5.20 shows a variance timeslice of one of the interpreted mounds that reach the top Naust reflection almost at the seafloor, and

a seismic line of the feature showing the hummocky structure and low to no seismic reflections. There are also some vertical columnar features below the mound interpreted in the previous chapter as chimneys.

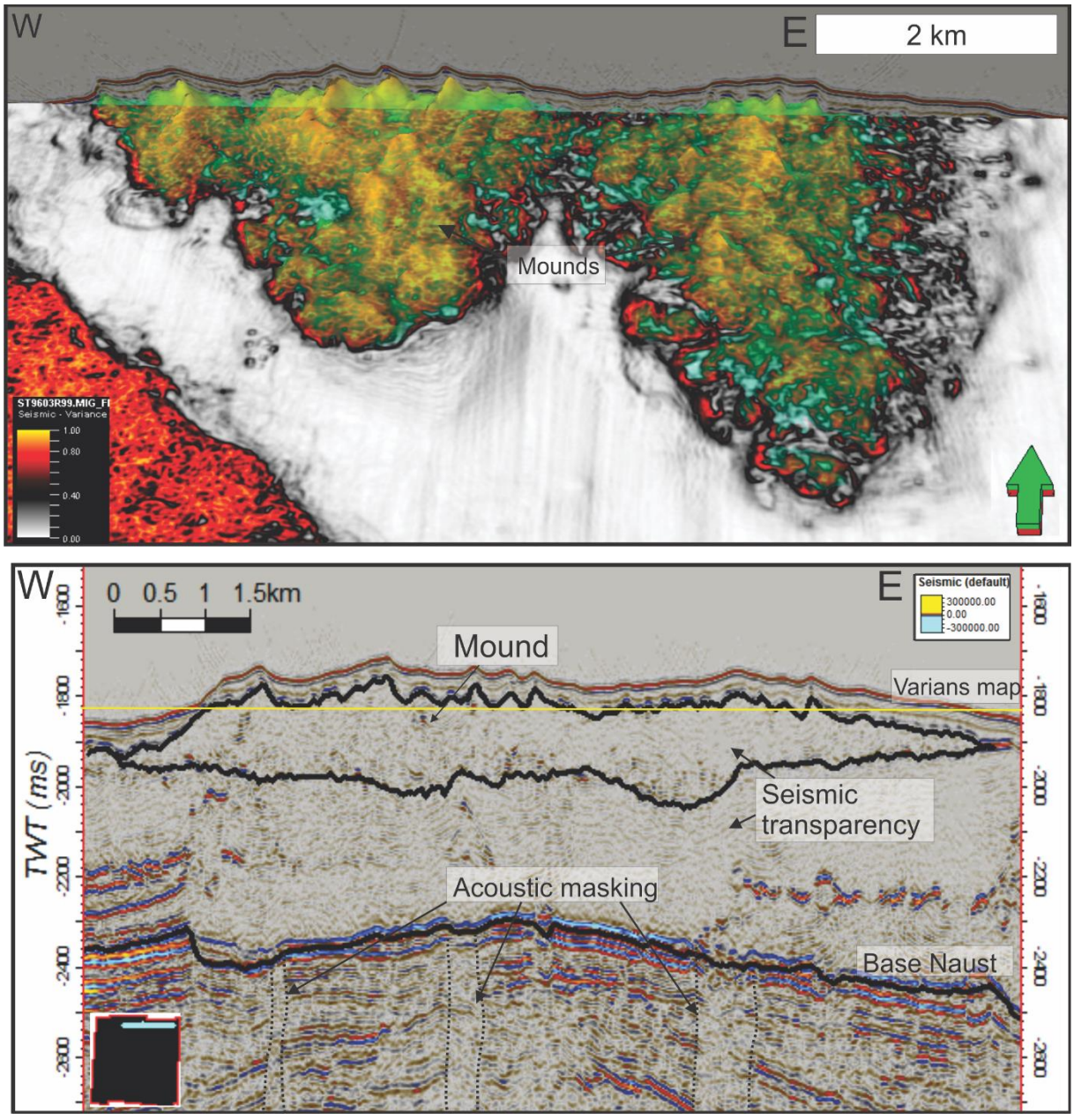

Figure 5.20 Above: 3D window of a timeslice of a variance attribute map with the interpreted top of the mound feature lain on top (green colour). Below: Seismic line showing the mounded feature near the seafloor. The variance timeslice is marked with a yellow line. Vertical amplitude anomalies, interpreted as fluid flow features in the previous chapter, are here marked with black dotted lines.

Figure 5.21 shows the mound that penetrates the base Naust reflector and a timeslice of a variance attribute map cutting through the feature, while figure 5.22 shows the surface of the top of the mound lain over the variance timeslice. This feature have the same internal structure

as the one penetrating the top Naust reflection. It is also hummocky on top, but with a lower relief than the other features (fig. 5.21 and fig. 5.22). This could possibly indicate that this feature at one point reached the seafloor, and as sediments in the Naust formation was deposited on top, the top of the feature was eroded.

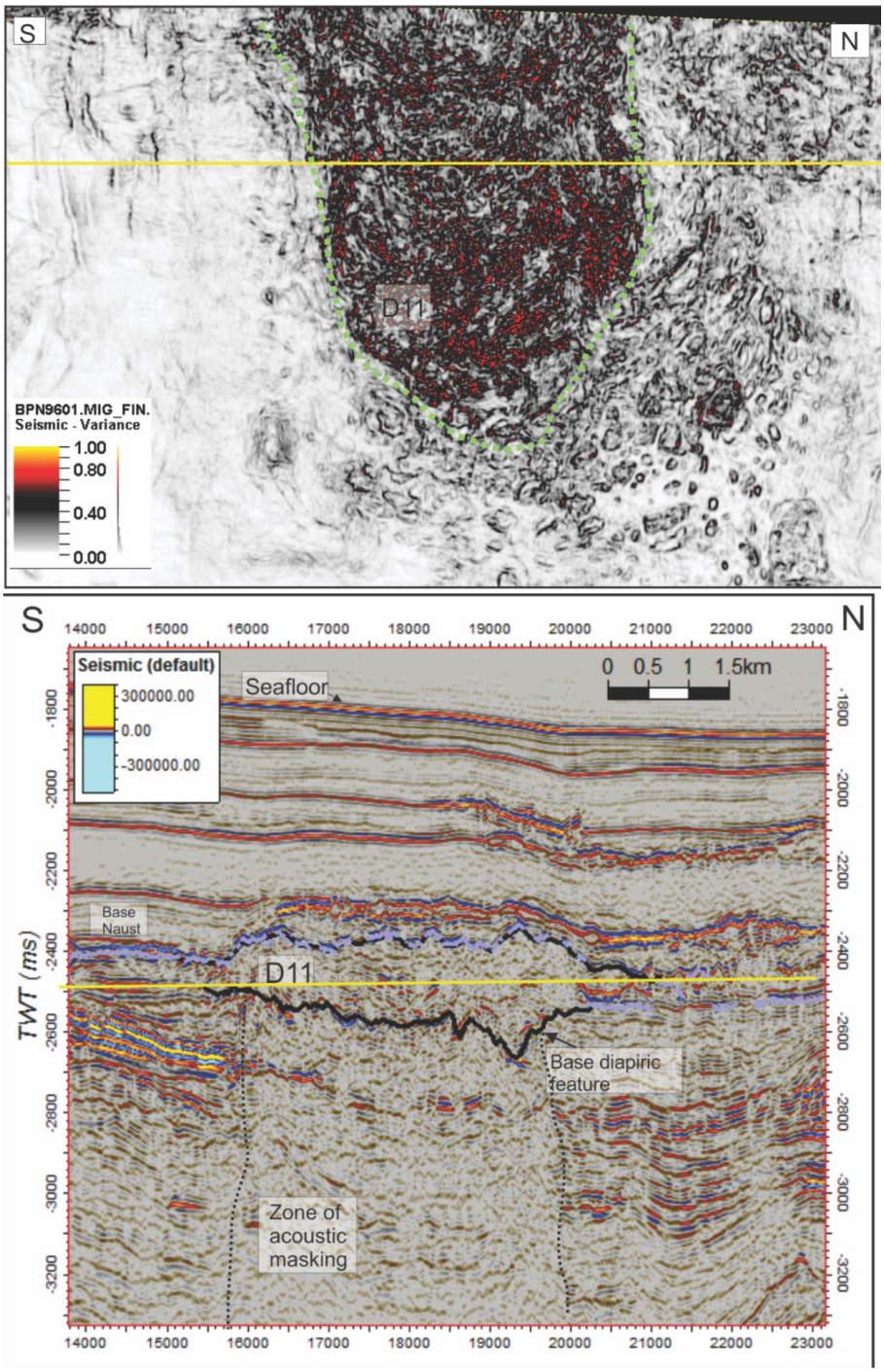

Figure 5.21 The deepest interpreted mound feature cutting through the base Naust reflection (purple horizon in lower section). The figure above shows a timeslice of a variance attribute map over the mound feature (outlined in black), and the yellow line indicates the position of the seismic line shown below. The lower figure shows a seismic line through the mound feature. The yellow line indicates the position of the variance timeslice.

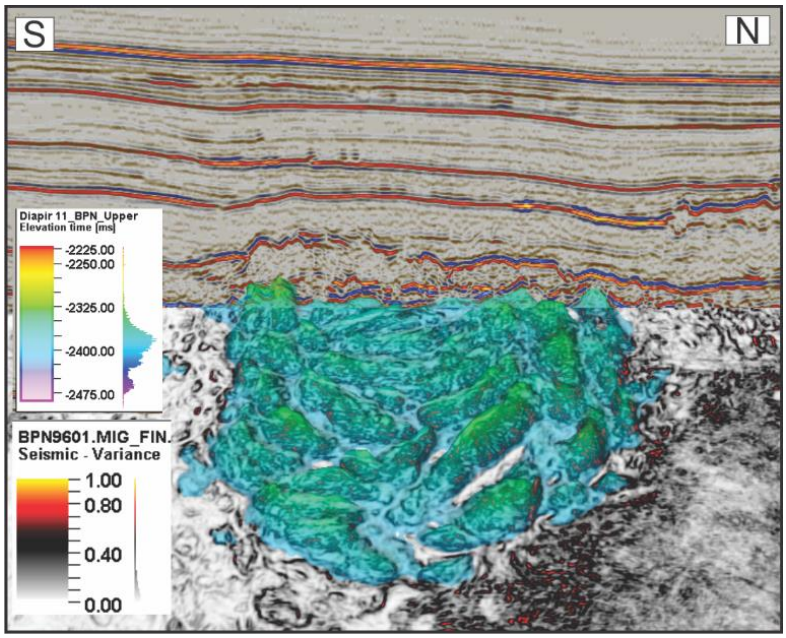

Figure 5.22 The same variance timeslice and mound feature as figure 5.17 shown in a 3D window with the generated surface of the top of the feature lain above the variance timeslice.

Figure 5.23 shows a 3D figure of mound feature D9, and is a good example of the hummocky upper surface of the mound features. The distance between the hummocks and troughs of these features can reach up to 300 ms and are quite steep.

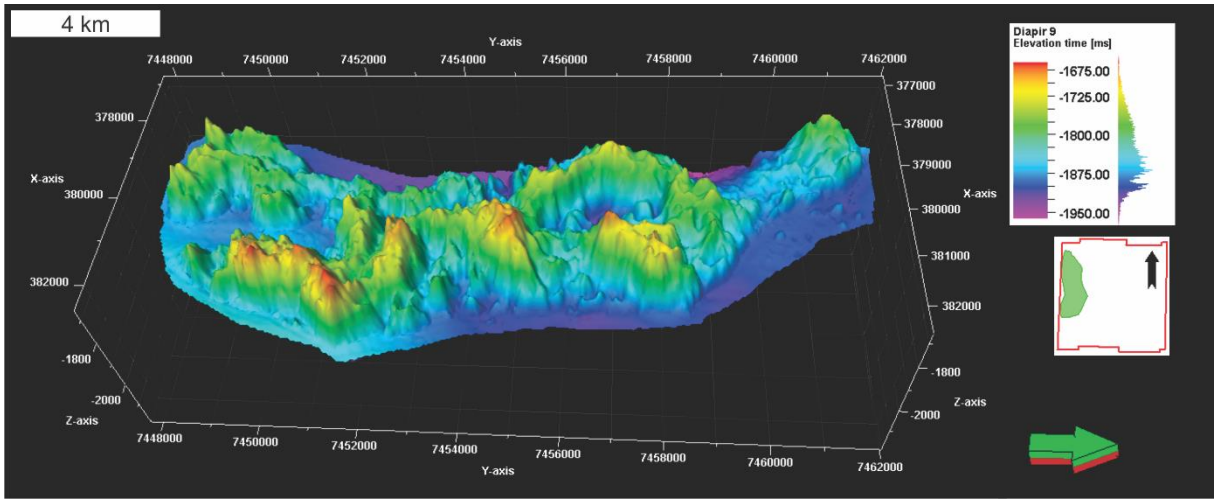

Figure 5.23 Surface map of interpreted mound feature D9 shown in a 3D window. This is a good example of the hummocky surface of the mound features. The distance between the hummocks and troughs of these features can reach up to 300 ms.

In table 5.2 the extent of the interpreted mounds are listed. The features vary in size, some of them being up to 10-13 km long while the smallest ones are only 1-2 km. Some of these features located at the edges of the 3D seismic surveys could also extend further outside of the study area.

Table 5.2 Summary of the interpreted mound features.

Diapiric mound feature	Dataset	Longest axis (km)	Shortest axis (km)	Vertical max. extent (ms TWT)
D1	ST9603R99	12.3 km	2.6 km	150 ms
D2	ST9603R99	3.7 km	3.5 km	370 ms
D3	ST9603R99	4.7 km	2.0 km	60 ms
D4	ST9603R99	2.2 km	0.8 km	160 ms
D5	BPN9601	5.6 km	4.1 km	130 ms
D6	BPN9601	2.8 km	2.5 km	120 ms
D7	ST9603R99	1.3 km	1.1 km	200 ms
D8	ST9603R99	13.5 km	7.3 km	350 ms
D9	ST9603R99	11.5 km	3.9 km	400 ms
D10	ST9603R99	11.2 km	4.6 km	250 ms
D11	BPN9601	4.6 km	4.3 km	280 ms

The mounds can be classified in three groups according to their size; big, medium and small. The big features are D1 and D8-10 and are located over the centre of the Vema dome (fig. 5.24). The medium size mounded features are D2-3, D5 and D11 and are mostly located towards the eastern end of the dome structure (fig. 5.24).

There also seems to be a characteristic difference in the base of the mounds, where the ones located on the eastern side of the dome have a flat base, while the one to the east have a deeper base. This distribution is shown in figure 5.24. Interestingly, the classification of these features delineates the crest of the Vema Dome.

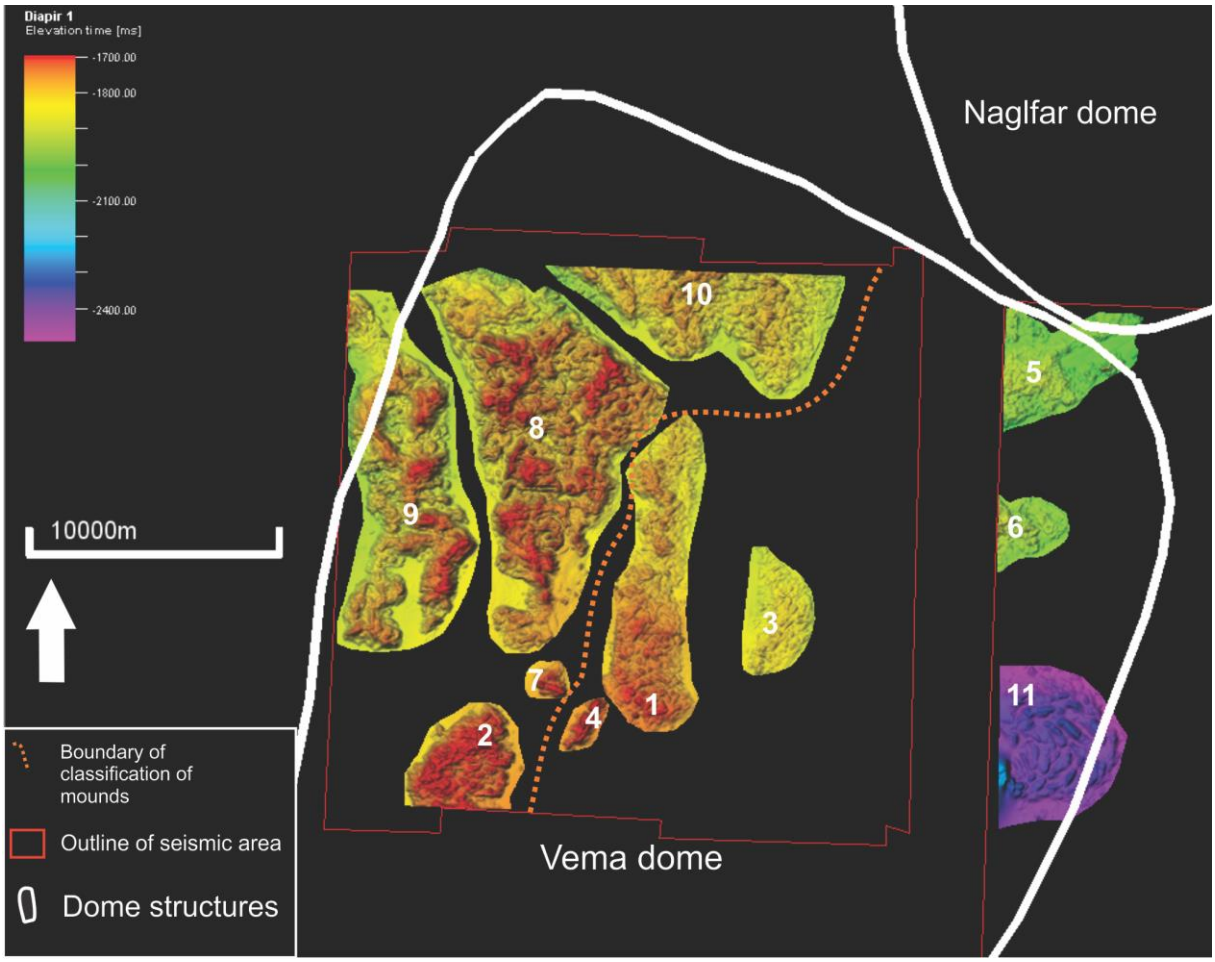

Figure 5.24 Overview map of the interpreted mound features. The orange line indicates a boundary where the mounds on the western side have deep bases whereas the feature to the east have flat bases.

Figure 5.25 shows a 3D window of two interpreted mounds, one with a flat base (D1) and one with a deep base (D10). The flat based feature D1 has a maximum vertical extent of 150 ms while D10 has a maximum vertical extent of 250 ms. The base in D10 are deepest at the centre of the mound feature. These features also show the hummocky upper boundary as shown in figure 5.23.

Thickness maps were generated between the upper and lower boundary of the mounds. Six of these are shown in figure 5.26. These thickness maps illustrate that the mounds are thickest around the center and thinning towards the flanks in all cases. Many of the mounds (D1, D2, D7, D9) also show a donut style thickness whereby a slight decrease in thickness is central to a flank of thicker structure.

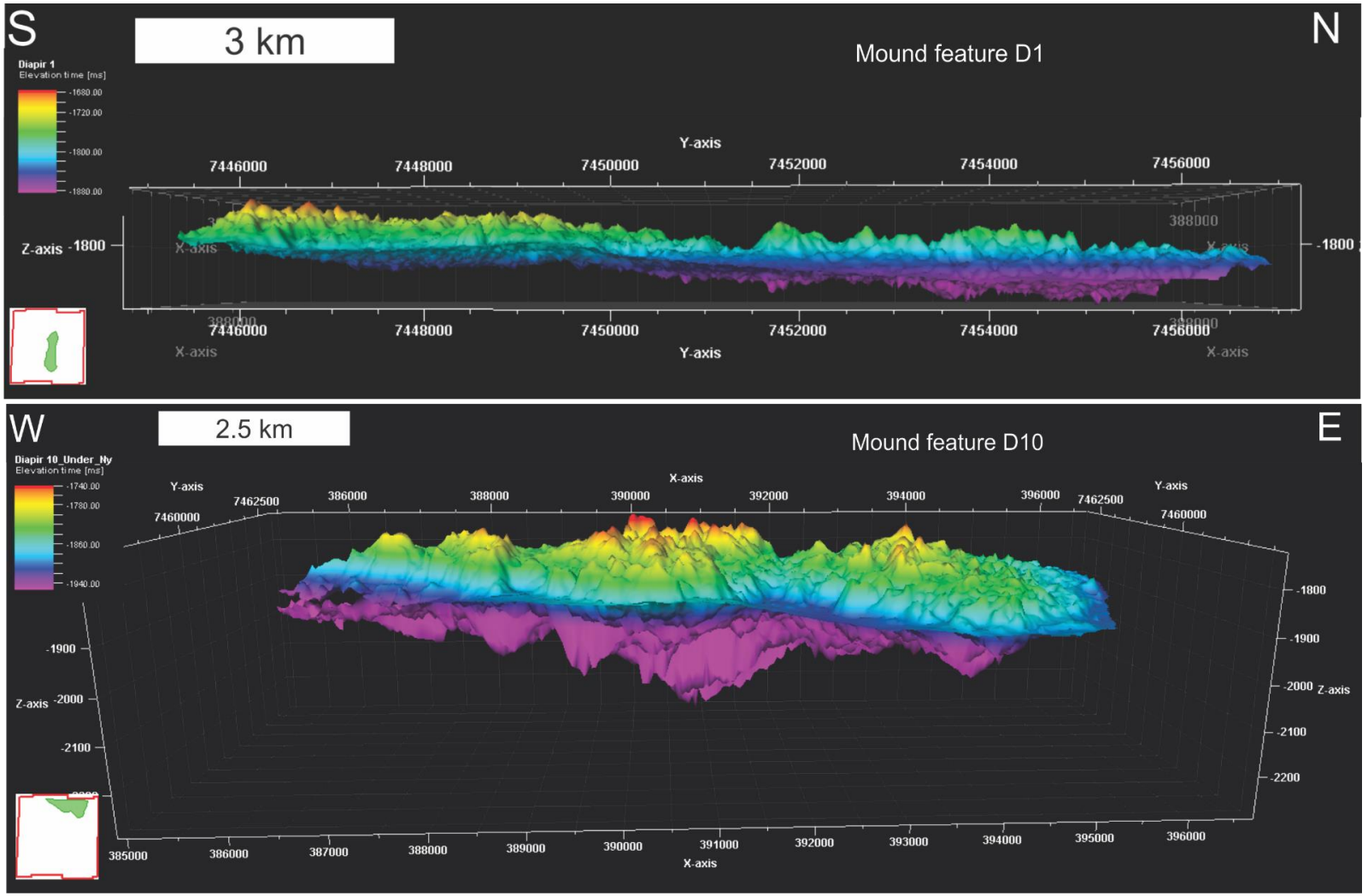

Figure 5.25 3D windows showing the interpreted mound features D1 and D10. Feature D1 is an example of the features with a flat base and D10 is an example of the mound featuers with a deep base.

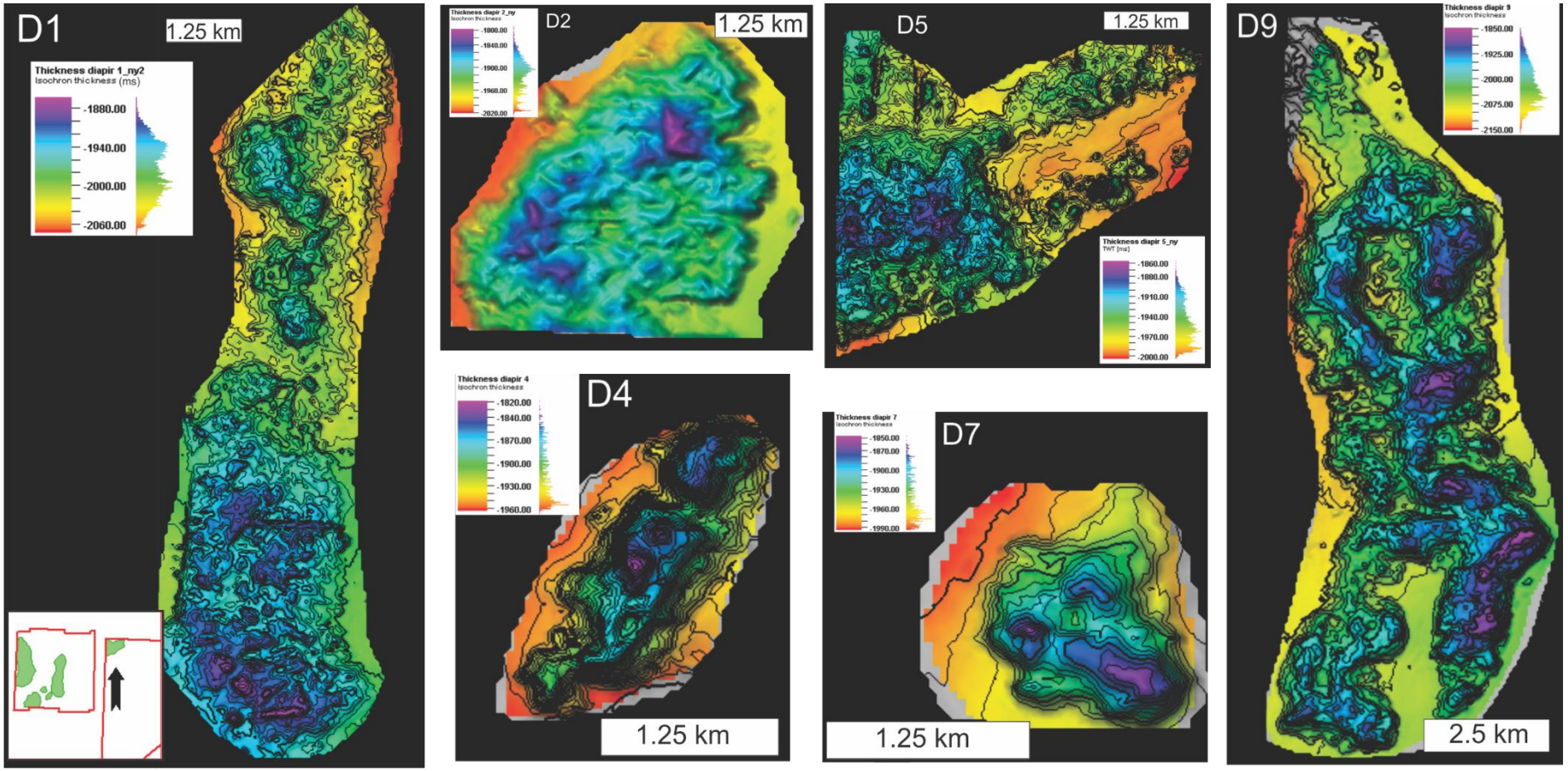

Figure 5.26 Thickness maps of six of the mounded features. The location of the mounds are shown in the polygons in the left lower corner.

Beneath these mounded features, there are indications in the seismic of many fluid migration pathways, such as chimneys and pipers, and some have also been interpreted as hydrothermal vents. These features were described in chapter 5.3. It is important to note that although vertical amplitude anomalies have been interpreted as fluid migration pathways, they could still be amplitude blanking due to scattering of seismic energy from the internal structure of the mound.

These mounded features with chaotic internal seismic pattern and very low seismic reflections have previously been studied by Hjelstuen et al., (1997) and Hovland et al., (1998) who interpreted these features as mud diapirs. This is a reasonable conclusion as they can be linked to the underlying plumbing system with sills and hydrothermal vent complexes (fig. 5.10, fig. 5.11, fig. 5.14, fig. 5.16 and fig. 5.20) and do not show any indications of the sediments coming from a lateral source. The donut pattern in thickness maps indicates that there is a distinct eruption site, similar to an eruption crater on a volcano where the thinned center is indicative of the location of outflow and the thickened flanks are the primary deposit location (Hovland and Judd, 1988)

5.5 Summary of interpretations

There are three major features which have been interpreted here; the sill complex, plumbing systems and diapirs. The sills were interpreted based off their anomalously high amplitude, cross-cutting relationship with the surrounding strata and characteristic shape (i.e. Planke et al., 2005). Sill emplacement is common throughout the Vøring basin so it is not unusual to find such features in this study area therefore the interpretation of these features is highly confident. Plumbing systems are interpreted based on the lowered amplitude, vertical nature and that they coincide with sill emplacements. The formation of hydrothermal vents in other parts of the Vøring Basin has been linked to sill intrusion and overpressure of fluids caused by the heat from the intrusions. These vents are normally seen close to the tip of sill intrusions. In this study area, the fluid migration pathways are also coincident with intrusion tips, and have characteristic amplitude blanking as well as forming near vertical pathways upwards in the sedimentary strata. All the vertical amplitude blanking zones in this study area have been interpreted as fluid migration pathways. However, amplitude blanking is common beneath structures such as diapirs due to energy scattering off complex structures could represent this effect. However in the preserved amplitude beneath the features it appears that there are disturbances in the sediment such as pull downs that are not consistent with the amplitude blanking being simply related to energy scattering above. Therefore, even though energy

scattering through the diapir structure could be contributing to the zone of amplitude blanking, they are still interpreted as migration pathways nonetheless because of their correspondence to sill tips. As all the migration pathways would presumably be acting as heat release vents for the sills, they could be termed hydrothermal vent systems and indeed some of the structures have a characteristic push-up/eye structure (fig. 5.12) as noted by Planke et al., (2005) as being common in buried hydrothermal vents.

Diapirs are mounded features which have chaotic internal reflections, a complex morphology and do not preserve any reflectivity from the surrounding strata. These three types of features interpreted here appear to be very well connected to each other, where diapirs often have large plumbing systems directly linking them to the sills beneath. The plumbing systems are often originating at the tip of the sills which is characteristic of sill-hosted hydrothermal systems (Planke et al., 2005). I interpret here that there is a relationship between the formation of the three features in this study area.

6 Discussion

This chapter will discuss the mound structures, amplitude anomalies and the possible fluid flow features observed in the 3D seismic surveys ST9603R99 and BPN9601. The goal is to integrate observations and interpretations to gain insight into the development and controlling factors of the diapiric mound structures, and how they relate to the fluid flow system in the Vøring Basin.

6.1 Polygonal faults and their relation to the fluid flow system

There is one set of polygonal faults limited to the southern end of survey BPN9601 and decreasing northwards in the survey area (fig. 5.6). As mentioned in chapter 2.3.2, the formation of polygonal fault systems is related to fluid flow processes where fluids are expelled from the sediments. This can be as a result of compaction and consolidation processes during burial, where compaction can lead to dewatering of sediments (Cartwright, 1996). Polygonal faults are often confined to lithological units consisting of fine-grained sediments where interconnected pore space is limited and so fluid overpressure forms faults in order to move towards lower pressure gradients.

The polygonal faults identified in the survey are all confined to an interval of 2500 ms and 2990 ms terminating in the base Naust reflector. Areas with polygonal faults have been identified within mud dominated sequences of upper Miocene to lower Pliocene age throughout the entire Vøring Basin (Berndt et al., 2004). Fluid migration in relation to these polygonal faults have previously been documented in other studies in the Vøring basin (i.e. Gay and Berndt, 2007 and Hustoft et al., 2007).

The formation mechanism of polygonal fault systems has been linked to fluid flow; however, polygonal faults are also documented to be migration pathways for fluids after the initial compaction-dewatering phase. Sibson (1996) shows the importance of small offset faulting and fracture networks as hosting significantly more fluid migration than in single, large offset faults for hydrothermally driven fluid migration. Ligtenberg (2005) shows that intersections in polygonal fault systems are a key feature for mud mound formation in other regions of the Vøring Basin, deeming areas with multiple intersecting planes ‘leaking’ vs. few intersections ‘sealing’. The polygonal fault system in this area 1) is not spatially coincident with diapirs and 2) does not show a significant number of intersections (fig. 5.6). Although dewatering of sediments outside the Vema Dome might have impacted the plumbing system on the Vema

Dome, it was not found any evidence in the data available that polygonal faulting was important in the formation of diapirism here.

6.2 Sill intrusions and overlying plumbing system

The mid-Norwegian continental margin consists of several volcanic basins such as the Møre and Vøring basins. Sill complexes of Palaeogene age have been identified in the Møre and Vøring basins that extend more than 80 000 km^2 (Planke et al., 2005).

Within the study area, five amplitude anomalies were mapped. These have the same seismic appearance that previous studies have identified as sill intrusions (Planke et al., 2005). The sill intrusions have been identified within 2795 ms and 4060 ms. The overall trend of the sill is to be relatively parallel with the host rock reflections which could indicate that the sills have been emplaced before doming took place. Although sill intrusions may follow a plane of weakness during emplacement, inferred dates of sill emplacement in the wider Vøring Basin and inferred doming in the region also supports that sill emplacement occurred before formation of the Vema Dome (Hovland et al., 1998, Planke et al., 2005). In the Vøring basin, magmatic intrusion was most active during the late Paleocene in relation to the continental rifting and breakup (Hjelstuen et al., 1999). The Vema Dome was mainly formed during Eocene until Late Pliocene times, but some minor uplift is thought to have continued until present (Blystad, 1995).

There seems to be a good spatial relationship between the sill intrusions and overlying fluid flow features, where the bigger chimneys and hydrothermal vents are located above the tip of sill intrusions (e.g. fig. 5.11, fig. 5.15). The formation of these chimneys and vents began to form after the emplacement of the sill complexes. These chimney features have then later acted as pathways for migrating fluids and mud.

Jamtveit et al (2004) studied hydrothermal vents in the Karoo Basin, where they suggested that during initial phases of vent formation, fluid pressure built up to well above lithostatic, disaggregating and brecciating the sedimentation. Initial venting was responsible for a marked pressure decrease, however the lowered pressure gradient in the brecciated material compared to the unaffected sediment was able to sustain fluid and sediment remobilization through the plumbing system on a smaller scale. This second stage with decreased pressure can be sustained for a long time which can have a long term effect for migration of fluids in a sedimentary basin (Planke et al., 2005)

As mentioned in chapter 2.1.2 heating from the emplacement of sills can cause dewatering and fracturing of the sedimentary host rock. If there is sufficient pressure build up due to fluid boiling, leading to overpressure, fluids can start to migrate upwards through hydrofractures and develop hydrothermal vents systems (Iyer et al., 2013, Jamtveit et al., 2004). Planke et al., (2005) also states that the presence of hydrothermal vents are affected by the geometry of the sills and the permeability and composition of the host rock.

In the study area, the plumbing system overlying the sills is mainly interpreted based on the seismic amplitude characteristics. There is one particular instance where the interpretation of a hydrothermal vent correlates to the classic description of hydrothermal vent systems in the Vøring Basin by Planke et al., (2005). However, the plumbing system described here need not be forming the typical crater, eye and mound structures to be hosting hydrothermally sourced fluid migration and therefore still influencing processes on the Vema Dome. In fact, any plumbing system that distributes heat from thermal anomalies through the subsurface may be termed hydrothermal systems regardless of surface expression (Norton, 1984). Intrusion hosted hydrothermal venting systems source fluid through either contact metamorphism and alteration processes which result in water generation, or by promoting circulation of fluid already contained within the host rock (Norton, 1984). Heat transport occurs at a faster rate, over a shorter time if much of the heat can be transported via convection rather than conduction, and when there is already fluid available in the host rock then much of the heat transport will take place via convection (Norton, 1984). In a marine sedimentary environment, there is already fluid contained within the pore space and so on the Vema Dome the sedimentary host rock likely contained fluid when sills emplaced. It is unlikely that compressional processes or mineral precipitation and alteration processes consumed all the pore fluids (Norton, 1984) before sill emplacement. Therefore, the nature of fluid sourced from the sills on the Vema Dome was most likely convection due to the pore space already containing fluid, and would have been hotter, occurring faster but less long-lived than a conductive system (Norton, 1984).

The compressional tectonic regime that created the Vema Dome would have most likely changed the nature of fluid redistribution through the plumbing system present. It has been shown that in compressional systems the mode of fracture and fault generation tends to be different from extensional environments (Sibson, 1996, Sibson, 2000). This in turn may have played a role in why the plumbing system redistributing heat in the subsurface on the Vema Dome appears different from the hydrothermal vent structures described by Planke et al. (2005).

The change towards a compressional environment during the doming process may have also played a role in the longevity of the fluid migration system once the thermal perturbations from sill emplacement had weakened.

6.3 Linking diapirs to underlying plumbing system

6.3.1 Possible source material

The hummocky appearance of the diapirs piecing the seafloor is also characteristic for other features, e.g. mass transport deposits (Hjelstuen et al., 1997). Laterally sourced material is possible, however if this is the case, the diapirs themselves would likely have a size-orientation correlation indicating the direction of where the material migrated from – i.e. they would gradually decrease in size away from the source. The features in this area do not show any such evidence of lateral movement, as the mounds are generally discreet lobate features with sharply unevenly distributed material (fig. 5.24). Mass transport deposits typically have certain internal characteristics based on 1) their proximity to the source and 2) the mechanical behaviour of the flow (Nardin et al., 1979). The hummocky upper reflector of the mounds in this area would correlate to plastic or elastic flows, so slides or slumps (Nardin et al., 1979). However, key characteristics of these types of deposits are a very high amplitude basal reflector, with either seismically transparent internal structure or evidence of non-disintegrated block material (Nardin et al., 1979). The internal structure of the mounds here does not show any of the characteristics of sliding or slumping (fig. 5.20, fig. 6.1), the basal reflector also has a low seismic amplitude and is difficult to define from the surroundings, suggesting that these are not slide or slump deposits (fig. 6.1). It is not likely that the source material is derived from the Naust debris flow material, as the diapirs then would most likely be as widespread as the Naust material is.

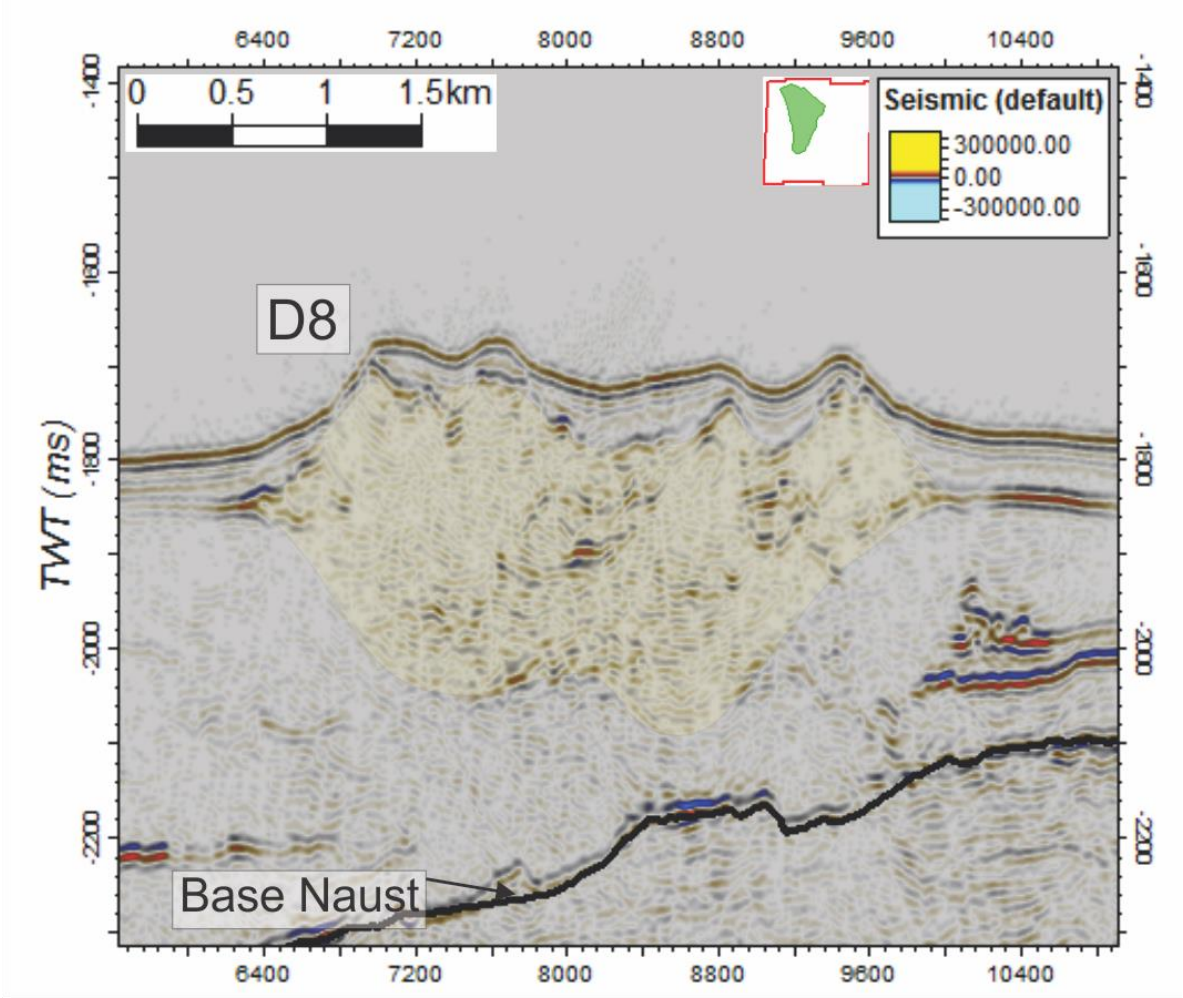

Figure 6.1 Seismic line showing the interpreted diapir D8 shaded in light yellow. the Base Naust reflection is marked with a black line. The lower base of the feature does not show any clear boundary with a strong amplitude indicating that this is not a slide of slump deposit.

If the source material does not derive from a lateral source, then it must have come from a vertical source somewhere in the subsurface. A more likely source are ooze sediments from the Brygge or Kai Formations. According to Hjelstuen et al. (1997), sediment cores taken over the diapirs and on the flanks of the Vema Dome indicates that the diapirs consist of coccolith ooze belonging to the Brygge and Kai formation. These sediments have a lower density and higher porosity than the overlying glacigenic debris flow sediments of the Naust formation which can initiate gravitational instability and be a contributing factor for diapirism (Hjelstuen et al., 1997). Additionally, as indicated in figure 5.26, the thickness maps indicate that these structures have a defined thick circular/ellipsoidal shape within the area interpreted as a diapiric structure with a thinned section in the middle. The thinned inner area with thicker flanks is indicative of a discreet expulsion site, with material expulsed depositing on the flanks. The

expulsion point remains thinner because the turbulence of ejected material stymies sediment deposition here (Hovland and Judd, 1988, Orange et al., 1999).

6.3.2 Linking diapirs to underlying plumbing system

As mentioned above, there is no indication of lateral mass movement connected to the features interpreted as diapirs and the source material must originate from the subsurface. As fluids and fluidized sediments move vertically towards the surface though sediment bedding planes, faults and vertical fluid flow features such as hydrothermal vent systems, the interpreted chimney features most likely act as migration pathways in this area.

The results in chapter 5 indicate that there is a clear correlation between the magmatic sill intrusions, acoustic chimneys and the mud diapirs. Figure 6.2 shows the sill intrusions overlain by the diapirs. This and figure 5.6, 5.8, 5.10 and 5.13 show that most of the diapirs are located directly above the sill complexes on the Vema Dome. As noted by Hjelstuen et al., (1997) mud diapirs are usually characterized by a consistent flow of mud from depth rather than episodic flows from a shallow source as in mud volcanism. Sill emplacement would provide a long-lived heat source leading to a constant flow of fluid towards the seafloor as opposed to episodic flow that a trigger point, for example seismicity/fault reactivation, would create. Additionally, remobilization of mud is dependent on overpressure which requires burial to relative significant depth (Huuse et al., 2010) The interpreted chimney features are clearly rooted at the tip of the sills and connect the sill intrusions to the diapir structures. Given the necessity of a plumbing system linking sediments at depth to the diapirs, and a triggering mechanism for a consistent flow of mud to the subsurface, it is highly likely that the imaged chimney structures are acting as fluid migration pathways. These chimney structures can be divided into two groups of chimneys, one being hydrothermal vents linked to the underlying sills, and the other being small faults, chimneys and pipes linked to overpressure in the subsurface (fig. 5.17). Some of the features might still appear broader or the anomalous low amplitude further weakened by energy scattering effects through the diapirs, however based on the physical constraints for diapir formation, the chimney structures are the best candidate for hosting fluid migration in the available datasets.

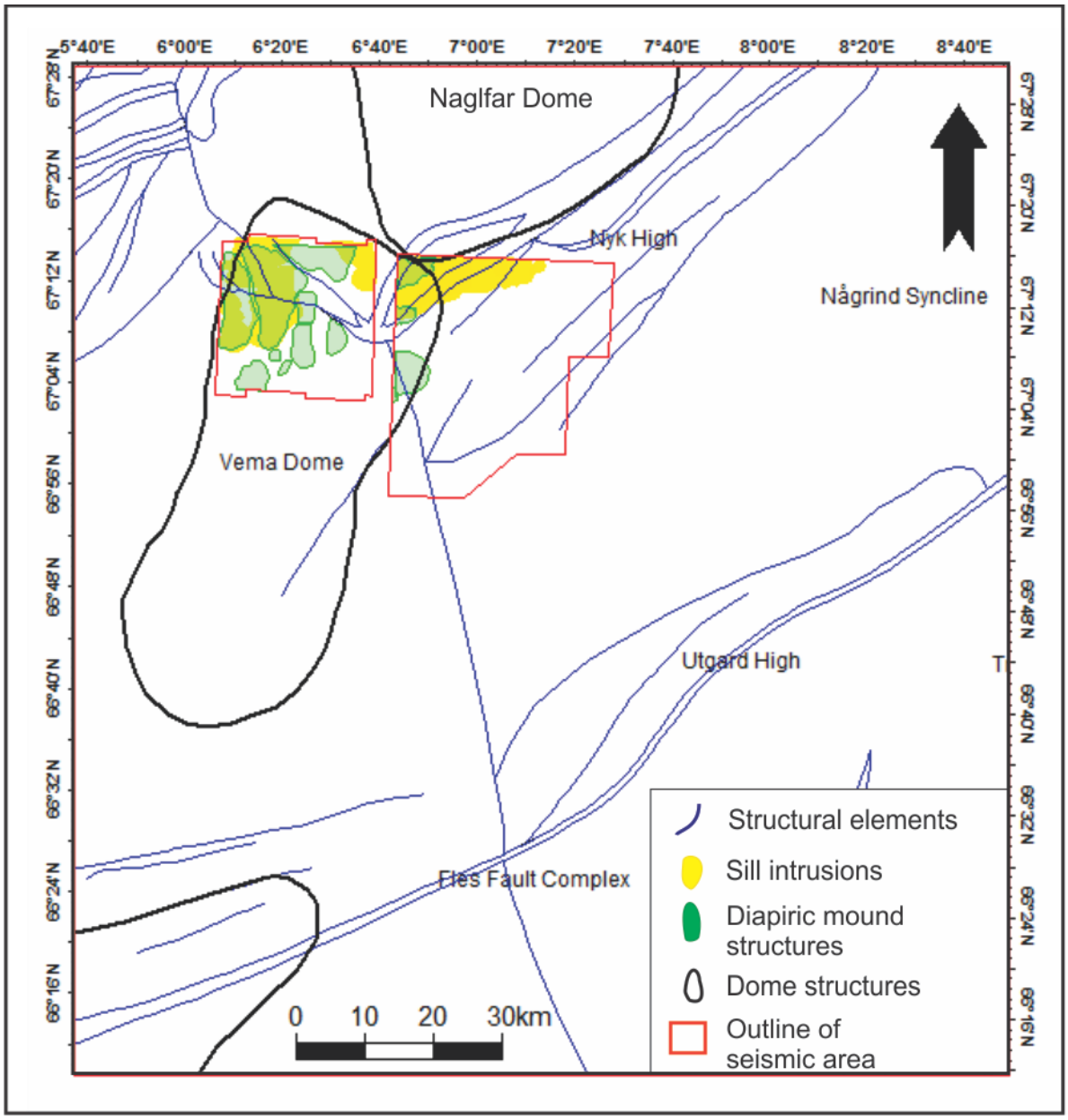

Figure 6.2 Overview of sill intrusions and diapiric mound structures lain on top of each other. Sill intrusions are yellow and diapirs are in green. The sill intrusions and diapirs correlate well over the northern part of the Vema dome.

Presence of gas is often associated with remobilization of mud and diapirism as gas provides additional buoyancy to the fluid which allows migration further towards the subsurface once the fluids reach hydrostatic pressure in the subsurface (Huuse et al., 2010). There is however no evidence of gas accumulations in the survey. Hovland et al., (1997) and Hjelstuen et al., (1997) both link the presence of gas to the formation of the diapirs, and lesser amounts of gas was found in well 6706/11-2. In the datasets, there is no evidence of negative amplitude anomalies, bright or flat spots, or enhanced crosscutting reflectors which generally indicate hydrocarbon accumulations. Since there is no clear acoustic indication of gas or heavier

hydrocarbons in the seismic data, the importance of hydrocarbons to the diapirs cannot be determined.

6.3.3 Importance of the Vema Dome

There is one main feature that differs from the area where there has been active diapirism and the surrounding where the seafloor is relatively featureless. Vertical fluid flow features and sill complexes have been documented in the entire Vøring Basin and the stratigraphy is also relatively the same throughout the basin. The main difference is the structural high, the Vema Dome.

Stuevold et al., (1992) suggest a model where continued doming after the initial mechanism of dome formation occurs due to increased sediment loading and differential subsidence. In this model, the increase in sediment loading occurs due to the debris flows of the Naust where considerable material is deposited in a short timespan. This increase in loading enhanced lateral instabilities in the pre-existing dome and reactivated faulting (Stuevold et al., 1992). Before the doming mechanism onset during the Miocene, the area was a structural high with low relief. Today the Vema Dome has a relief of 1800-3000 m and it is thought that the doming mechanisms are still active (Hjelstuen et al., 1997).

Doming of the stratigraphy causes weaknesses in the material which, with an increase in strain can breach to faults depending on the mechanical strength of the rock (Bott, 1981, Hardy and McClay, 1999). These faults and fracture networks can further increase the permeability and work as migration pathways. Dome formation generally happens in compressive environments as the maximum compressive stress needs to be acting in the horizontal plane generally (Zoback et al., 1989) which implies that there has been a local change in tectonic regime over the dome area to induce a compressive feature in an extensional basin (fig. 6.2). As the doming mechanism is likely to create planes of weakness, or faulting, in the strata, that otherwise would not be present over the greater Vøring Basin, fluid flow related to sill intrusions and overpressuring mechanisms haves an already established plumbing system to utilize rather than ‘forcing’ hydrothermal vent structures. Therefore, the Vema Dome faulting and stress regime coupled with the availability of appropriate material and the presence of sill intrusions promoting fluid flow has led to localised diapirism on the Vema dome where in the rest of the Vøring Basin the fluid flow processes are expressed by other modes, for example hydrothermal venting and polygonal faulting.

The sills may have had a contributing factor in enhancing the doming by heating the surrounding rocks. The doming process could "push" the fluids and mud through the system as the doming generated faults and fractures which also work as migration pathways.

6.3.4 Longevity of diapirism over the Vema Dome

The longevity of diapirism on the Vema Dome is difficult to determine based on the available data. Within the survey area there is only one diapir that does not breach the top Naust reflection and can therefore be regarded as the oldest one (fig. 5.21). The rest of the diapirs breach the top Naust reflection, most of them with some sedimentation on top (fig. 5.20). There are no diapirs recognised which are emplaced within the centre of the Naust. Whether there has been a period between the deepest diapir and the shallow diapirs with no active diapirism here is hard to determine as Hjelstuen et al., (1997) show the diapir field extends further north than the data in this study covers. Hjelstuen et al., (1997) has also mapped diapirs in the subsurface within the Naust outside of the available data. Since there is one diapir in the study area that is apparently older, and mud diapirism is associated with a constant flow one could possibly argue that diapirism has been active in the area throughout the Naust deposition – i.e. the time between the deepest and shallowest diapirs. Another possibility is that the deepest diapir is not related to the rest of the diapirs at all and might actually be a result of a single event as it is deeper than the rest of the mapped diapirs and has a more circular shape than the rest. It also has a more distorted feeding zone underlying compared to the rest. The deep diapir imaged could therefore be 1) an old mud volcano 2) a sediment remobilization feature that has emplaced in the subsurface rather than breaching the seafloor or 3) evidence of the onset of diapirism on the Vema Dome. If it were an old mud volcano, there should be evidence of stacking flows (Huuse et al., 2010), however this feature has the same internal structure as all the other diapirs. The slightly differing shape could imply a sub-seafloor emplacement, however in this case there should be evidence within the Naust of overlying sediment accommodating the emplacement. The differing shape might also be representative of erosion over the top of the feature during Naust deposition. As the Naust predominantly deposited as large debris flows, the top of the diapir would be more prone to erosion and redeposition processes than under the present-day conditions. As there is no evidence above the deepest diapir that would imply a sub-seafloor emplacement, the logical conclusion is that the deepest diapir in this area is also likely the oldest. This suggests that the process of diapirism started around the onset of Naust deposition, with these datasets suggesting a hiatus in diapirism but other studies (i.e. Hjelstuen et al., 1997)

suggesting continued diapiric activity. This implies that the hypothesis by Stuevold et al., (1992) and Hovland et al., (1998) that sediment loading has increased differential pressure has been important in triggering diapirism.

7 Summary and conclusion

- Using two seismic datasets from the Vema Dome region of the Vøring Basin, this study aimed to link diapiric mound features to underlying fluid flow features and sill complexes.
- One set of polygonal faults is observed in the lower part of the Naust formation. There is no evidence suggesting that these have been important in the development and triggering of the diapirs as they are not spatially coincident with the diapirs.
- Three main features have been documented; diapiric mound structures, underlying plumbing system and sill intrusions.
- The sill intrusions are recognized in the seismic as high amplitude anomalies confined to an interval between 2785 ms – 4060 ms. The sills were mapped and interpreted on RMS amplitude maps and vertical seismic sections. The sills show a dip up towards the center of the Vema Dome indicating that they were emplaced before compressional tectonics produced the Vema Dome structure.
- Vertical columnar areas with low seismic amplitude are interpreted as focused fluid flow pathways, known as chimneys, pipes and leaking faults. These fluid flow structures can be divided into two separate types. The smaller pipes and faults have been linked to overpressure in the subsurface. The bigger chimneys can be linked to the tip of sills and termed hydrothermal vents. Both these features can be linked to the overlying diapirs, and make up the plumbing system in the survey area.
- Eleven diapirs have been mapped in the survey area and are recognized in variance attribute maps. Ten of these penetrate the top Naust reflection and show a thin layer of recent sediments on top, while one cuts the base Naust reflection. The dataset indicates that diapirism started in the area at the onset of Naust deposition, and that there has been a hiatus in diapirism.
- Thickness maps of the diapirs indicate that the diapiric structures have a defined thick circular/ellipsoidal shape with a thinned section in the middle indicating a discrete eruption site where material has been deposited on the flanks.

- The results in this study indicate that diapirism on the Vema Dome seem to be a result of three mechanisms acting together or successively; 1) the emplacement of sills leading to hydrothermal vents and other chimney features representing pathways for fluid migration into the shallow overburden, 2) buoyancy due to density difference of oozes

of the Kai and Brygge formations overlain by rapidly deposited glacigenic debris flows of the Naust formation, and 3) the uplift of the Vema Dome leading to the development of overpressures, faults and fractures. The results and discussion suggest the following timing of events:

1. Emplacement of sill complexes during Paleogene times which caused boiling of fluids that lead to overpressure and hydrothermal fluid flow.
2. The rising of the Vema Dome then started during Eocene times causing additional weaknesses, small scale faults, and a localized variation in the stress regime and further overpressure.
3. Deposition of glacigenic debris flow sediments over the oozes in the Kai and Brygge formations caused sediment loading and compaction and buoyancy forces remobilized ooze sediments to start migrate upwards.

8 References

ANDREASSEN, K., NILSSEN, E. G. & ØDEGAARD, C. M. 2007. Analysis of shallow gas and fluid migration within the Plio-Pleistocene sedimentary succession of the SW Barents Sea continental margin using 3D seismic data. *Geo-Marine Letters,* 27**,** 155-171.

ANDRESEN, K. J. 2012. Fluid flow features in hydrocarbon plumbing systems: What do they tell us about the basin evolution? *Marine Geology,* 332**,** 89-108.

BERG, R. R. 1975. Capillary pressures in stratigraphic traps. *AAPG bulletin,* 59**,** 939-956.

BERNDT, C. 2005. Focused fluid flow in passive continental margins. *Philosophical Transactions of the Royal Society of London A: Mathematical, Physical and Engineering Sciences,* 363**,** 2855-2871.

BERNDT, C., BÜNZ, S., CLAYTON, T., MIENERT, J. & SAUNDERS, M. 2004. Seismic character of bottom simulating reflectors: examples from the mid-Norwegian margin. *Marine and Petroleum Geology,* 21**,** 723-733.

BERNDT, C., BÜNZ, S. & MIENERT, J. 2003. Polygonal fault systems on the mid-Norwegian margin: a long-term source for fluid flow. *Geological Society, London, Special Publications,* 216**,** 283-290.

BJØRLYKKE, K. 2010. Petroleum Geoscience: From Sedimentary Environments to Rock Physics., chap. Introduction to petroleum geology. Springer Science.

BLYSTAD, P. 1995. Structural elements of the Norwegian continental shelf. Part 2: The Norwegian Sea region. *NPD Bull.,* 8.

BOTT, M. 1981. Crustal doming and the mechanism of continental rifting. *Developments in Geotectonics.* Elsevier.

BROWN, K. & WESTBROOK, G. 1988. Mud diapirism and subcretion in the Barbados Ridge accretionary complex: the role of fluids in accretionary processes. *Tectonics,* 7**,** 613-640.

BROWN, K. M. 1990. The nature and hydrogeologic significance of mud diapirs and diatremes for accretionary systems. *Journal of Geophysical Research: Solid Earth,* 95**,** 8969-8982.

BUKOVICS, C. & ZIEGLER, P. A. 1985. Tectonic development of the Mid-Norway continental margin. *Marine and Petroleum Geology,* 2**,** 2-22.

BULAT, J. 2005. Some considerations on the interpretation of seabed images based on commercial 3D seismic in the Faroe‐Shetland Channel. *Basin Research,* 17**,** 21-42.

CARTWRIGHT, J. 2007. The impact of 3D seismic data on the understanding of compaction, fluid flow and diagenesis in sedimentary basins. *Journal of the Geological Society,* 164**,** 881-893.

CARTWRIGHT, J. 2011. Diagenetically induced shear failure of fine-grained sediments and the development of polygonal fault systems. *Marine and Petroleum Geology,* 28**,** 1593-1610.

CARTWRIGHT, J., JAMES, D. & BOLTON, A. 2003. The genesis of polygonal fault systems: a review. *Geological Society, London, Special Publications,* 216**,** 223-243.

CARTWRIGHT, J. & SANTAMARINA, C. 2015. Seismic characteristics of fluid escape pipes in sedimentary basins: implications for pipe genesis. *Marine and Petroleum Geology,* 65**,** 126-140.

CARTWRIGHT, J. A. 1996. Polygonal fault systems: a new type of fault structure revealed by 3-D seismic data from the North Sea Basin.

CARTWRIGHT, J. T. & DEWHURST, D. 1998. Layer-bound compaction faults in fine-grained sediments. *Geological Society of America Bulletin,* 110**,** 1242-1257.

CHAND, S., RISE, L., KNIES, J., HAFLIDASON, H., HJELSTUEN, B. & BØE, R. 2011. Stratigraphic development of the south Vøring margin (Mid-Norway) since early Cenozoic time and its influence on subsurface fluid flow. *Marine and Petroleum Geology,* 28**,** 1350-1363.

DALLAND, A., WORSLEY, D. & OFSTAD, K. 1988. A lithostrategraphic scheme for the Mesozoic and Cenozoic succession offshore mid- and northern Norway. *NPD-Bulletin NO 4*.

DEEGAN, C. T. & SCULL, B. J. 1977. *A standard lithostratigraphic nomenclature for the Central and Northern North Sea*, HMSO.

DEWHURST, D. N., CARTWRIGHT, J. A. & LONERGAN, L. 1999. The development of polygonal fault systems by syneresis of colloidal sediments. *Marine and Petroleum Geology,* 16**,** 793-810.

EIDVIN, T., BUGGE, T. & SMELROR, M. 2007. The Molo Formation, deposited by coastal progradation on the inner Mid-Norwegian continental shelf, coeval with the Kai Formation to the west and the Utsira Formation in the North Sea. *Norwegian Journal of Geology/Norsk Geologisk Forening,* 87.

FALEIDE, J. I., TSIKALAS, F., BREIVIK, A. J., MJELDE, R., RITZMANN, O., ENGEN, O., WILSON, J. & ELDHOLM, O. 2008. Structure and evolution of the continental margin off Norway and the Barents Sea. *Episodes,* 31**,** 82-91.

GUDMUNDSSON, A. 2000. Active fault zones and groundwater flow. *Geophysical Research Letters,* 27**,** 2993-2996.

GUDMUNDSSON, A. 2001. Fluid overpressure and flow in fault zones: field measurements and models. *Tectonophysics,* 336**,** 183-197.

GUZZETTA, G. & CINQUEGRANA, R. 1987. "Fluid tectonics": a little appreciated facet of buoyancy tectonics. *Tectonophysics,* 139**,** 321-324.

HANSEN, J., CARTWRIGHT, J., HUUSE, M. & CLAUSEN, O. R. 2005. 3D seismic expression of fluid migration and mud remobilization on the Gjallar Ridge, offshore mid‐Norway. *Basin Research,* 17**,** 123-139.

HARDY, S. & MCCLAY, K. 1999. Kinematic modelling of extensional fault-propagation folding. *Journal of Structural Geology,* 21**,** 695-702.

HENRIKSEN, S. & VORREN, T. O. 1996. Late Cenozoic sedimentation and uplift history on the mid-Norwegian continental shelf. *Global and Planetary Change,* 12**,** 171-199.

HJELSTUEN, B. O., ELDHOLM, O. & SKOGSEID, J. 1997. Vøring Plateau diapir fields and their structural and depositional settings. *Marine Geology,* 144**,** 33-57.

HJELSTUEN, B. O., ELDHOLM, O. & SKOGSEID, J. 1999. Cenozoic evolution of the northern Vøring margin. *Geological Society of America Bulletin,* 111**,** 1792-1807.

HJELSTUEN, B. O., SEJRUP, H. P., HAFLIDASON, H., BERG, K. & BRYN, P. 2004a. Neogene and Quaternary depositional environments on the Norwegian continental margin, 62 N–68 N. *Marine Geology,* 213**,** 257-276.

HJELSTUEN, B. O., SEJRUP, H. P., HAFLIDASON, H., NYGÅRD, A., BERSTAD, I. M. & KNORR, G. 2004b. Late Quaternary seismic stratigraphy and geological development of the south Vøring margin, Norwegian Sea. *Quaternary Science Reviews,* 23**,** 1847-1865.

HOVLAND, M. & CURZI, P. V. 1989. Gas seepage and assumed mud diapirism in the Italian central Adriatic Sea. *Marine and petroleum geology,* 6**,** 161-169.

HOVLAND, M. & JUDD, A. 1988. *Seabed pockmarks and seepages: impact on geology, biology, and the marine environment,* Springer.

HOVLAND, M., NYGAARD, E. & THORBJØRNSEN, S. 1998. Piercement shale diapirism in the deep-water Vema Dome area, Vøring Basin, offshore Norway. *Marine and Petroleum Geology,* 15**,** 191-201.

HUUSE, M., JACKSON, C. A. L., VAN RENSBERGEN, P., DAVIES, R. J., FLEMINGS, P. B. & DIXON, R. J. 2010. Subsurface sediment remobilization and fluid flow in sedimentary basins: an overview. *Basin Research,* 22**,** 342-360.

IYER, K., RÜPKE, L. & GALERNE, C. Y. 2013. Modeling fluid flow in sedimentary basins with sill intrusions: Implications for hydrothermal venting and climate change. *Geochemistry, Geophysics, Geosystems,* 14**,** 5244-5262.

JAMTVEIT, B., SVENSEN, H., PODLADCHIKOV, Y. Y. & PLANKE, S. 2004. Hydrothermal vent complexes associated with sill intrusions in sedimentary basins. *Physical geology of high-level magmatic systems,* 234**,** 233-241.

KJOBERG, S., SCHMIEDEL, T., PLANKE, S., SVENSEN, H. H., MILLETT, J. M., JERRAM, D. A., GALLAND, O., LECOMTE, I., SCHOFIELD, N. & HAUG, Ø. T. 2017. 3D structure and formation of hydrothermal vent complexes at the Paleocene-Eocene transition, the Møre Basin, mid-Norwegian margin. *Interpretation,* 5**,** SK65-SK81.

LIGTENBERG, J. 2005. Detection of fluid migration pathways in seismic data: implications for fault seal analysis. *Basin Research,* 17**,** 141-153.
LÜDMANN, T. & WONG, H. K. 2003. Characteristics of gas hydrate occurrences associated with mud diapirism and gas escape structures in the northwestern Sea of Okhotsk. *Marine Geology,* 201**,** 269-286.
LØSETH, H., GADING, M. & WENSAAS, L. 2009. Hydrocarbon leakage interpreted on seismic data. *Marine and Petroleum Geology,* 26**,** 1304-1319.
NARDIN, T. R., HEIN, F., GORSLINE, D. S. & EDWARDS, B. 1979. A review of mass movement processes sediment and acoustic characteristics, and contrasts in slope and base-of-slope systems versus canyon-fan-basin floor systems.
NORTON, D. L. 1984. Theory of hydrothermal systems. *Annual Review of Earth and Planetary Sciences,* 12**,** 155-177.
ORANGE, D. L., GREENE, H. G., REED, D., MARTIN, J. B., MCHUGH, C. M., RYAN, W. B., MAHER, N., STAKES, D. & BARRY, J. 1999. Widespread fluid expulsion on a translational continental margin: mud volcanoes, fault zones, headless canyons, and organic-rich substrate in Monterey Bay, California. *Geological Society of America Bulletin,* 111**,** 992-1009.
OSBORNE, M. J. & SWARBRICK, R. E. 1997. Mechanisms for generating overpressure in sedimentary basins: A reevaluation. *AAPG bulletin,* 81**,** 1023-1041.
PÉREZ-BELZUZ, F., ALONSO, B. & ERCILLA, G. 1997. History of mud diapirism and trigger mechanisms in the Western Alboran Sea. *Tectonophysics,* 282**,** 399-422.
PLANKE, S., RASMUSSEN, T., REY, S. S. & MYKLEBUST, R. Seismic characteristics and distribution of volcanic intrusions and hydrothermal vent complexes in the Vøring and Møre basins. Geological Society, London, Petroleum Geology Conference series, 2005. Geological Society of London, 833-844.
REN, S., FALEIDE, J. I., ELDHOLM, O., SKOGSEID, J. & GRADSTEIN, F. 2003. Late Cretaceous–Paleocene tectonic development of the NW Vøring basin. *Marine and Petroleum Geology,* 20**,** 177-206.
RISE, L., CHAND, S., HJELSTUEN, B., HAFLIDASON, H. & BØE, R. 2010. Late Cenozoic geological development of the south Vøring margin, mid-Norway. *Marine and Petroleum Geology,* 27**,** 1789-1803.
ROVERE, M., GAMBERI, F., MERCORELLA, A., RASHED, H., GALLERANI, A., LEIDI, E., MARANI, M., FUNARI, V. & PINI, G. A. 2014. Venting and seepage systems associated with mud volcanoes and mud diapirs in the southern Tyrrhenian Sea. *Marine Geology,* 347**,** 153-171.
SCHLUMBERGER. 2015. *file:///C:/Users/lha208/Downloads/Petrel_Recommended_Seismic_Volume_Attributes_2015_Poster.pdf* [Online]. [Accessed].
SCHOWALTER, T. T. 1979. Mechanics of secondary hydrocarbon migration and entrapment. *AAPG bulletin,* 63**,** 723-760.
SHERIFF, R. 1985. Aspects of Seismic Resolution: Chapter 1.
SIBSON, R. H. 1996. Structural permeability of fluid-driven fault-fracture meshes. *Journal of Structural Geology,* 18**,** 1031-1042.
SIBSON, R. H. 2000. Fluid involvement in normal faulting. *Journal of Geodynamics,* 29**,** 469-499.
SIBSON, R. H. 2003. Brittle-failure controls on maximum sustainable overpressure in different tectonic regimes. *AAPG bulletin,* 87**,** 901-908.
SKOGSEID, J., PEDERSEN, T. & LARSEN, B. 1992. Vøring Basin: subsidence and tectonic evolution. *Structural and Tectonic Modelling and Its Application to Petroleum Geology, NPF Spec. Publ,* 1**,** 55-82.
STUEVOLD, L. M., SKOGSEID, J. & ELDHOLM, O. 1992. Post-Cretaceous uplift events on the Vøring continental margin. *Geology,* 20**,** 919-922.
TWISS, R. J. & MOORES, E. M. 1992. *Structural geology,* Macmillan.

VADAKKEPULIYAMBATTA, S., BÜNZ, S., MIENERT, J. & CHAND, S. 2013. Distribution of subsurface fluid-flow systems in the SW Barents Sea. *Marine and Petroleum Geology,* 43**,** 208-221.

YILMAZ, Ö. 2001. Seismic data analysis: Processing, inversion, and interpretation of seismic data.

ZOBACK, M. L., ZOBACK, M. D., ADAMS, J., ASSUMPCAO, M., BELL, S., BERGMAN, E., BLÜMLING, P., BRERETON, N., DENHAM, D. & DING, J. 1989. Global patterns of tectonic stress. *Nature,* 341**,** 291.